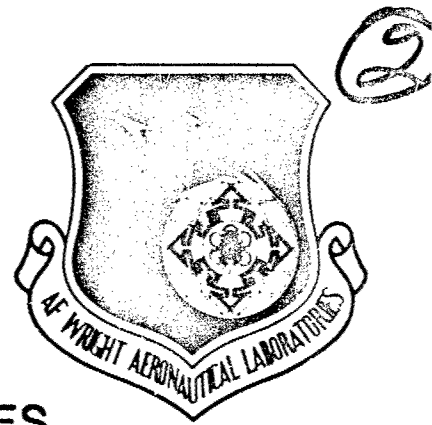AD-A170 601

AFWAL-TR-85-2006

COMPATIBILITY OF SODIUM AND LITHIUM IN SUPERALLOY HEAT PIPES
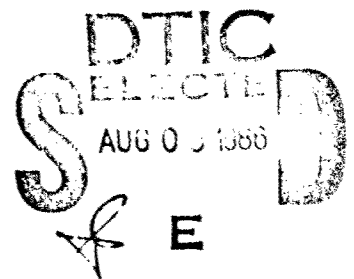
Warner B. Kaufman
Leonard K. Tower

Tower and Kaufman
Fairview Park, OH 44126

April 1985

Final Report for Period 1 January - 31 December 84

Approved for public release, distribution unlimited

DTIC
ELECTE
AUG 0 5 1986
E

AERO PROPULSION LABORATORY
AIR FORCE WRIGHT AERONAUTICAL LABORATORES
AIR FORCE SYSTEMS COMMAND
WRIGHT-PATTERSON AIR FORCE BASE, OHIO 45433

86   8   4   1
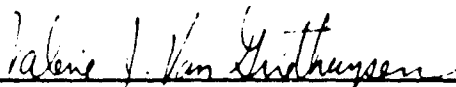
SECURITY CLASSIFICATION OF THIS PAGE

AD-A170 601

REPORT DOCUMENTATION PAGE

1a. REPORT SECURITY CLASSIFICATION	1b. RESTRICTIVE MARKINGS
UNCLASSIFIED	

2a. SECURITY CLASSIFICATION AUTHORITY	3. DISTRIBUTION/AVAILABILITY OF REPORT
	APPROVED FOR PUBLIC RELEASE:
2b. DECLASSIFICATION/DOWNGRADING SCHEDULE	DISTRIBUTION UNLIMITED

4. PERFORMING ORGANIZATION REPORT NUMBER(S)	5. MONITORING ORGANIZATION REPORT NUMBER(S)
	AFWAL-TR-85-2006

6a. NAME OF PERFORMING ORGANIZATION	6b. OFFICE SYMBOL (If applicable)	7a. NAME OF MONITORING ORGANIZATION
Leonard K. Tower and Warner B. Kaufman		Air Force Wright Aeronautical Laboratories Aero Propulsion Laboratory (AFWAL/POOS-3)

6c. ADDRESS (City, State and ZIP Code)	7b. ADDRESS (City, State and ZIP Code)
Firview Park Ohio 44126	Wright-Patterson AFB OH 45433

8a. NAME OF FUNDING/SPONSORING ORGANIZATION	8b. OFFICE SYMBOL (If applicable)	9. PROCUREMENT INSTRUMENT IDENTIFICATION NUMBER
Aero Propulsion Laboratory	AFWAL/POOS-3	F33615-81-C-2012

8c. ADDRESS (City, State and ZIP Code)	10. SOURCE OF FUNDING NOS.			
Wright-Patterson AFB, Ohio 45433	PROGRAM ELEMENT NO.	PROJECT NO.	TASK NO.	WORK UNIT NO.
	62203F	3145	19	49

11. TITLE (Include Security Classification) COMPATIBILITY OF SODIUM AND LITHIUM IN SUPERALLOY HEAT PIPES

12. PERSONAL AUTHOR(S)
Kaufman, Warner B. and Tower, Leonard K.

13a. TYPE OF REPORT	13b. TIME COVERED	14. DATE OF REPORT (Yr., Mo., Day)	15. PAGE COUNT
Final	FROM 1 Jan 84 TO 31Dec84	April 1985	118

16. SUPPLEMENTARY NOTATION
This report represents part of a program to transfer space heat pipe technology from NASA LeRC to Aero Propulsion Laboratory

17.	COSATI CODES		18. SUBJECT TERMS (Continue on reverse if necessary and identify by block number)
FIELD	GROUP	SUB. GR	HEAT PIPE, SPACECRAFT POWER SYSTEMS, SUPERALLOYS, CORROSION
22	02		SODIUM, LITHIUM, HEAT TRANSFER
10	03		

19. ABSTRACT (Continue on reverse if necessary and identify by block number)

Heat pipes of superalloy materials are attractive for low power terrestrial topping cycle and space power systems because of availability and relatively low cost. Six pipes of each material, stainless steel 304L and 310S, Hastalloy X and B, and Haynes 188 were tested. Eighteen pipes used sodium as a working fluid and were tested in an air environment to study both internal and external compatibility. The remaining twelve used lithium as a working fluid and were tested in a vacuum environment to study internal compatibility and external vaporization of material components. Some pipes had screen wicks and others had metal fiber wicks. Test facilities and procedures are discussed in detail. Compatibility as well as performance of sodium pipes and lithium pipes is compared. As a aid in explaining the performance of the pipes, a simple theoretical analysis was made, and the results are discussed.

20. DISTRIBUTION/AVAILABILITY OF ABSTRACT	21. ABSTRACT SECURITY CLASSIFICATION
UNCLASSIFIED/UNLIMITED ☒ SAME AS RPT. ☐ DTIC USERS ☐	Unclassified

22a. NAME OF RESPONSIBLE INDIVIDUAL	22b. TELEPHONE NUMBER (Include Area Code)	22c. OFFICE SYMBOL
V. J. Van Griethuysen	513-255-6235	AFWAL/POOS-3

DD FORM 1473, 83 APR   EDITION OF 1 JAN 73 IS OBSOLETE

1/11

SECURITY CLASSIFICATION OF THIS

FOREWORD

The information in this report was assembled for the University of Dayton as Task 20 of Contract No. F33615-81-C-2012 with the Air Force Wright Aeronautical Laboratories/Aero Propulsion Laboratory, of the Aeronautical Systems Division, Air Force Systems Command.

Ms. V.J. Van Griethuysen of the Energy Conversion Branch at the Aero Propulsion Laboratory (AFWAL-POOC) served as Project Engineer. The work was in support of Project 31451949, Thermal Energy Storage, Heat Pipes, and Heat Transfer Investigation. The report was prepared by Warner B. Kaufman and Leonard K. Tower, principal investigators. As members of the Chemical Systems Branch, Space Propulsion and Power Division of NASA Lewis Research Center, these investigators previously had conducted heat pipe compatibility tests on a group of superalloy materials with sodium and lithium fluids. The results were never reported because of a de-emphasis of heat pipe research at the Lewis Center.

This report represents part of a program to transfer space heat pipe technology from NASA Lewis to Aero Propulsion Laboratory. It describes the facilities and test procedures as well as compatibility results on five superalloy materials over thousands of hours of operation. The work was performed during the period 1 January to 31 December 1984.

The authors are indebted to the following personnel at NASA Lewis for consultation and assistance in the execution of this work: Dr. Stuart Fordyce, Chief, Space Power Technology Division; Major Alan Willoughby, retired, formerly Air Force Systems Command Liaison Officer; and Mr. William Frey, technician, associated with the life test evaluations conducted at the NASA Lewis Research Center.

TABLE OF CONTENTS

TABLE OF CONTENTS (continued)

LIST OF ILLUSTRATIONS

LIST OF ILLUSTRATIONS (continued)

LIST OF TABLES

SECTION I

INTRODUCTION

Heat pipes employing liquid metal working fluids have been widely investigated for applications in high temperature energy conversion systems in both space and terrestrial applications. The severity of the pipe operating environment, both internal and external, causes materials compatibility to be the major problem encountered.

The Lewis Research Center of NASA studied heat pipes as components of space power systems employing thermionic energy conversion (Ref. 1). Many innovative assembly techniques were devised in the course of constructing unusual heat pipes for testing (Ref. 2).

PROGRAM

The scope of applications for pipes grew to include terrestrial power plants, in which topping systems were advocated to supplement the conventional power cycle. Such applications placed economic constraints not considered important in space systems. For instance, the pipes should be capable of simple fabrication from readily available materials which can withstand the environment to which they are exposed.

In support of this effort, the Lewis Research Center initiated studies of sodium filled heat pipes to screen various container materials for possible terrestrial thermionic power systems and topping cycles. The peak temperatures envisioned for the terrestrial applications were somewhat lower than those for the space thermionic heat pipes. During the planning stage it became apparent that a possible niche existed in space power for heat pipes operating in this lower temperature range. Such systems would perform at lower power densities than the high temperature thermionic systems. Accordingly, the scope of

1

the investigation was enlarged to include vacuum environment for some pipes.

At the same time, lithium was added as a working fluid candidate suitable for a higher temperature range than sodium. The lower vapor pressure of lithium lessens the tendency of the envelope to creep, among other factors. For example, at a temperature of 1000 °C, the vapor pressure of sodium is about 47 times that of lithium.

The investigation was intended to be part of an ongoing study of liquid metal heat pipe materials and compatibility with the internal and external environment. Performance was to have been studied in later generations of pipes.

The test facilities were designed to permit unattended life testing over extended periods. In their design, provisions were made for simulating corrosive combustion gas environments at a later time. The program actually conducted was limited to air and vacuum. All candidate container materials were tested in both environments, although some were better suited to one than the other.

Before the work in this program could be completed, a de-emphasis of heat pipe research occurred at Lewis Research Center. The work was terminated with no report of the test results. The specialized test equipment was eventually transferred to the Air Force Wright Aeronautical Laboratories. Interest remains in liquid metal heat pipes operating in the temperature range of these pipes, especially for space applications. For this reason the status of the Lewis pipes at the time of shutdown was examined and is reported herein. Also, to facilitate the recommissioning of the test facilities, and to aid in the design of new facilities, a comprehensive discussion of the test facilities and their operation is included.

2

CHOICE OF MATERIALS

Prior to procurement of heat pipes, an extensive survey of the behavior of candidate alloys for inclusion in this program was conducted by Mr. James F. Morris, formerly of Lewis Research Center. Some of the rationale for the choice of materials, and some problems which were anticipated from the working fluid, container, and contaminant combinations (Ref. 3) will be discussed herein.

EXTERNAL ENVIRONMENT CONSIDERATIONS

The heat pipe environments in this study were air and vacuum. The additional intention of testing in an atmosphere simulating combustion flue gases which are encountered in electric power topping cycles was not realized because of the aforementioned de-emphasis of heat pipe research.

Since the original focus of the program was on terrestrial applications, the materials selections were guided by this consideration. When the scope of the program was enlarged to include space applications, the list of envelope materials chosen for air testing was extended to vacuum, with the knowledge that vaporization was a potential problem. Indications have been given that materials suitable for use in one situation at elevated temperatures may be undesirable in another (Ref. 4). Thus alloying constituents added to increase oxidation resistance may vaporize readily in vacuum. However, the materials choices ultimately were constrained by commercial availability and the expectation of compatibility with the liquid metals to be used.

To economize on the number of tests required in the screening, only sodium was used in the air pipes, and for the most part, lithium in the vacuum pipes. The assumption was made that the internal and external environments could not interact if the pipes were in good condition. Table 1

3

TABLE 1
SCHEDULE OF ENVELOPE MATERIALS, EXTERNAL ENVIRONMENT, AND WORKING FLUIDS

Environment	Envelope Material	Fluid
Air	304L	Sodium
	310S	
	Hastalloy X	
	Haynes 188	
	Hastalloy B	
Vacuum	304L	Sodium
	310S	Lithium
	Hastalloy X	
	Haynes 188	
	Hastalloy B	

4

shows the schedule of envelope materials, external environment, and working fluids which was tested.

DESCRIPTION OF THE PIPES

The outside dimensions for all the pipes were 1.27 cm diameter and 91.5 cm in length. The wall thickness was about 0.18 cm. The end caps and wicking structure were of the same material as the envelopes.

The stainless steel pipes contained screen of 60, 100, or 200 mesh stainless material wrapped to make a four layer wick. The original intention was to employ screen wicks in all pipes. Because screen was not available in Haynes 188, Hastalloy X, and Hastalloy B without undue delay, the wicks for these pipes were fabricated of metal fiber matching the container material. The metal fiber wicks were 0.08 cm thick, with a porosity of about 80 percent. The material was rolled into a single layer.

The pipes were cleaned chemically, honed inside, and vapor degreased. They were baked out at around 1000 °C, with wicks installed, at initial background pressure of $6x10^{-5}$ N/m^2 ($4.5x10^{-7}$ mm of Hg). The end caps were then electron beam welded and the pipes baked out again. After bake-out they were bagged in an inert atmosphere of ultra high purity argon.

At the time of filling they were suspended vertically in a furnace under an inert atmosphere and the working fluid was introduced with a heated syringe. With an initial background pressure of about $2x10^{-4}$ N/m^2 ($1.5x10^{-6}$ mm of Hg), they were then heated at the bottom for 5 to 10 min to outgas the working fluid. An orifice at the end of the pipe prevented serious loss of working fluid. After cooling, the pipes were pumped out and closed with a small bead of envelope material by a proprietary process of the vendor.

Table 2 provides an index of material pipe number, external environment, wick type, working fluid, and

5

TABLE 2

INDEX OF PIPE NUMBER, MATERIAL, ENVIRONMENT, WICK TYPE, WORKING FLUID, AND RECOMMENDED MAXIMUM TEMPERATURE

Material	Pipe Number	Environment	Wick type		Working fluid	Temperature limit, °C
			Screen (mesh)	Metal fiber		
304L	L-1[a]	Air	200	--	Sodium	880[c]
	L-2		200	--		
	L-7[a]		100	--		
	L-8		100	--		
	L-3	Vacuum	200	--		
	L-9	Vacuum	100	--		
310S	S-1	Air	60	--	Sodium	880[c]
	S-2	Air		--	Sodium	
	S-3	Air		--	Sodium	
	S-7	Vacuum		--	Lithium	
	S-8	Vacuum		--	Lithium	
	S-9	Vacuum		--	Lithium	
Hastalloy X	HX-7	Air	---		Sodium	930[c]
	HX-8[b]	Air	---		Sodium	
	HX-9	Air	---		Sodium	
	HX-2	Vacuum	---		Lithium	
	HX-5	Vacuum	---		Lithium	
	HX-11	Vacuum	---		Lithium	
Haynes 188	HA-5	Air	---		Sodium	980[c]
	HA-6	Air	---		Sodium	
	HA-8	Air	---		Sodium	
	HA-1	Vacuum	---		Lithium	
	HA-2	Vacuum	---		Lithium	
	HA-4	Vacuum	---		Lithium	
Hastalloy B	HB-1	Air	---		Sodium	980[c]
	HB-2	Air	---		Sodium	
	HB-3	Air	---		Sodium	
	HB-5	Vacuum	---		Lithium	
	HB-6	Vacuum	---		Lithium	
	HB-8	Vacuum	---		Lithium	

[a]Destroyed in prototype test facility.
[b]Returned to manufacturer for modification, not tested.
[c]Temperature for failure after 1000 hr at 2×10^7 N/m^2 (3000 psi).

6

recommended maximum temperature. The recommended maximum
temperature represents the maximum temperature for which
an alloy is regarded as structurally suitable (Ref. 5).

The facilities were designed with the capability of testing heat pipes in the temperature range of 500 to 1000 °C. The tests were to be conducted in a vacuum environment for space applications and in an air, corrosive gas, and/or water vapor environment (exhaust and stack gases) for terrestrial applications. The corrosive gas and water vapor tests were intended for second or third generation pipes. Therefore, the required equipment to introduce a particular gas or combination of gases into the test chambers and the required venting, etc., for safety considerations was not incorporated for the work described herein.

TEST STANDS

Each of the two test stands pictured in Fig. 1 consisted of two instrument cabinets housed side by side in a steel frame. Six test stations, three on a side, were supported on opposite sides of each frame. The test stations were numbered 1 through 12, starting from the top left of the left stand. Since each of the five heat pipe material combinations was to be tested in a vacuum environment as well as an air environment, Stations 1, 2, 3 (Stand 1) and 7, 8, 9 (Stand 2) were designated as vacuum test stations. The remaining Stations, 4, 5, 6 (Stand 1) and 10, 11, 12 (Stand 2) were operated with open ports on the ends of the chambers to permit room air to circulate by convection and were designated as air environment stations.

A 1000 liter/sec Vac-Ion pump was housed in the base of each of the two test stands. The vacuum stations were connected to 15.2 cm diameter manifolds by 3.8 cm diameter flexible metal hoses. The manifolds were installed vertically on their respective Vac-Ion pump inlets. Each pump
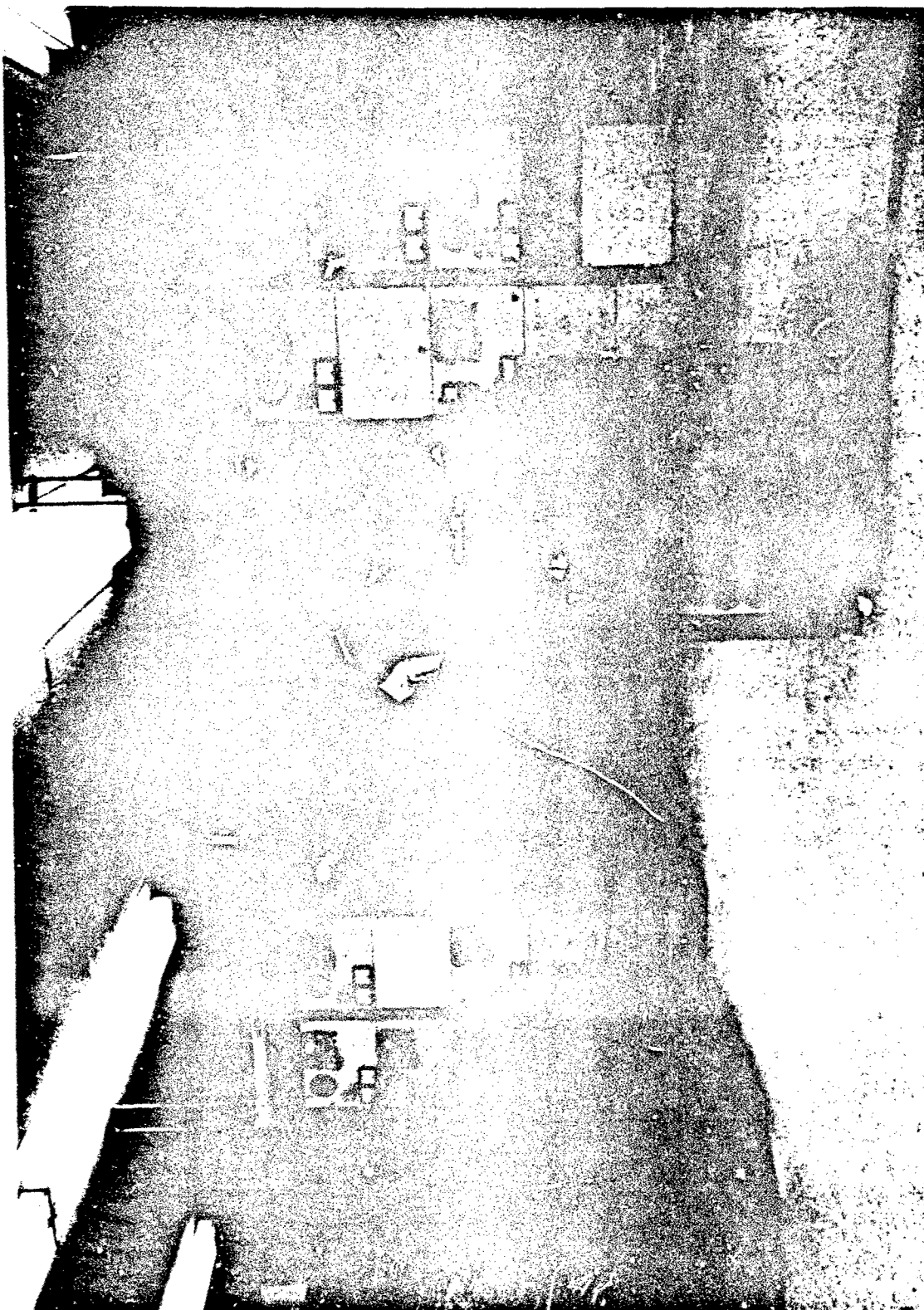
FIGURE 1. - SUPERALLOY HEAT PIPE TEST FACILITY.

was capable of maintaining a vacuum of about 10^{-6} N/m^2 (10^{-8} mm of Hg) in the three test chambers it served while the heat pipes were at operating temperatures.

Because Vac-Ion pumps will not start at pressures above 6×10^{-2} N/m^2 (5×10^{-4} mm of Hg), two 500-liter/sec turbomolecular pumps (foreground of Fig. 1) were used as forepumps. These pumped down from atmospheric pressure to about 10^{-4} N/m^2 (10^{-6} mm of Hg).

Five individual sets of controls and instrumentation can be seen on each stand. Since there were only five material groups of heat pipes, only five of the six chambers on each stand were used; three vacuum and two air on the left stand, and two vacuum and three air on the right stand. While all twelve chambers were installed, only ten control panels were completed. Eight of the ten were identical. One air station, 6, and one vacuum station, 9, were fitted with larger capacity powerstats to provide a higher heat input capability for those pipes which showed high heat transport promise. They were located in a lower panel in their respective stands because of size and weight. Also apparent in a lower panel of each stand is a control unit for each of the respective Vac-Ion pumps.

The left test stand is pictured in Fig. 2. In the upper left corner of each of the respective control panels can be seen a powerstat to regulate power input to the heat pipe evaporator heater. Below it is a panel power on-off switch, indicating light, powerstat on-off switch, fuseholder, ammeter, and voltmeter. On the right side of each panel is a four position thermocouple selector switch and a temperature indicating meter with a temperature limiting pointer. Visible below these is an elapsed-time meter, temperature meter on-off switch, indicating light, and the temperature limit relay reset button.

Three air environment test stations can be seen on the right side of the stand in Fig. 2. The top and bottom stations have the chambers removed and one chamber lies on the

TEMPERATURE
METER

VACUUM
VALVE

POWERSTAT

U CHANNEL

HEAT
EXTRACTOR

SUPPORT
DISK

ADJUSTMENT
SCREWS

END
PLATE

EVAPORATOR
HEATER

COOLING
WATER/
SUPPORT
TUBES
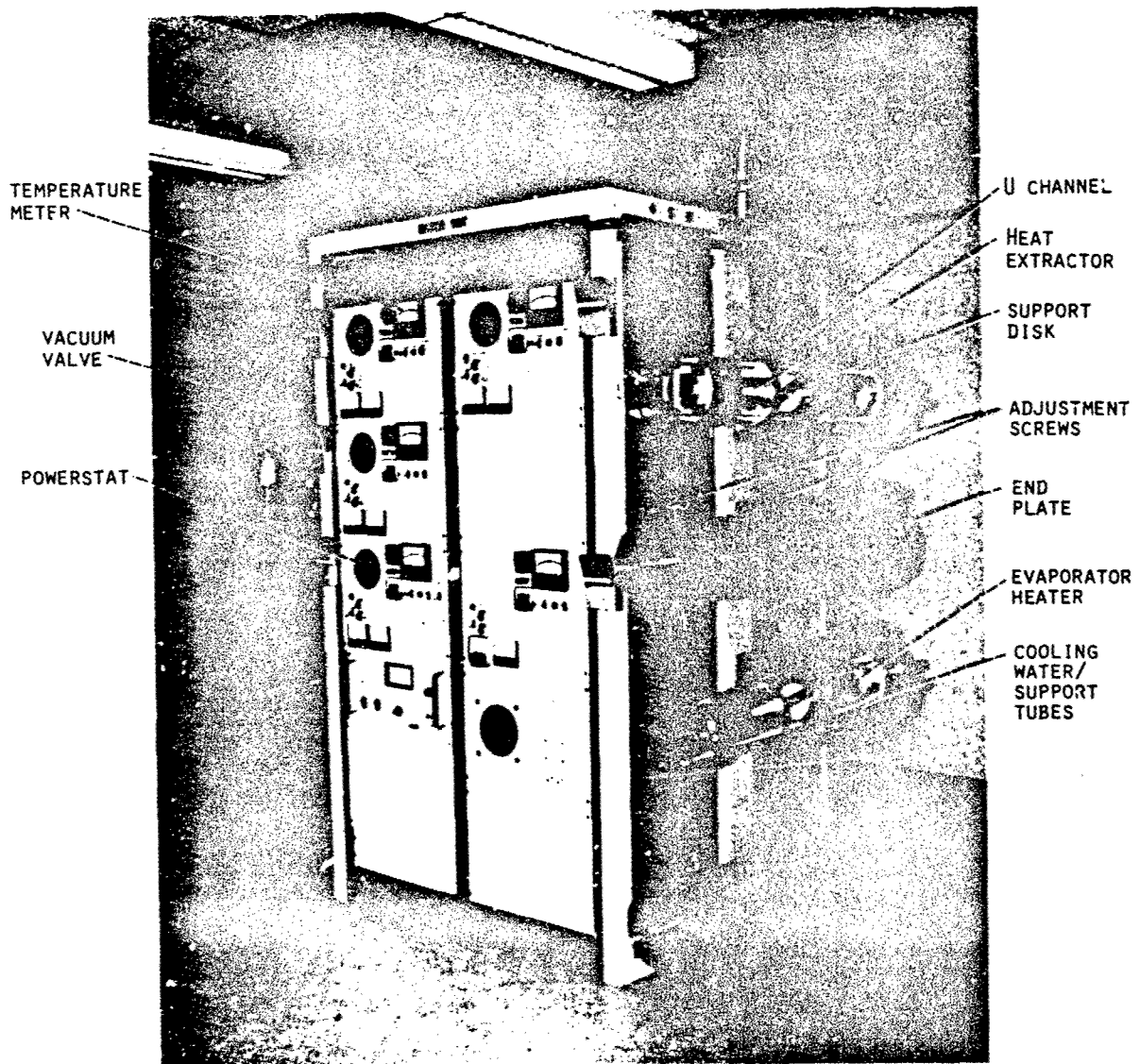
FIGURE 2. - LEFT TEST STAND SHOWING STATION DETAIL.

12

floor. The chamber end plate and internal structure of each station were supported by two bolts that passed through the heavy gauge U-shaped channel at its far end and were threaded into the edge of the end plate, top and bottom. In a vacuum environment station, the chamber was bolted to the end plate using a copper gasket as a seal. For an air environment station, the chamber was bolted loosely to leave about a half centimeter gap. No seal was required. The assembly was also supported at the midpoint of the chamber by adjustment screws that threaded through the near end of the U-shaped channel at the top and bottom.

The U-channel was pivoted at midpoint of the assembly on a 3.8 cm diameter stud that protruded through the center channel of the test stand frame. The whole assembly could be inclined at a chosen angle, negative or positive, and held in position by tightening the nut on the end of the pivot stud.

Each chamber had a port located at about midpoint of the heat pipe evaporator and another at midpoint of the heat pipe condenser. In addition, a port was located in the center of the end plate and in the center of the end of the chamber. For the air stations, these two ports were left open for air circulation, but for vacuum stations, vacuum valves were fitted to both ports. A 3.8 cm diameter flexible metal hose was connected between the end plate valve and vacuum manifold to permit inclination of the assembly about the pivot stud. This valve was used to isolate the particular station from the Vac-Ion pump system so that the chamber could be brought up to atmospheric pressure for removal and installation of heat pipes without disturbing the other two stations on the same vacuum system. The vacuum valves, visible on the chamber ends on the left side of the test stand, Fig. 2, could be connected to one of the turbomolecular forepumps by a flexible metal hose for initial pump-down of the station to be put on test. An ionization-type vacuum gauge was installed on

13

the port over the heat pipe evaporator in each vacuum chamber to monitor internal pressure.

Chambers were installed for the air environment tests to "doubly contain" the sodium working fluid. Thus, in the event of pipe wall failure, leaking sodium would condense on the cooler chamber surfaces and oxidize rather than spray out into the surrounding area.

The uncovered stations 4 and 6 in Fig. 2 show, right to left, the end plate, the evaporator heater, the cooling water/support tubes, four support disks, heat pipe support channel, U-channel, and the heat extractor. Not shown is a cylindrical insulation added to the adiabatic section of those pipes tested in air and described later. Also not visible in Fig. 2 is a copper disk located between the end plate and the front evaporator heater support disk. The copper disk, supported by the cooling tubes, shielded the back of the end plate from heat radiation from the evaporator heater.

In addition to the two stainless steel coolant tubes and the large port at the center of the end plate, six small feed-through ports that could be vacuum sealed with copper gaskets were welded into the end plate. One of them was used as a feed-through for the thermocouple leads. Two more were used for evaporator heater electrical leads. The remaining three were spares.

The two cooling tubes not only supplied coolant to the heat extractor, but also supported the internal assembly. The support disks were slipped over the cooling tubes and positioned to support each end of the evaporator heater and each end of the condenser heat extractor. A thin gauge channel can be noted spanning the diameter of the second disk from the right. This channel and a similar one fastened to the facing side of the third disk supported the heat pipe. The channels were formed of the same material as the particular heat pipe they supported in order to prevent transfer of any deleterious constituent from it to the

14

pipe which would obscure the external corrosion mechanism in metallographic studies.

At the near end can be seen a rectangular fixture that was fabricated in two halves so that it could be clamped onto the ends of the coolant tubes with bolts to add rigidity to the structure. Two special "0"-ring-sealed adjusting screws can be observed, one on the top, one on the bottom, of the near end of the chambers. After the chamber was assembled over the internal structure with its heat pipe installed, these screws were adjusted until their ends contacted the top and bottom of the rectangular fixture to add additional support to the internal structure.

The recirculating cooling system serviced both test stands. At each station, part of the coolant flowed into one of the cooling water/support tubes, through the heat extractor coil, and out the other tube. The rest of the coolant was directed through the copper coil brazed to the outside of the chamber wall over the area of the heat pipe evaporator and adiabatic sections.

EVAPORATOR HEATER - AIR

Components of the original heater for use in the air environment tests are illustrated in Fig. 3(a). The heating element wire was wound on a 4.8 cm diameter by 35.5 cm long tube of 98 percent alumina. The tube was cast with a 0.32 cm wide by 0.16 cm deep helical groove from each end to the midpoint. At midpoint was a 0.64 cm square circumferential groove. Kanthal A resistance wire was used to wind coils in the helical grooves from the ends of the alumina tube toward the midpoint groove. The ends of the two coils meeting in the midpoint groove were twisted together and lead to the forward end of the heater in a small alumina tube. The leads from the outer ends of the coils were twisted together to form the other lead. Therefore, the coils operated in parallel. A separate piece of wire was wrapped in the midpoint groove and in each end

15

INSULAT[...] END WAS[...]

ALUMINA END WASHER

CAST CERAMIC FIBER TUBE

ALUMINA COVER TUBE

GROOVED ALUMINA TUBE WITH WIRE

MIDPOINT GROOVE
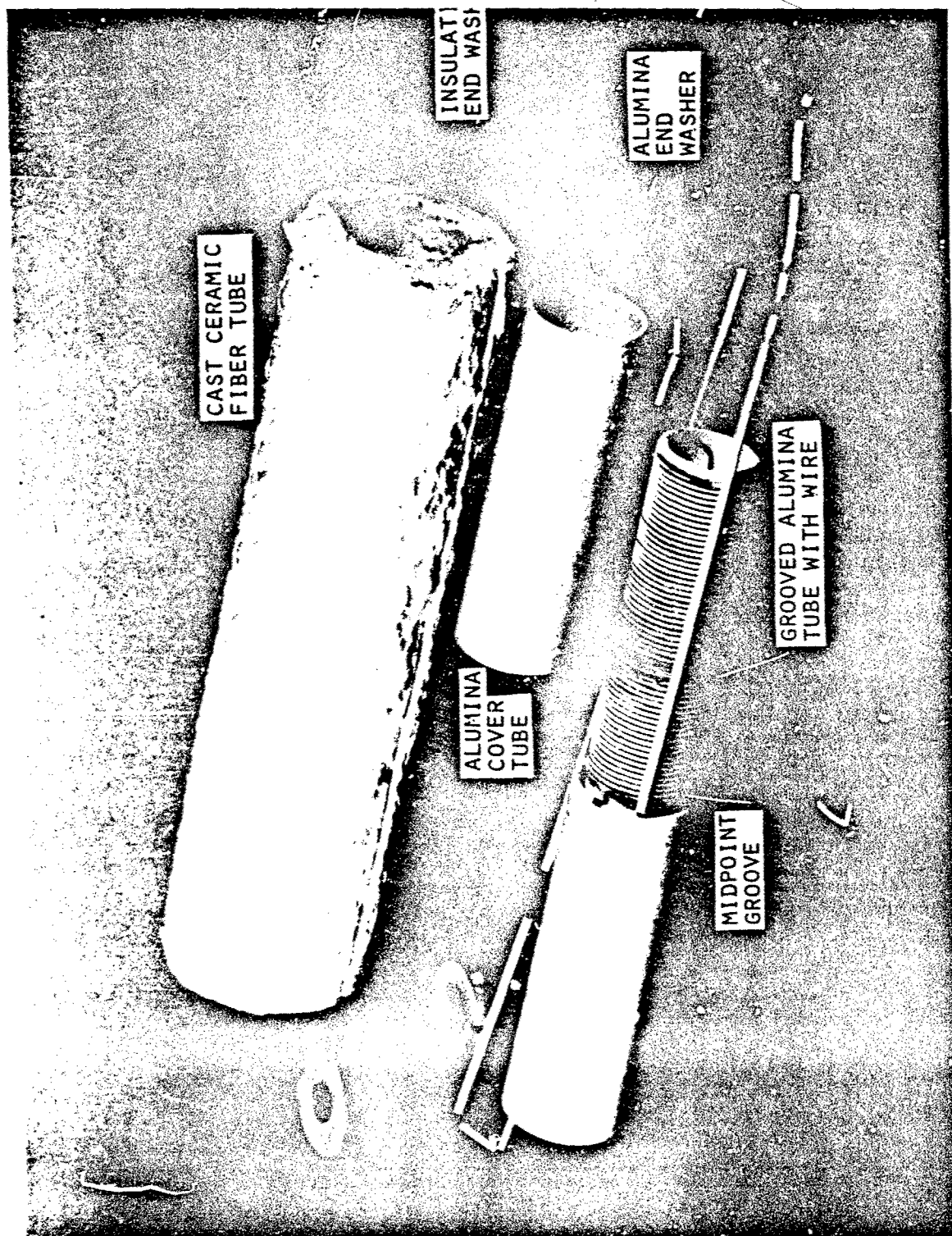
(A) HEATER AS ORIGINALLY DESIGNED.

FIGURE 3. - EVAPORATOR HEATER FOR AIR ENVIRONMENT STATIONS.

16

groove over the last coil. The ends were twisted together to prevent the coils from loosening.

Each half of the wound tube was covered with a 5.1 cm I.D., 99 percent alumina tube. This assembly was then inserted into a 10 cm O.D., vacuum formed insulating tube of asbestos-free alumina-silica fiber. An alumina washer was inserted in the alumina cover tube against each end of the grooved tube. Finally, a 2.54 cm thick insulating washer was inserted in each end of the outside insulating tube to decrease heater end losses from direct radiation.

These heaters were designed to produce about 1200 W and operate to 1200 °C. However, when tested in a proto-type facility with a superalloy 304L stainless steel heat pipe, not only did the heater collapse into a melted lump of material, but extensive external reaction destroyed the heat pipe. Unfortunately, chemical or metallurgical anal-ysis of the failure was not made, but observation suggested that the small percentage of silica present in the grooved tube was primarily responsible.

A second evaporator heater was constructed using a commercially available electric heating element housed in silica-free alumina (Electro-Applications, Inc. Model SK-118). The 4.1 cm I.D. cylindrical tube was comprised of two halves as shown in Fig. 3(b). The wire ends of each half were twisted together so that the two halves operated in parallel to provide 1200 W. The unit, capable of temperatures to 1200 °C was inserted into the 10 cm O.D. insulating tube of cast alumina-silica fiber. Two layers of heavy gauge aluminum foil were wrapped over the outside of the tube followed by one layer of alumina-silica ceramic fiber blanket about 1.27 cm thick. Admittedly, the cast tube and the blanket contained silica but they operated at a much lower temperature than the heater core of the origi-nal heater. The whole assembly was then wrapped with another layer of aluminum foil. End losses were minimized by washers about 5 cm thick machined from lava.

17

CERAMIC FIBER BLANKET

ALUMINUM FOIL

ALUMINUM FOIL

HEATER

CAST CERAMIC FIBER TUBE

LAVA END WASHER

(B) HEATER, FINAL DESIGN.

FIGURE 3. - EVAPORATOR HEATERS FOR AIR ENVIRONMENT STATIONS.

18

Both heaters were supported and centered about the heat pipe by 1.3 cm long stainless steel cylindrical sections fastened to the first and second support disks. While a few failures were experienced over the course of the tests, the heaters as a whole operated satisfactorily as long as 15,000 to 23,000 hr of continuous testing.

EVAPORATOR HEATER-VACUUM

The evaporator heaters for the vacuum environment tests required a different design from those for the air environment tests. Outgassing the insulating tube, the insulating blanket, and the several closely-packed layers would have been time consuming, if not impossible. Therefore, the heaters were constructed, as seen in Fig. 4, using a silica-free, 4.8 cm diameter alumina tube cast with a helical groove in its outer surface. Unlike the similar tube of the first air heater design, it had a continuous groove the full 33.8 cm of length. A 0.10 cm diameter molybdenum (moly) wire was wrapped in the helical groove. A 0.10 cm diameter tantalum wire was wound over the last turn on each end of the moly coil to prevent the coil from loosening or unraveling. The moly element wire was bent at 90° where it came off the last turn of the coil to provide a short length of lead at the ends. These ends were joined to 0.15 cm diameter tantalum wire by a short coupling crimped over the ends of the two wires.

The heater core was inserted into a 7.9 cm diameter high purity alumina cover tube that extended about 1.27 cm beyond the core ends. The assembly was then inserted into a radiation shield consisting of four concentric cylinders. The inner two were fabricated of 0.0127 cm thick moly sheet. Corrugated strips of 0.0127 cm thick moly separated the innermost cylinder from the alumina tube and the second cylindrical shield from the first. Because of poor ductility of moly, the two inner shields could not be

19
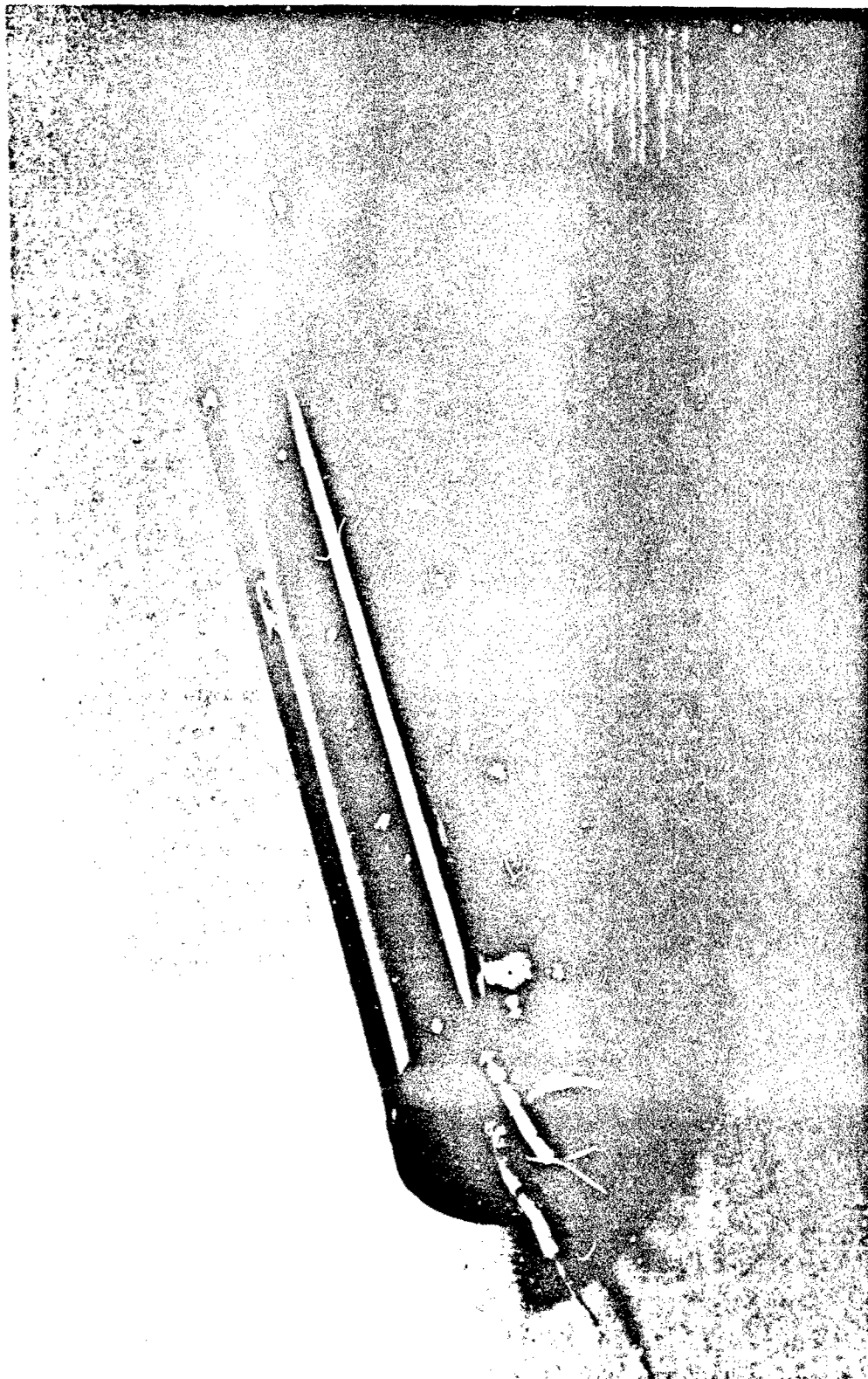
(A) ASSEMBLED.

FIGURE 4. – EVAPORATOR HEATER FOR VACUUM ENVIRONMENT STATIONS.

MOLY SHIELD
DISKS

END SHIELDS

MOLY SEPARATOR
STRIP

MOLY SHIELDS

STAINLESS STEEL
SHIELDS

ALUMINA
COVER TUBE

HEATER
CORE

CONNECTING
STRIPS

SUPPORT
DISK
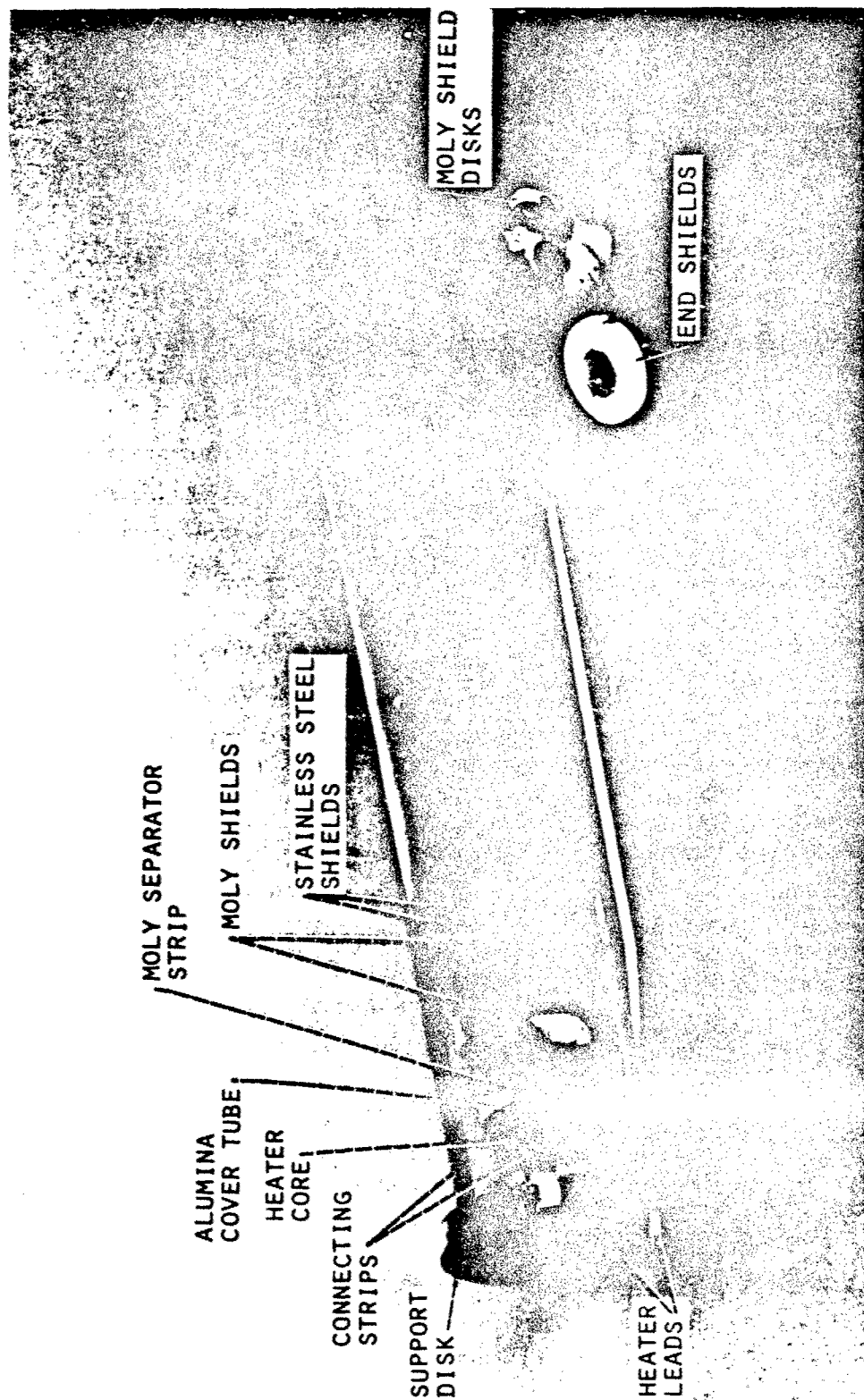
HEATER
LEADS

(B) INTERNAL PARTS.

FIGURE 4. - EVAPORATOR HEATER FOR VACUUM ENVIRONMENT STATIONS.

21

simply dimpled as were the two outer 0.020 cm thick stainless steel cylinders for separation spacing.

The innermost heat shields to prevent end losses were disks of 0.63 cm thick boron-nitride. Outside these were four moly disks, each 0.012 cm thick. The disks were spaced apart by small moly tabs spot welded to the disks. The heater element leads were electrically insulated from the metal end shields as they exited the assembly by short sections of high purity alumina tube. The aft lead was brought to the front end of the heater in a length of the same kind of tubing. The end flanges were tied together by three vee-shaped connecting strips of stainless steel sheet. The heater assembly was supported on each end by short cylindrical sections welded to the first and second support disks.

The heaters were capable of operating at 1200 W which proved to be greater than required for this group of pipes. There were no failures among the five heaters used. Four operated in excess of 25,800 hr each.

HEAT EXTRACTOR

The heat extractor, as originally designed, is pictured in Fig. 5(a). It was to be capable of removing about 600 W from the condenser section of a 1.27 cm diameter heat pipe by conduction from the pipe wall to the cooling water. It consisted of twelve pairs of stainless steel fingers and a helical coil of 0.63 cm diameter copper tubing. Each finger was ~2.5 cm wide and 2.86 cm long. The fingers were 0.79 cm thick along most of their length for strength purposes. In order to provide a thermal resistance between the condenser and the heat sink, the thickness was decreased to about 0.24 cm near the ends that were brazed to the copper coil. A 0.63 cm radius was machined into the inside surfaces to accommodate the heat pipe diameter. Two bolts inserted through one side of each pair and threaded into the other were used to draw

22

COPPER TUBE

STAINLESS STEEL FINGERS

HEAT CHOKE

HEAT PIPE
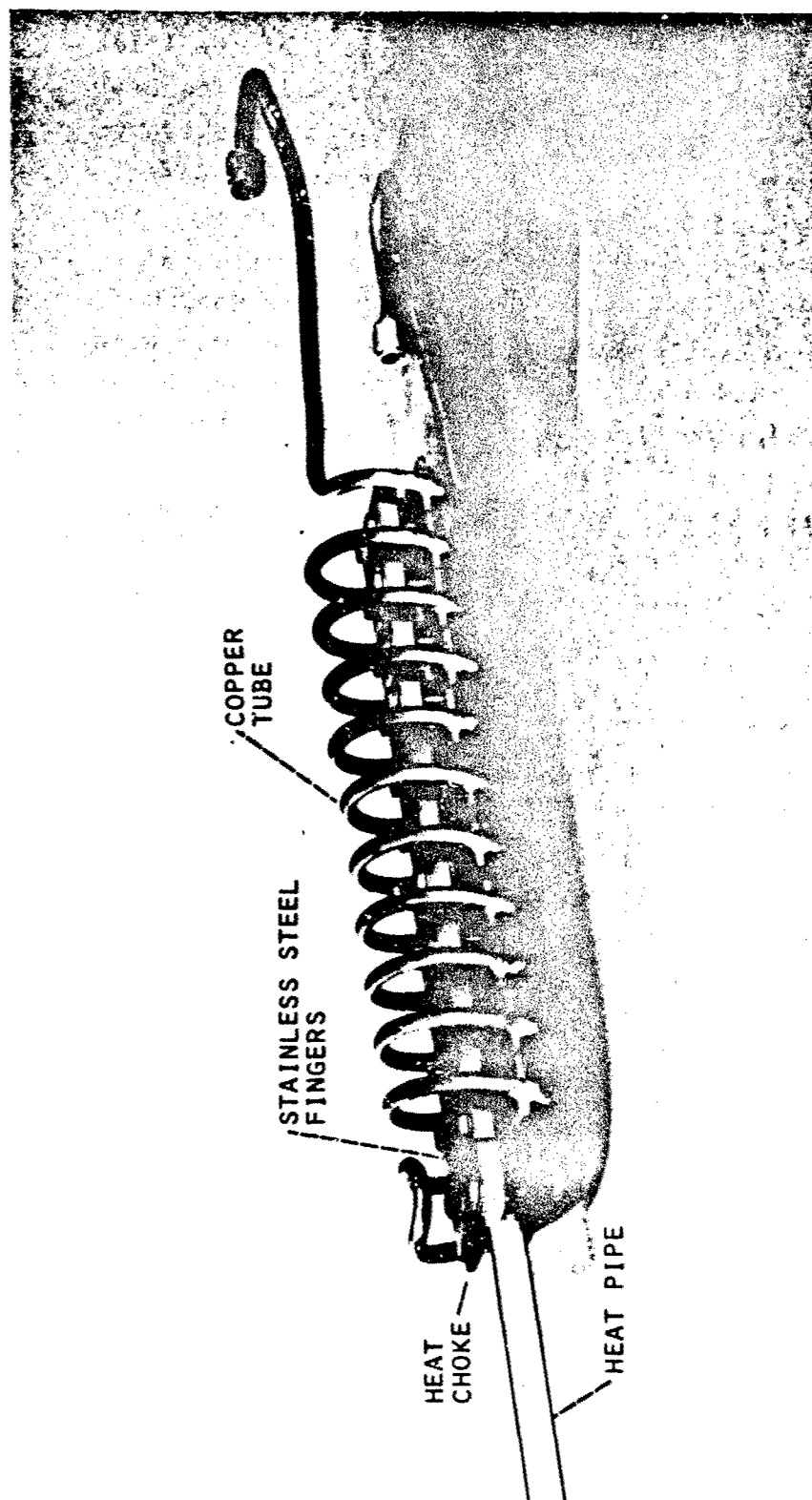
(A) CONDUCTION MODEL.

FIGURE 5. - HEAT EXTRACTOR DESIGNS.

23

the fingers against the condenser section of the pipe. The copper tube was coiled with a double lead so that the inlet and outlet connections would be on the same end. The heat extractor was supported in the same manner as the evaporator heater, but from the third and fourth support disks.

The fingers could be sprung out of contact with the heat pipe by loosening the two bolts in alternate pairs, every third pair, or whatever combination was necessary to obtain the desired heat flow rate from the condenser. With this latitude for controlling the heat flux, it was hoped the condenser and, therefore, the heat pipe could be set and maintained at the desired operating temperature. The design was tested in the prototype facility where it became evident that the heat transport capability of the superalloy pipes would require only a fraction of the heat extractor. Thus a simpler heat extractor would be sufficient.

A simple heat extractor, such as the one shown in Fig. 5(b), was used during the test program. It consisted merely of a copper tube wound in a helical coil of the same diameter as the original design. The coil was covered with a copper cylinder that was split longitudinally to permit it to be drawn tightly over the copper coil and secured with stainless steel hose clamps. Fairly good contact was maintained with the coil in this manner. Radiation to the copper cylinder was sufficient to cool a pipe for these heat pipe material selection tests.

COOLING SYSTEM

A schematic sketch of the cooling system is shown in Fig. 6. It was a recirculating system that serviced all twelve superalloy heat pipe test stations as well as seven refractory heat pipe test stations. Water was pumped from a 422 liter stainless steel reservoir by a 190 liter/min pump through a heat exchanger to the heat pipe test facilities at about 55 °C. A solution of ethylene glycol and

24
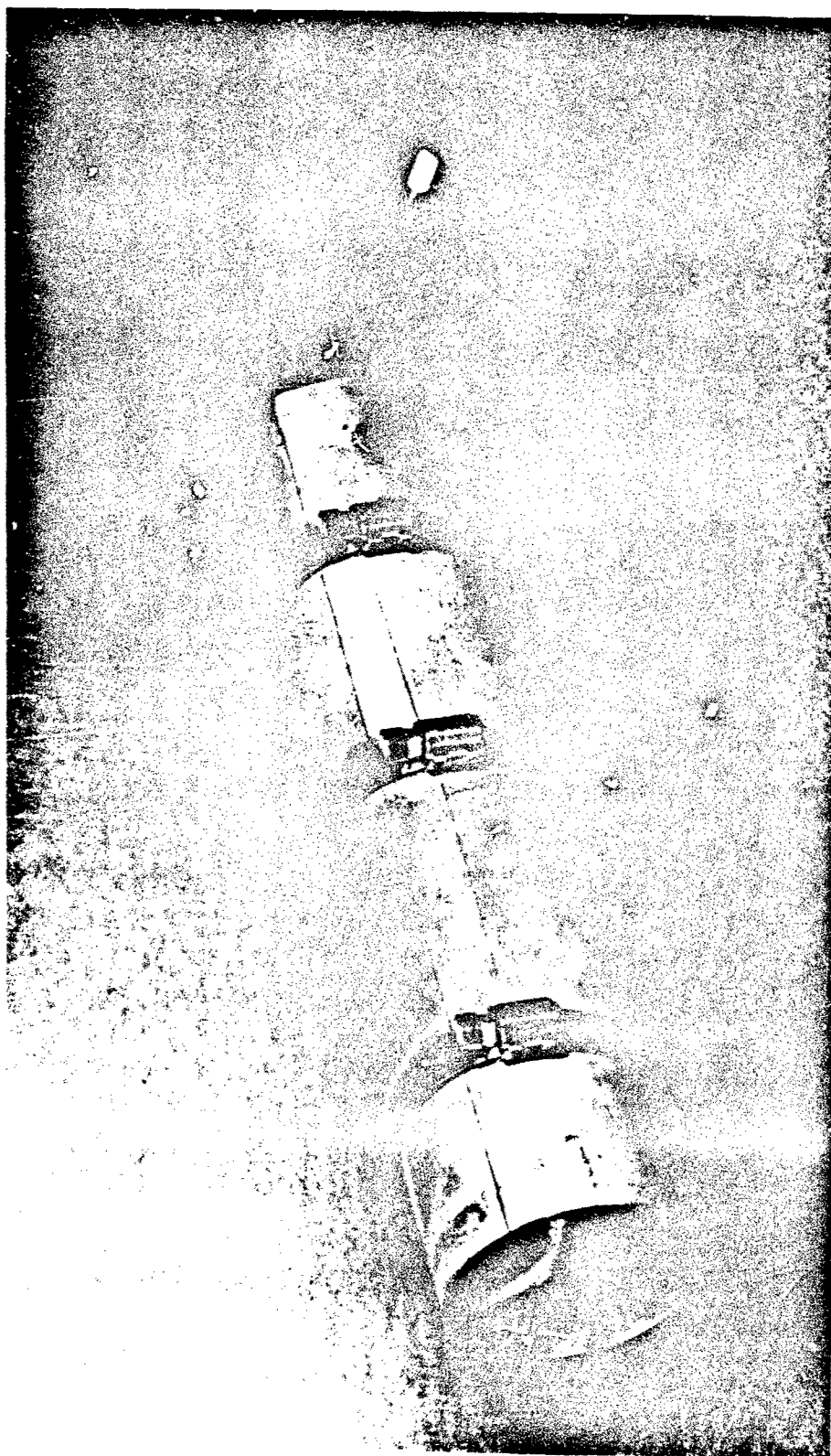
(B) RADIATION MODEL.

FIGURE 5. - HEAT EXTRACTOR DESIGNS.
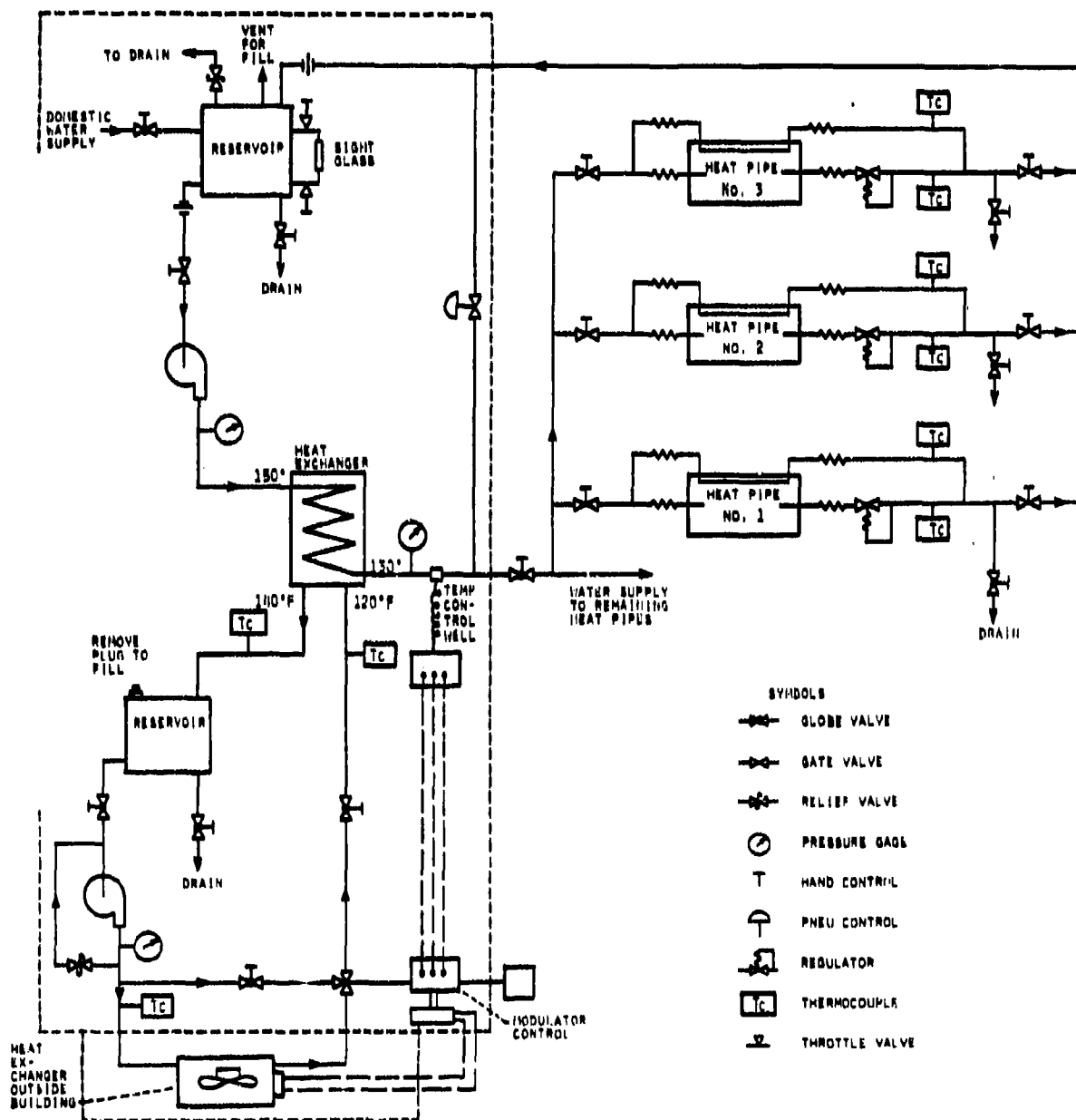
FIGURE 6. - COOLING SYSTEM SCHEMATIC DRAWING.

26

water was circulated through the heat exchanger by a second 190 liter/min pump to a second heat exchanger located outside the building. The temperature of the cooling water reaching the test facilities was controlled automatically by a motorized valve operated by a coolant outlet temperature sensor. The valve regulated the rate of ethylene glycol solution between a bypass loop and the second heat exchanger. The complete system operated continuously, trouble free, for a period of over three years.

THERMOCOUPLE INSTALLATION

Five 24 gauge chromel-alumel thermocouples were spot welded along the top center line of each pipe at the locations indicated in Fig. 7. Thermocouple no. 1, and the spare, were shielded by a strip of the same material as the heat pipe itself from direct radiation from the evaporator heater. The bare thermocouple wires were led through two-hole high purity alumina tubes to a point about 50 cm from the evaporator end of the pipe. The tubes were held in place with straps of the same material as the respective pipe material that were spot welded to the pipe. From this point to a terminal strip fastened to the top cooling tube, the wires were led through two-hole, high purity alumina beads. From the terminal strip out, the wires had ordinary glass type thermocouple electrical insulation and were terminated at the selector switch.

Any one of the four thermocouple outputs could be read on the panel-mounted temperature meter during data taking. At all other times the selector switch was set to send the output of thermocouple no. 1 to the meter. A temperature limiting pointer on the meter scale could be set to the temperature not to be exceeded. In the event of over-temperature, a relay would open causing electrical power to the evaporator heater to be shut off.
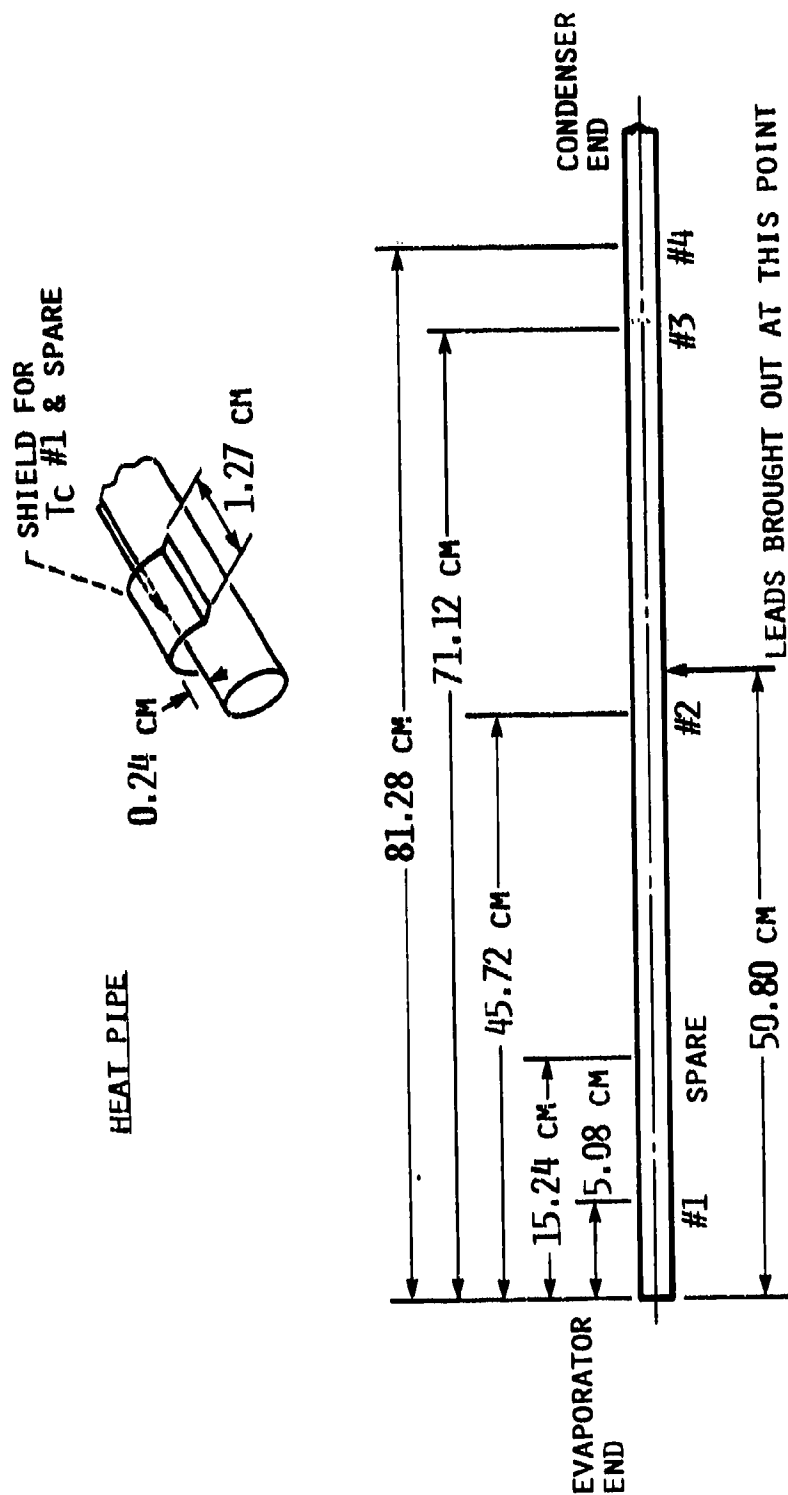
FIGURE 7. – THERMOCOUPLE LOCATIONS.

28

The spare thermocouple was connected to the selector switch in the event that thermocouple no. 1 failed. Thermocouple failures were generally due to wire breakage adjacent to the spot-welded junction bead.

SECTION III
TEST PROCEDURE

PREHEAT

Early in the program it proved difficult or impossible to start up some of the heat pipes. There was concern that during manufacture, the working fluid may have been driven to the condenser end where it solidified and left the evaporator dry. Because of the low thermal conductivity of the tube materials, not enough heat could be transported at start up to liquefy the working fluid and allow it to be drawn into the evaporator. Therefore, before installation in a test station, each pipe was "preheated" in a bench apparatus. The heat pipe was suspended vertically, evaporator end down, in the center of a 5 cm diameter open tube. A 1200 W heat gun was positioned above the tube so that hot air was blown down the tube over the heat pipe. The heat pipe evaporator temperature, as indicated by thermocouple no. 1, was read on a portable potentiometer. Hot air was blown over the heat pipe for a minimum of 2 hr while the indicated temperature was well above the melting point of sodium, 98 °C, or lithium, 186 °C. In this manner the working fluid should have been fluid enough to be pulled to the evaporator end of the pipe by gravity.

INSTALLATION

A pipe was installed by sliding it through the heat extractor, support channels, and evaporator heater, until the tip of the evaporator was just short of the forward end of the evaporator heater. The two pipe support channels were adjusted until the pipe was centered in the heater and heat extractor.

The adiabatic sections of those pipes installed in air stations were fitted with an insulating tube similar to the one surrounding the evaporator heaters. The tube was split

31

in half for installation purposes. It was held in place by being jammed between the edges of the heat pipe support channels. Figure 8 shows a heat pipe in operation with one half of the insulating tube removed. The thermocouple wires were led out through the split in the insulating tube and connected to the thermocouple terminal strip. A single layer of aluminum foil was wrapped around the two halves. A piece of wire wrapped over the aluminum foil at each end and twisted held the unit together.

The chamber was then carefully drawn over the assembly and, in the air stations, bolted loosely to the end plate leaving a small gap. In the vacuum stations the chamber was bolted tightly using a copper sealing gasket between the end plate and the chamber flange. The adjustment screws at the near end of the U-channel, Fig. 2, were tightened to support the chamber. Those at the near end of the chamber also were adjusted to just contact the rectangular fixture inside.

It was intended to operate the pipes at an adverse tilt (evaporator up) of at least 5°. However, it soon became apparent that most of the pipes would not pump the working fluid to the evaporator at anything less than 5° negative (evaporator down). At a negative tilt the working fluid flows to the evaporator helped by gravity. As will be seen later, some pipes would not function even at this favorable tilt.

OPERATION

When the station to be started up was a vacuum station, the flexible metal hose from a turbomolecular pump was connected to the vacuum valve on the end port of the chamber. The vacuum valve on the end plate was in the closed position to isolate the particular test station from the Vac-Ion pump manifold during "bake-out". The turbo-pump was started and as the chamber pressure, indicated by the ionization gauge, decreased, heater power was
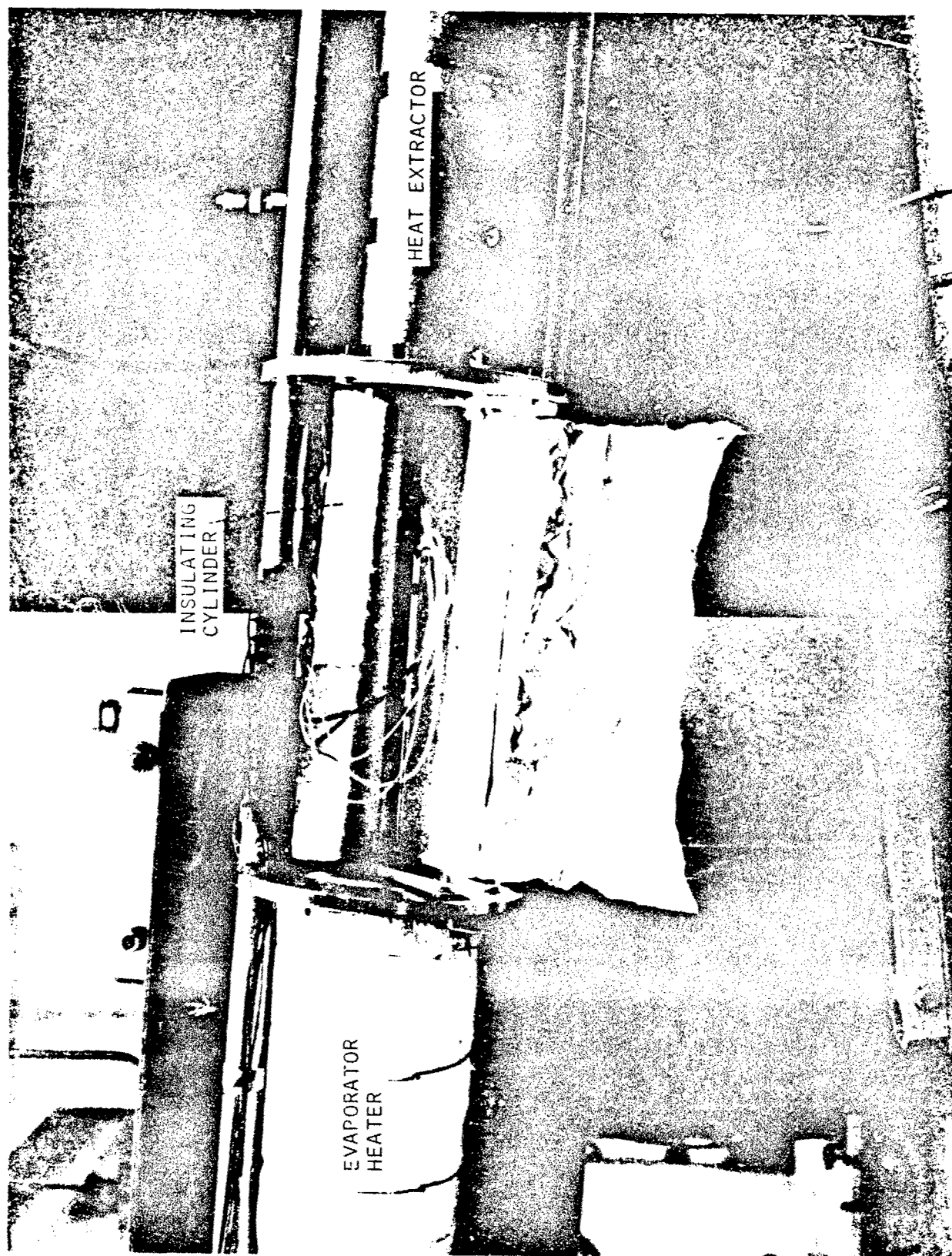
32

HEAT EXTRACTOR

INSULATING CYLINDER

EVAPORATOR HEATER

FIGURE 8. – ADIABATIC SECTION INSULATING TUBE, AIR STATIONS.

33

increased. Finally, when chamber pressure reached about 6×10^{-2} N/m^2 (5×10^{-4} mm of Hg) at evaporator operating temperature, the valve to the turbo-pump was closed. If the chamber pressure was maintained with both valves closed, the station was assumed to be baked out and leak tight. The valve on the end plate was then opened to the manifold. Normally, only a momentary increase in manifold pressure was observed.

Cooling water was then supplied to the heat extractor and the housing, and power to the evaporator heater was adjusted to obtain operating temperature at thermocouple no. 1 on the heat pipe evaporator. For those heat pipes in air environment stations, initial pump down and "bake-out" were, of course, not required. Heater power and coolant flow were gradually increased until the maximum operating temperature was reached.

Data were generally recorded once each day and consisted of visual observation of the pipe color through view ports and hand logging of current, voltage, temperature at the four locations on the pipe, and elapsed time since start of test. For vacuum stations, the vacuum pressure was recorded also.

The pipes remained on test until failure was indicated, either by the appearance of oxides of lithium or sodium on view ports and other structures, or by a change in the temperature profile or color pattern of the pipe.

After a pipe failure and its removal from the station, any lithium or sodium oxide was cleaned off the internal structure and the inside of the chamber using isopropyl alcohol. On occasion a small puddle of lithium or sodium might be covered over with oxide. In this case, brief squirts of alcohol were impinged on the puddle to disturb the oxide and cause it to react with the fluid slowly.

34

SECTION IV
RESULTS

Although superalloy heat pipe testing continued through October 1981, the program was not actively pursued after June 1979 due to the loss of project leaders and a shift of technological emphasis of Lewis Research Center effort. Unfortunately, some of the test records, metallurgical specimens, and photos were lost or misplaced between 1979 and the writing of this report. However, the writers have attempted to reconstruct the results to the best of their ability from existing records, data logs, photos, the available heat pipes, and from memory. General conclusions on the merits of each material group will be presented.

PIPE PERFORMANCE

Since materials compatibility was the prime consideration at the outset of the program rather than pipe performance, the pipes were fitted with only four thermocouples. However, performance comparisons can be made between the sodium filled pipes and the lithium filled pipes and between those with screen wicks and those with metal fiber wicks from the temperature profiles.

Early in the program difficulty was experienced starting up the pipes. Therefore, each pipe was preheated on the bench as described earlier. Observation of the data shows that preheating made little or no noticeable difference on startup. Most of the pipes were operated at a favorable tilt. The evaporator end was 8 to 10 cm below the condenser end in an attempt to improve startup and temperature profile. A favorable tilt seemed to help some pipes slightly. A few sodium pipes with screen wicks, L-2, L-8, and S-1, performed as well at an adverse tilt of 5 to 10° as they did at a favorable tilt of the same amount. The sodium pipes with metal fiber wicks had to be operated

at a favorable tilt because of liquid flow resistance and variation of wick uniformity. Even a favorable tilt of up to 15° did not alter the profiles of the lithium filled pipes.

Figure 9 presents representative temperature profiles during startup of the sodium pipes. The profiles are plotted for several levels of increasing input power to the evaporator heater. The power numbers are only meant to illustrate relative values as no attempt was made to determine the actual heat transported down the pipes. The indicated temperatures at T_1, T_2, T_3, and T_4 are plotted and connected together with straight lines for convenience. Pipe temperatures between these points probably do not lie on the lines.

The profiles in Fig. 9(a) are from the data of a 304L stainless steel pipe (L-2) which had a screen wick of 200 mesh. The profiles in Fig. 9(b) are plotted from the data of Hastalloy B pipe HB-1, which had a metal fiber wick. A pipe was considered to be "started" and operating as a heat pipe when T_1-T_4 was less than 30 °C. For the sodium pipes the temperature indicated at T_1, 5 cm from the evaporator end cap, had to reach about 640 to 670 °C before the pipe started. Start up did not seem to be affected by the rate at which power was increased. For instance, if, when power was initiated, it was set immediately at a level which would rapidly bring T_1 to 800 °C when equilibrium was reached, the pipe would start when T_1 passed through about 640 °C. If on the other hand, power was initially set at a level which at equilibrium produced a temperature at T_1 of say 600 °C, T_1-T_4 would remain substantially greater than that of a started pipe. When power was then increased and T_1 reached about 640 °C the temperatures at T_3 and T_4 would suddenly increase to give a relatively flat started pipe profile. Further increases in power would result in a higher and higher profile until

36
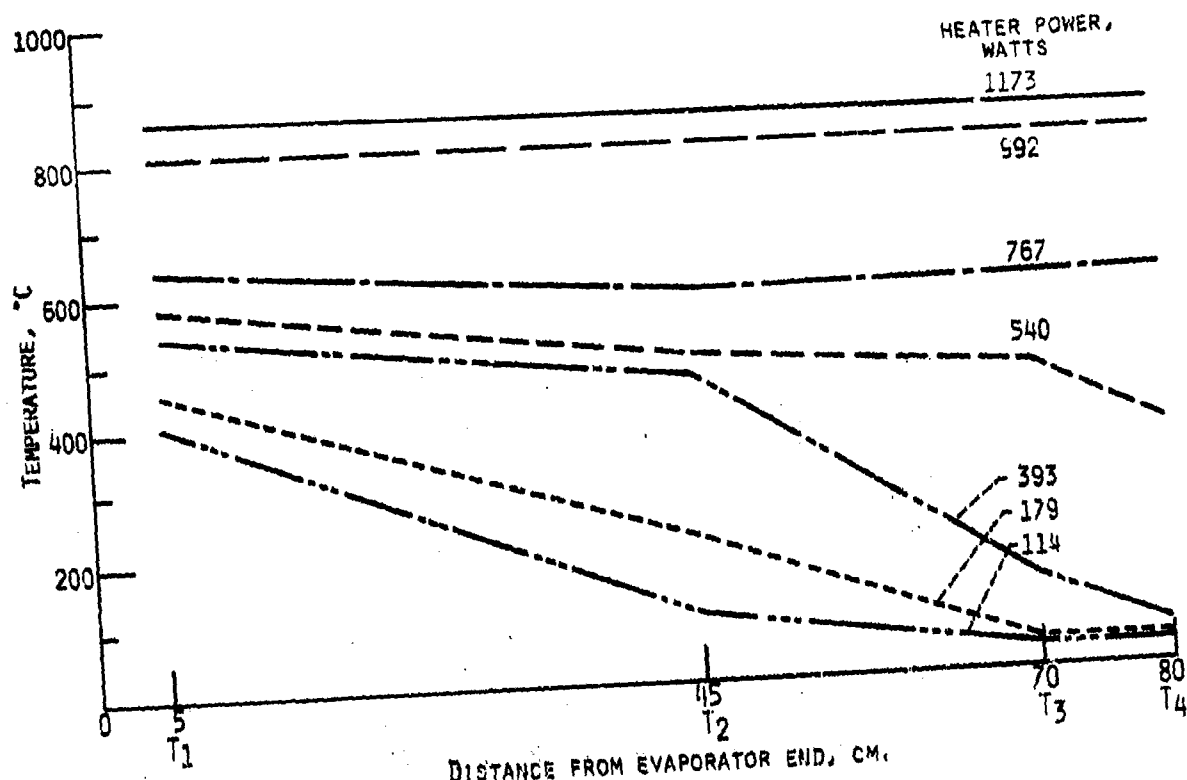
(A) SCREEN WICK - 304L, PIPE L-2.

FIGURE 9. - REPRESENTATIVE TEMPERATURE PROFILES DURING START-UP, SODIUM WORKING FLUID.
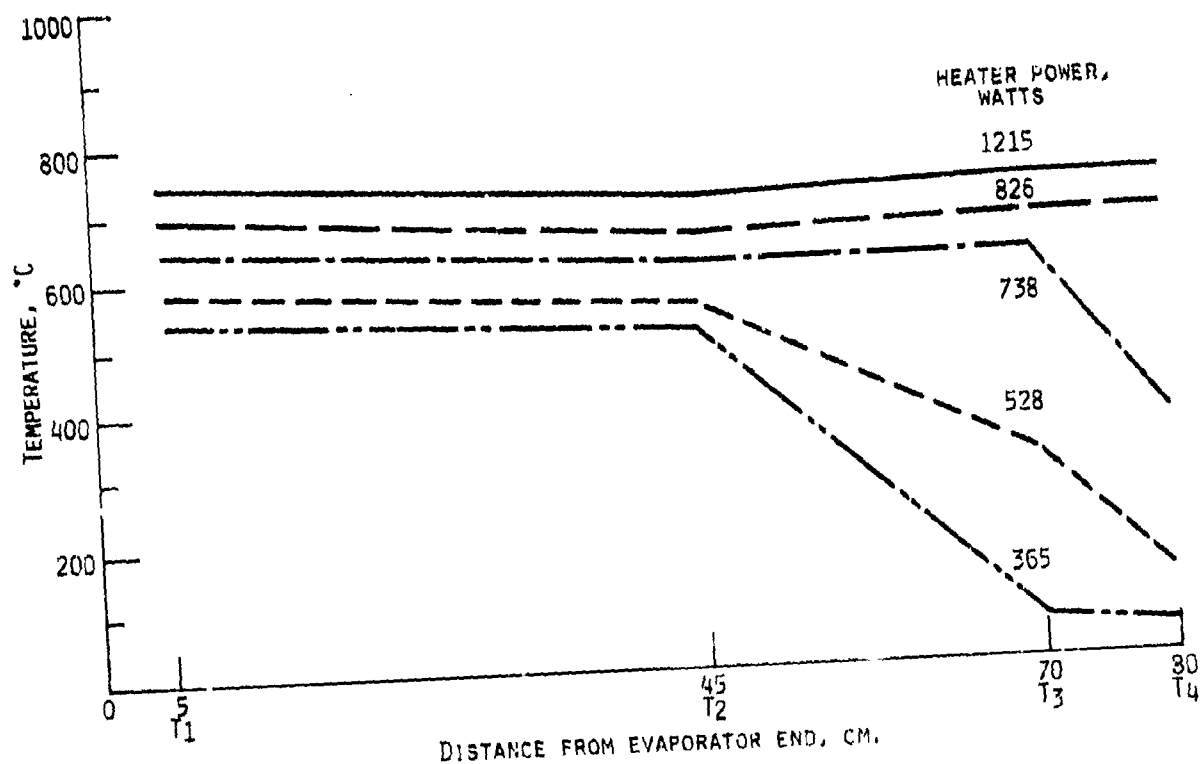
(B) METAL FIBER WICK, HASTALLOY B, PIPE HB-1.

FIGURE 9. - REPRESENTATIVE TEMPERATURE PROFILES DURING START-UP, SODIUM WORKING FLUID.

37

the target temperature at T_1 for the particular pipe material was reached.

Start up temperature profiles for two of the lithium pipes can be seen in Figs. 10(a) and (b). The profiles in Fig. 10(a) are for a 310S stainless steel pipe (S-7) which, like the sodium pipe of Fig. 9(a), had a screen wick. Similar profiles are observed for the Haynes 188 pipe (HA-4) plotted in Fig. 10(b). Pipe HA-4, like HB-1 of Fig. 9(b), had a metal fiber wick. These two profile plots, representing the best of those for lithium pipes, indicate that the pipes were operating poorly at the temperatures reached. If higher evaporator temperature had been achieved, flatter profiles might have been attained in the lithium pipes. A subsequent section, Analysis of Performance, deals with this matter further.

Sodium pipes started up and worked well with both metal fiber wicking and screen wicking; lithium pipes did not work well with either type of wick. It may be concluded, therefore, that the poor operation was due to the working fluid and not the type of wick.

The steady state temperature profiles on Figs. 11(a) through (e) show that all 14 pipes with sodium as the working fluid did function. Those with screen wicks of 200 mesh (L-2 and L-3) and 100 mesh (L-8) (Fig. 11(a)), seemed to provide a slightly flatter profile and were more consistent than those having 60 mesh screen wicks (S-1 to S-3) (Fig. 11(b)). All the pipes having screen wicks appeared to perform better than those with metal fiber wicks (Figs. 11(c) to (e)). Pipe HA-8 (Fig. 11(d)), appears to represent a case of a damaged or improperly installed wick.

Steady state profiles along lithium pipes are shown in Fig. 12. Those for 310S stainless steel pipes, S-7, S-8, and S-9 which had 60 mesh screen wicks are essentially the same as those for the pipes with metal fiber wicks. Since the pipes were heated along the 30.5 cm long
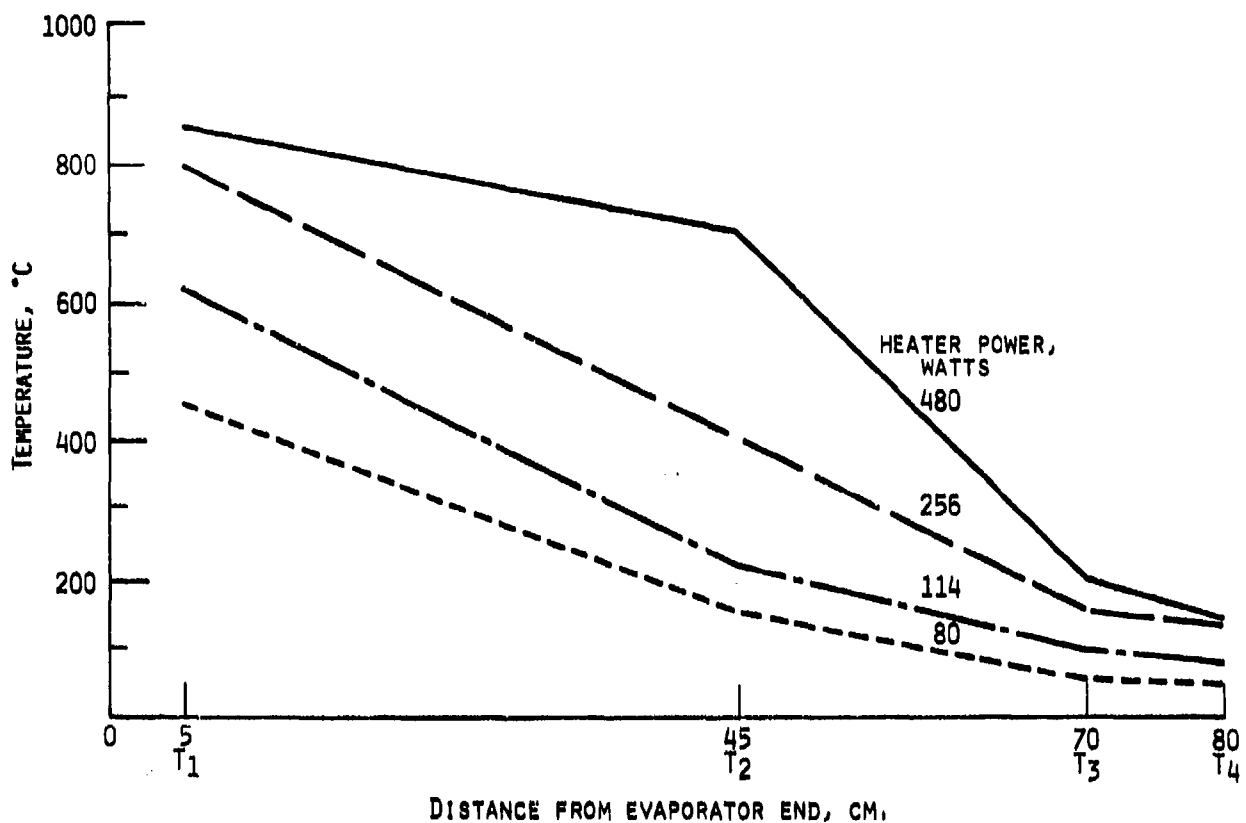
(A) SCREEN WICK, 310S, S-7.

FIGURE 10. - REPRESENTATIVE TEMPERATURE PROFILES DURING START-UP, LITHIUM WORKING FLUID.
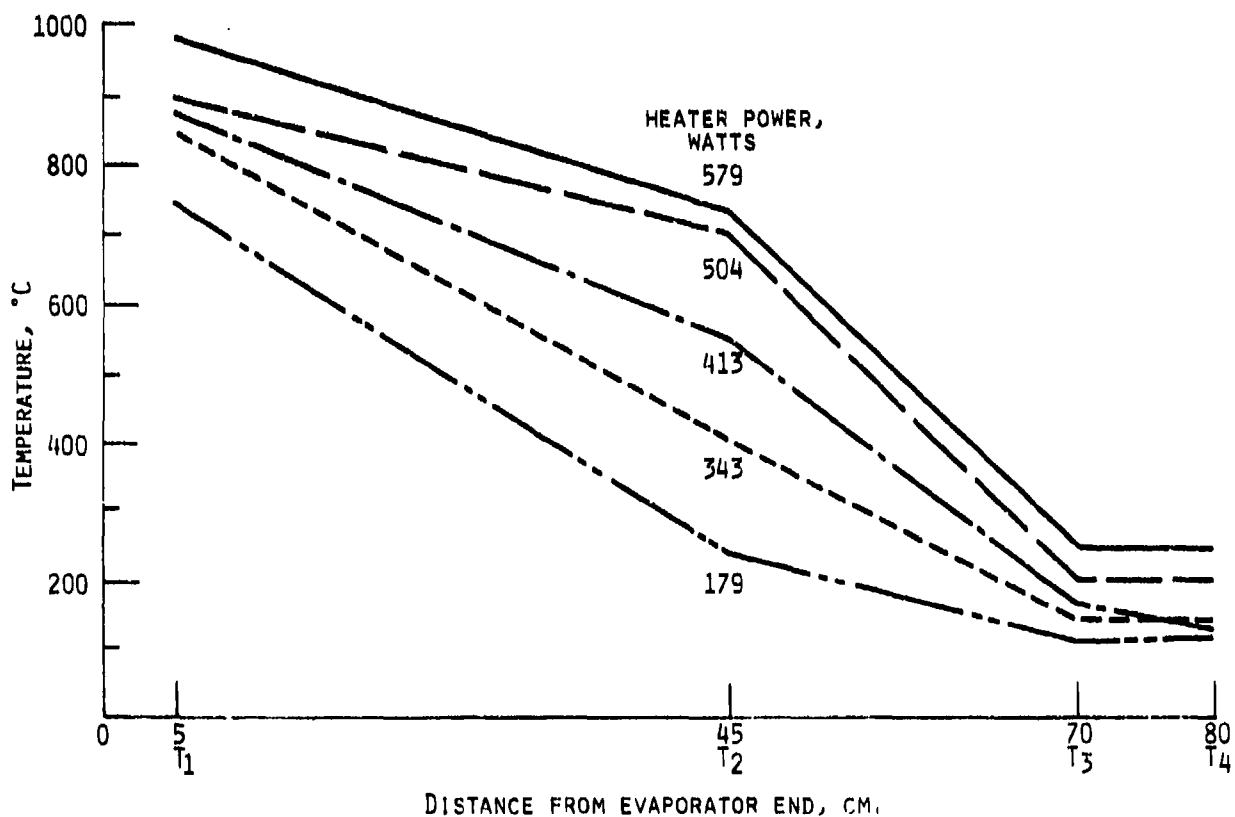
(B) METAL FIBER WICK, HAYNES 188, HA-4.

FIGURE 10. - REPRESENTATIVE TEMPERATURE PROFILES DURING START-UP, LITHIUM WORKING FLUID.

DISTANCE FROM EVAPORATOR END, CM.
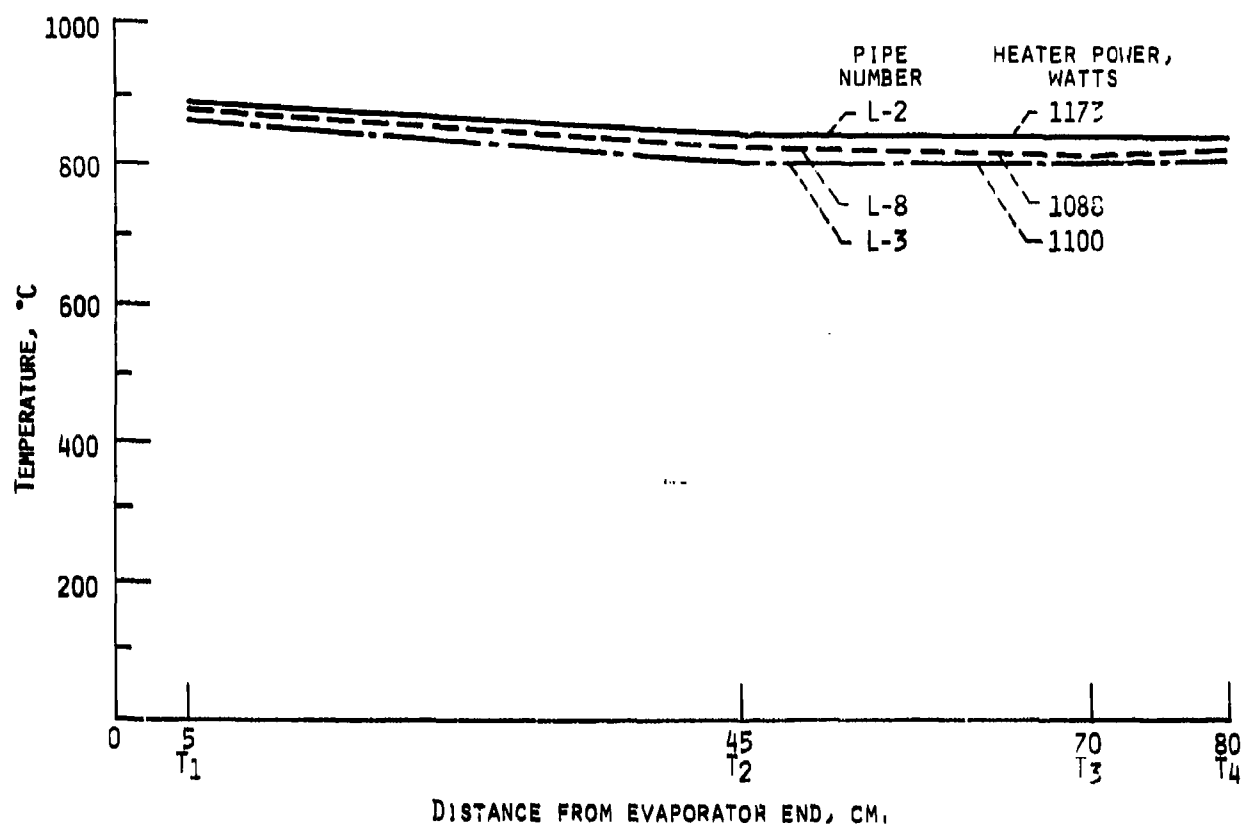
(A) SCREEN WICKS, 304L PIPES.

FIGURE 11. - TYPICAL STEADY-STATE TEMPERATURE PROFILES FOR SODIUM FILLED PIPES.

DISTANCE FROM EVAPORATOR END, CM.
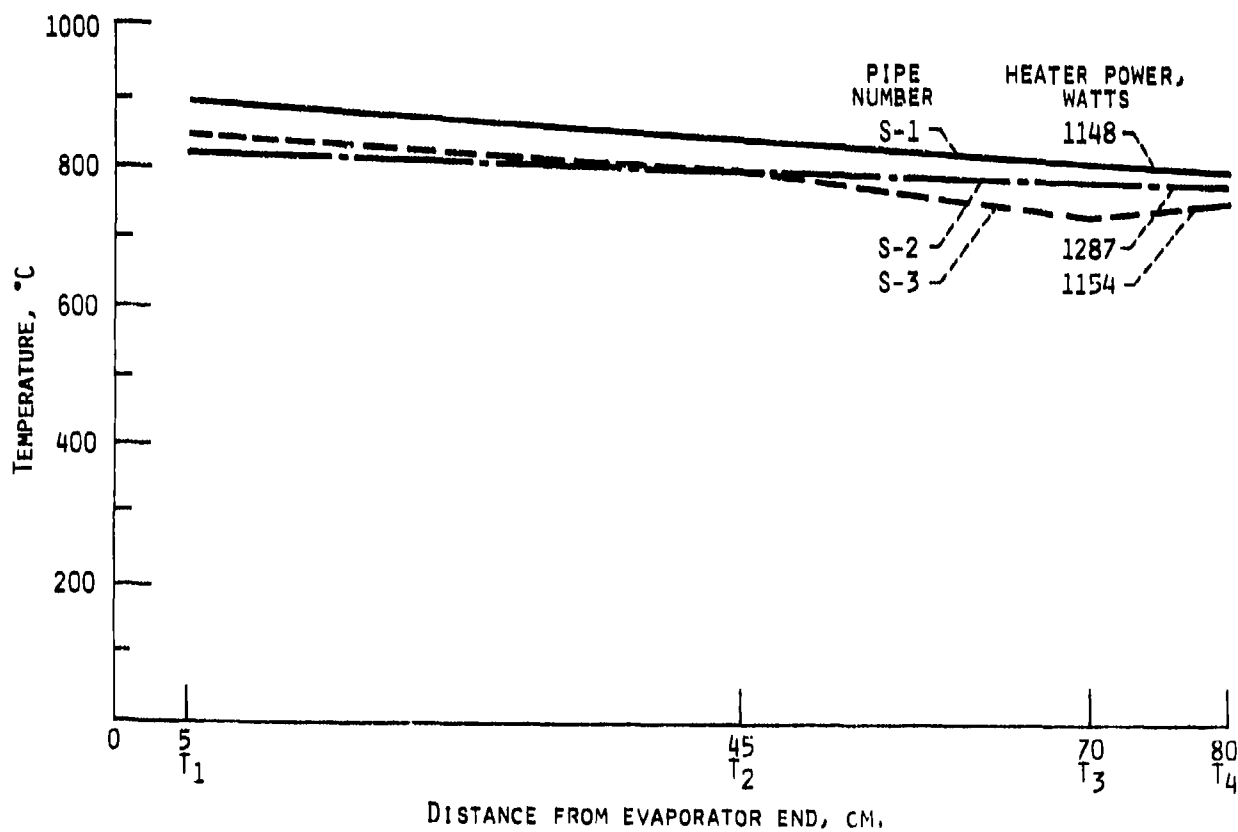
(B) SCREEN WICKS, 310S PIPES.

FIGURE 11. - TYPICAL STEADY-STATE TEMPERATURE PROFILES FOR SODIUM FILLED PIPES.
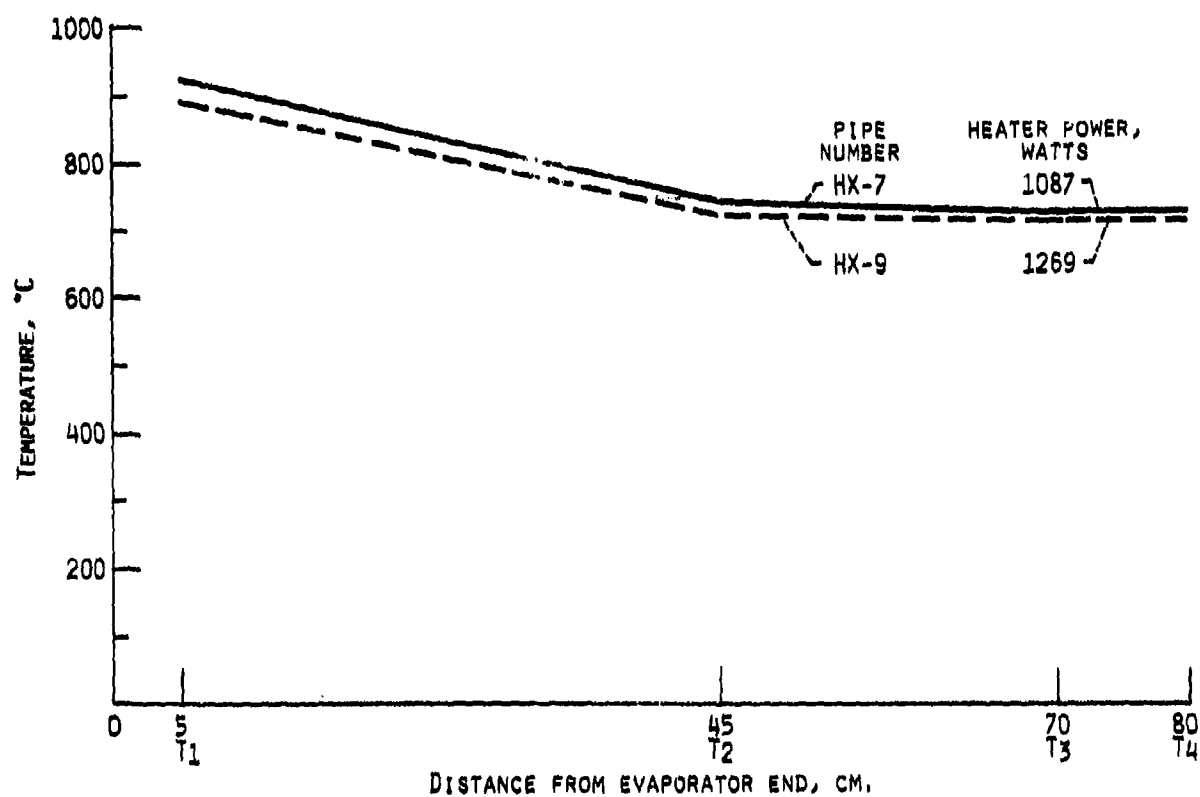
(C) METAL FIBER WICKS, HASTALLOY X PIPES,

FIGURE 11, - TYPICAL STEADY-STATE TEMPERATURE PROFILES FOR SODIUM-FILLED PIPES,

41
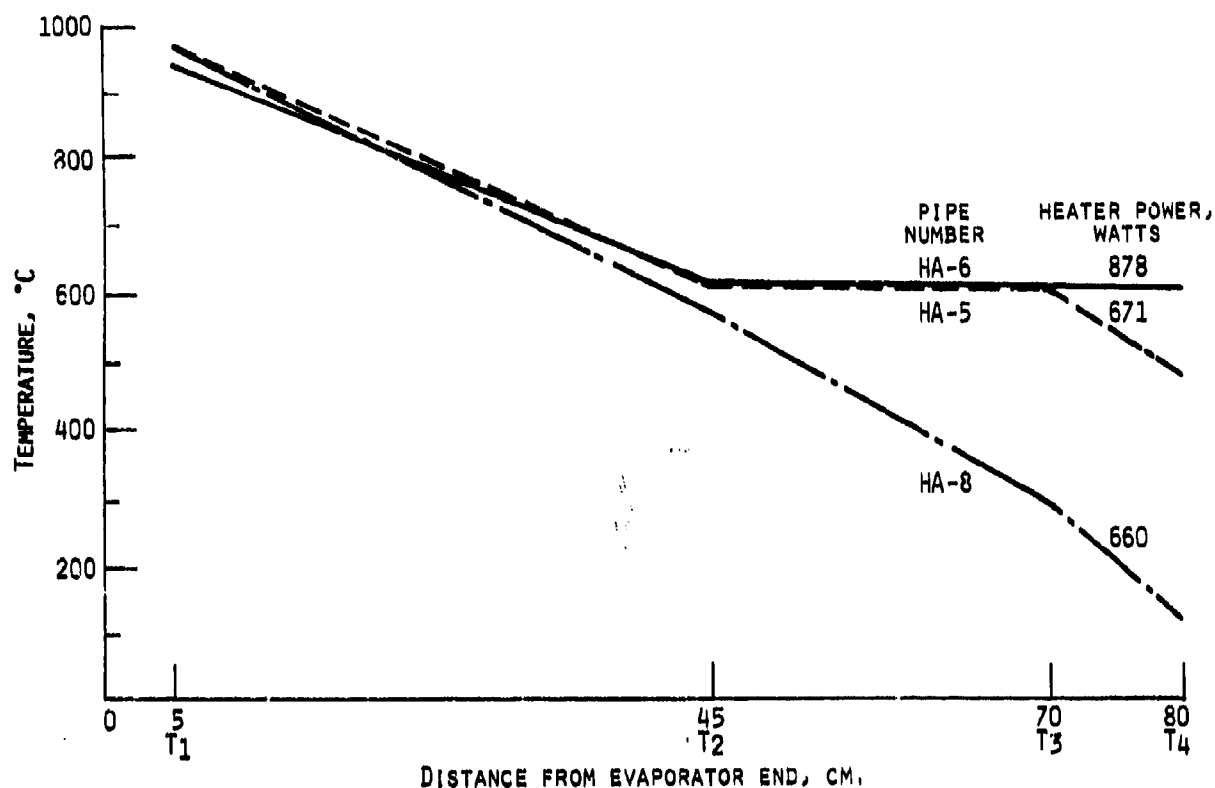
(D) METAL FIBER WICKS, HAYNES 188 PIPES.

FIGURE 11. - TYPICAL STEADY-STATE TEMPERATURE PROFILES FOR SODIUM-FILLED PIPES.
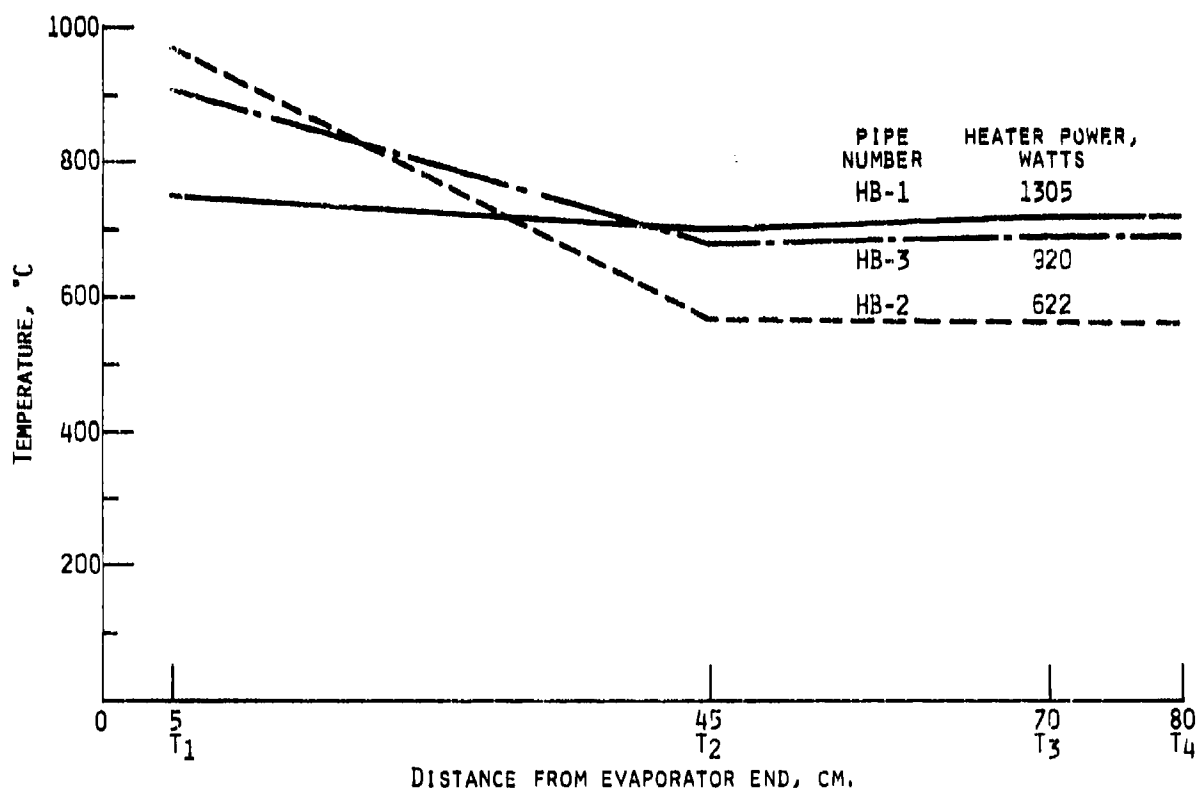
(E) METAL FIBER WICKS, HASTALLOY B PIPES.

FIGURE 11. - TYPICAL STEADY-STATE TEMPERATURE PROFILES FOR SODIUM-FILLED PIPES.
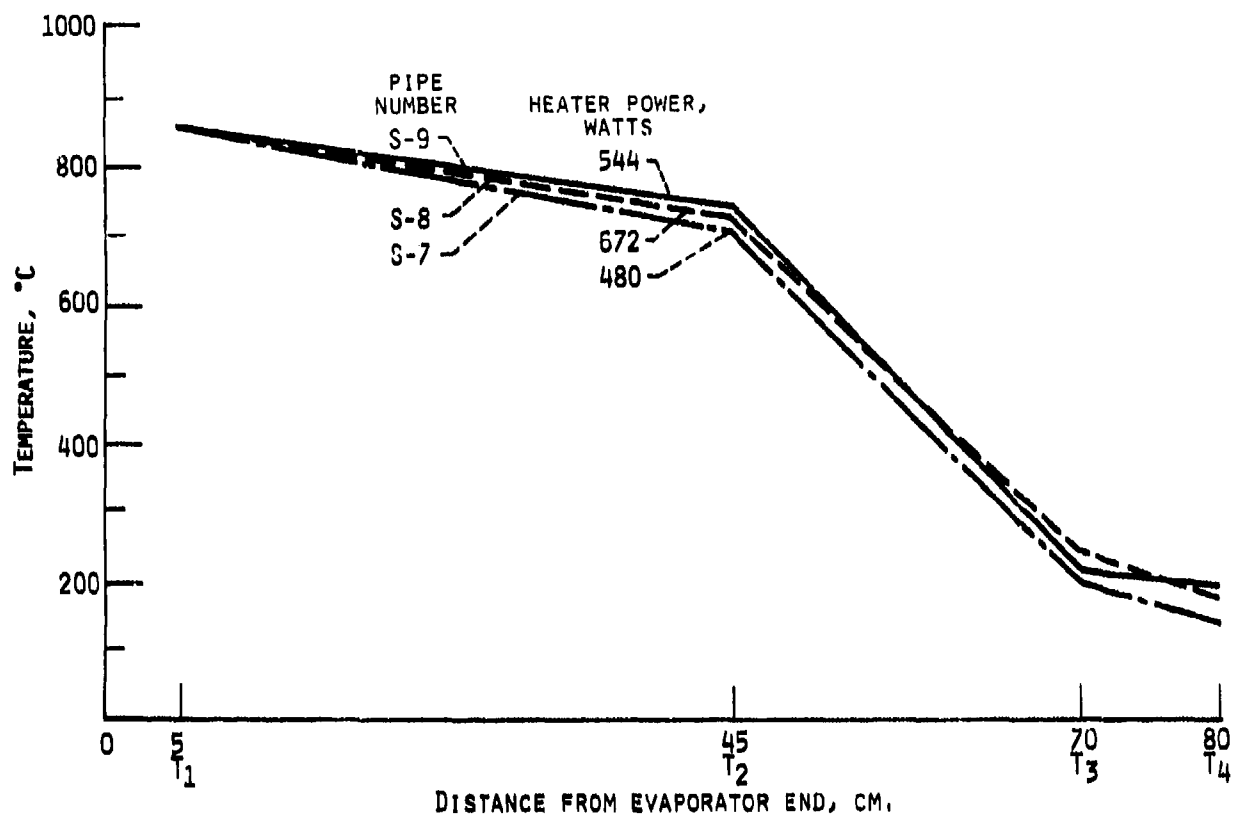
(A) SCREEN WICK, 310S PIPES.

FIGURE 12. - TYPICAL STEADY-STATE TEMPERATURE PROFILES FOR LITHIUM-FILLED PIPES.
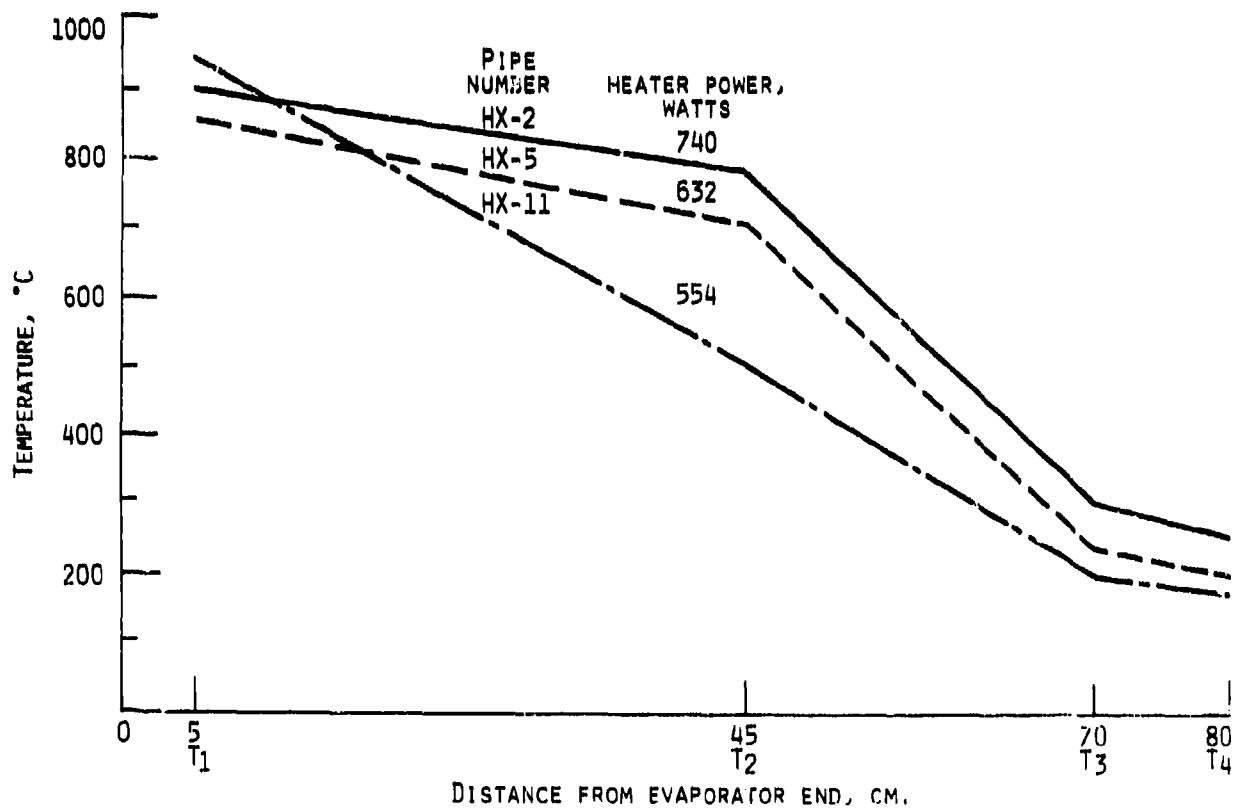
(B) METAL FIBER WICKS, HASTALLOY X PIPES.

FIGURE 12. - TYPICAL STEADY-STATE TEMPERATURE PROFILES FOR LITHIUM-FILLED PIPES.

43
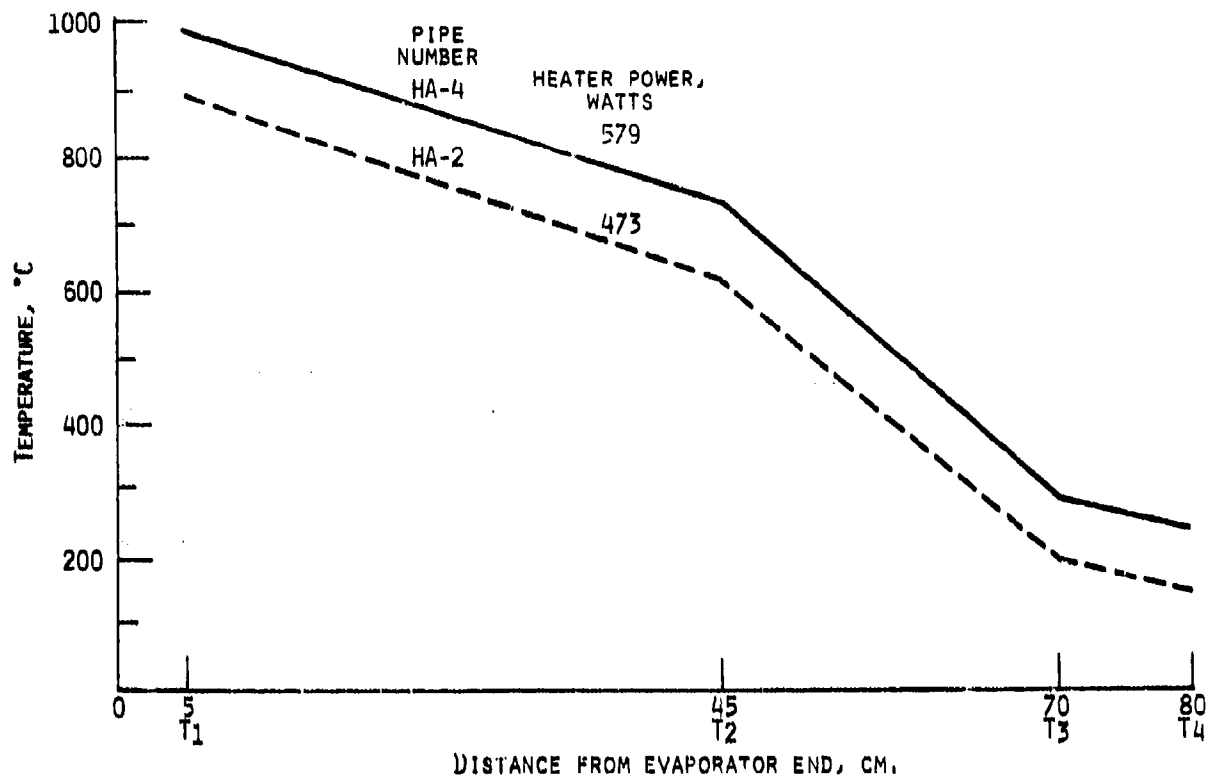
(C) METAL FIBER WICKS, HAYNES 188 PIPES.

FIGURE 12. - TYPICAL STEADY-STATE TEMPERATURE PROFILES FOR LITHIUM-FILLED PIPES.
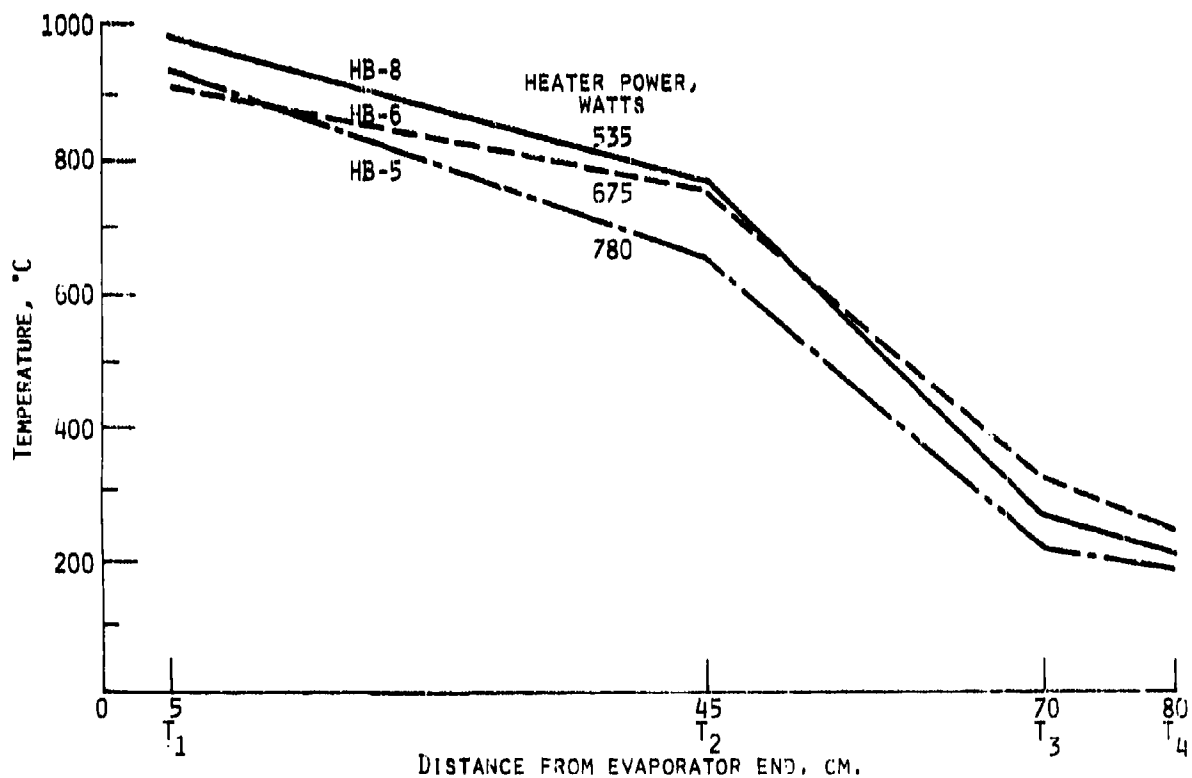
(D) METAL FIBER WICKS, HASTALLOY B PIPES.

FIGURE 12. - TYPICAL STEADY-STATE TEMPERATURE PROFILES FOR LITHIUM-FILLED PIPES.

44

evaporator, one might expect the indicated temperature at T_2 to be due to heat conduction down the pipe walls. However, in Section V evidence is presented to indicate that the observed performance is possibly all that might have been attainable at the temperatures reached.

COMPATIBILITY

The intended application for the sodium pipes was to be for low temperature thermionic topping cycles in terrestrial power plants. Therefore, the external oxidation/corrosion rate in air was investigated in addition to the internal corrosion rate of the working fluid. All but three of the sodium pipes were tested in an air environment.

The intended application for the lithium pipes was in low power thermionic space systems. Therefore, the lithium pipes were tested in a vacuum environment. Thus the evaporation rate of the constituents of the pipe materials could be studied at the same time as the internal corrosion rate of lithium on the materials. No pipes constructed of 304L stainless were filled with lithium because the literature already indicated poor compatibility with this combination. However, three sodium 304L pipes were included with the vacuum group.

Air Environment

A brief summary of the pipes tested in air is given in Table 3. Four pipes are listed with the 304L group because two of them were used for testing evaporator heaters for the air tests in a prototype facility and were inadvertently destroyed. One of the Hastalloy X pipes, HX-8, was returned to the manufacturer unused to have the metal fiber wick replaced with a screen wick and the pipe filled with lithium. The program was terminated before HX-8 could be returned and put on test.

45

TABLE 3

AIR ENVIRONMENT RESULTS

Material-pipe number	Test time, hr	Maximum temperature, °C	Cause of failure
304L			
L-1	0	----	Destroyed in prototype heater tests
L-2	2,100	880	External corrosion of evaporator wall
L-7	0	----	Destroyed in prototype heater tests
L-8	4,070	900	External corrosion of evaporator wall
310S			
S-1	25,417	885	No failure
S-2	1,492	925	External corrosion due to heater overtemp.
S-3	16,874	880	No failure
Hastalloy X			
HX-7	29,657	1000	No failure
HX-8	------	----	Returned to manufacturer for screen wick
HX-9	11,557	925	No failure
Haynes 188			
HA-5	22,574	920	No failure
HA-6	2,324	990	Crack in evaporator wall
HA-8	15,982	965	No failure apparent - pipe never pumped
Hastalloy B			
HB-1	1,186	1000	External corrosion at evaporator end weld
HB-2	14,445	1020	No failure
HB-3	547	910	External corrosion at evaporator end weld

46

The test times listed are total hours of operation and were not necessarily continuous. Shutdowns due to power interruption, over-temperature, heater failure, thermocouple failure, etc., were inevitable over the long tests. The maximum temperatures listed were those indicated by thermocouple no. 1 (T_1) over at least a 24 hr period.

The evaporator sections of ten of the fourteen pipes tested in air are shown in Fig. 13. Pipe S-2 of the 310S group, pipe HA-8 of the Haynes 188 group, and pipe HB-2 of the Hastalloy B group were lost or misplaced between removal from the test stands and this writing, making further inspection of these three pipes impossible.

The oxidation of the surface varied with the material involved. For instance, heavy external oxidation was evident on both 304L pipes. Between 5 and 25 cm from the evaporator end the wall thickness of each was reduced considerably. The wall of pipe L-2 became so thin a crack or hole developed that may have allowed sodium to escape rapidly. The evaporator heater failed at the same time, indicating the escaping sodium may have ignited forming a hot torch for a short period. A thick, porous, metallic deposit coated the first 13 cm of the evaporator. X-ray diffraction analysis showed the deposit material to be iron oxide. Iron is the largest constituent of 304L stainless steel.

Oxidation also caused a leak in pipe L-8 about 13 cm from the evaporator end. The wall thickness in this area was reduced from 0.2 cm to about 0.08 cm. The leak rate was probably slower than that of L-2 so that sodium vapor oxidized as it escaped and condensed on cooler surfaces.

The extent of external oxidation can be seen more clearly in Fig. 14. Figure 14(a) presents a cross section of the evaporator at the location of thermocouple no. 1, 5 cm from the evaporator end along with a cross section at about 3.8 cm from the condenser end. Figure 14(b) shows

47

L-2 | L-8 | S-1 | S-3 | HX-7 | HX-9 | HA-5 | HA-6 | HB-1 | HB-3
3041 | | | 310S | | HASTALLOY X | | HAYNES 188 | | HASTALLOY B

48
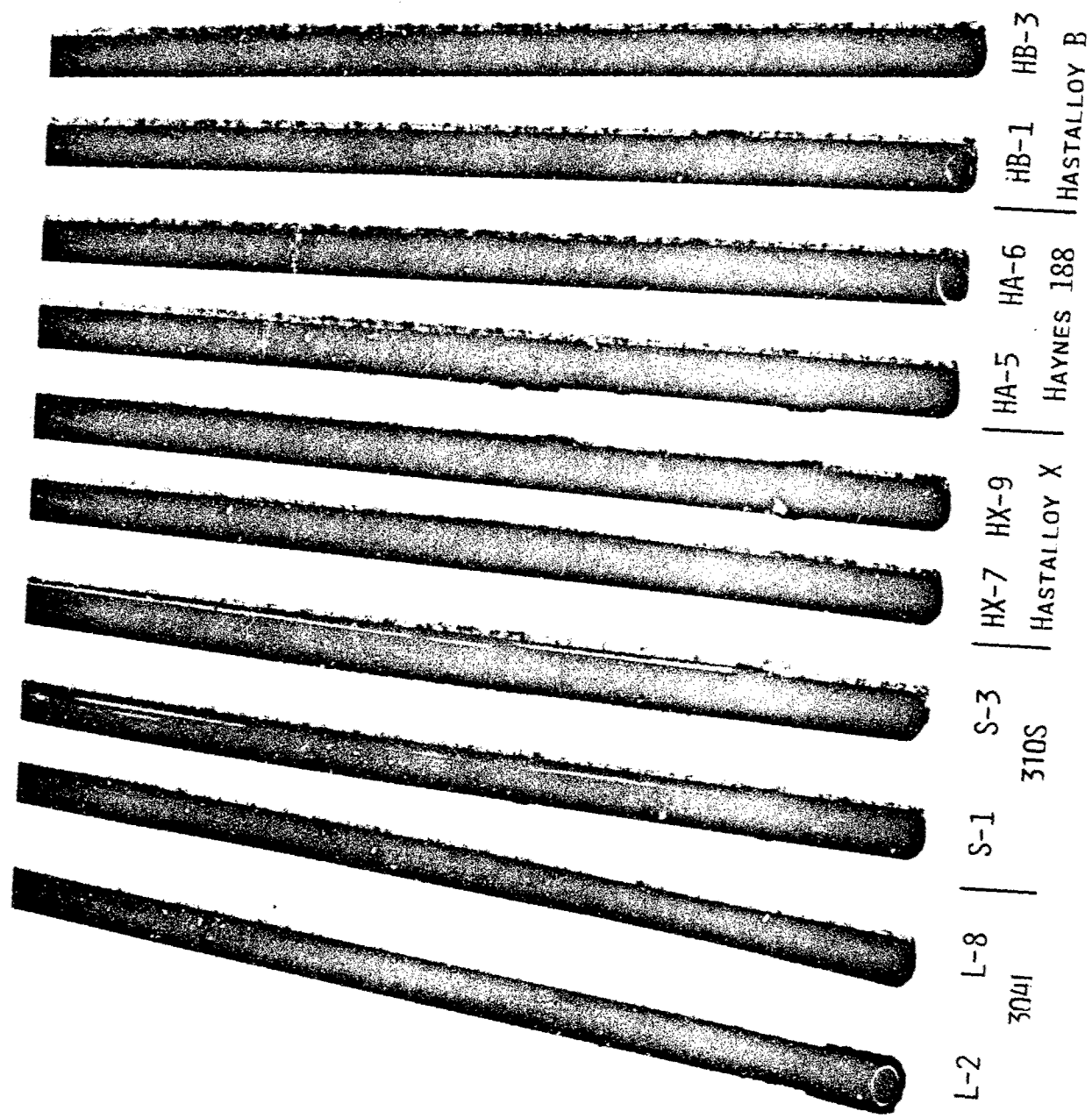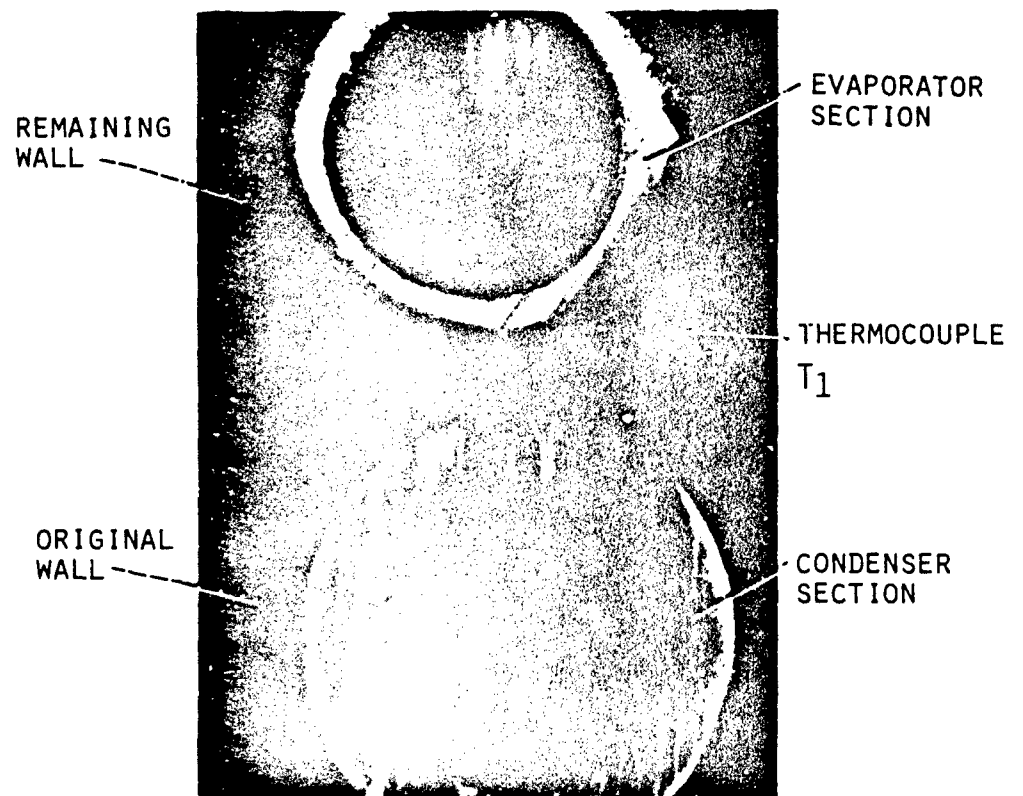
(A) COMPARISON OF EVAPORATOR AND CONDENSER CROSS-SECTIONS OF PIPE L-2.
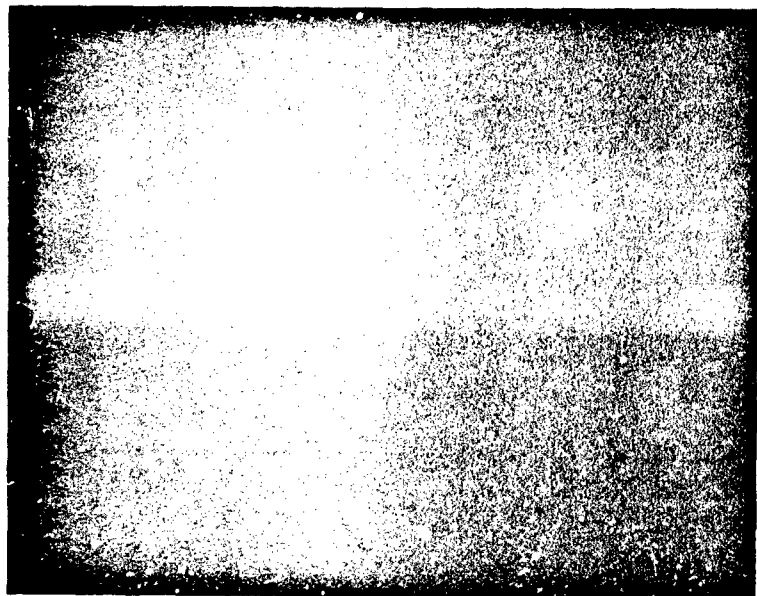
(B) EXTERNAL COATING AND SCALING, EVAPORATOR END, PIPE L-2.

FIGURE 14. - EXTERNAL/INTERNAL CORROSION IN STAINLESS STEEL 304L PIPES.

the thick deposit on the evaporator end. The temperature recorded by T_1 ran as high as 800 to 830 °C while that near the cut through the condenser registered only about 40° less, hardly enough difference to cause such a great disparity in external oxidation. Further, examination of a cross section taken near the downstream end of the evaporator showed the wall thickness to be nearly the same as that in the condenser. From an enlargement of Fig. 14(a) measurements were made of the original wall thickness of the condenser section and the expanded wall thickness and remaining wall thickness of the evaporator section. Calculations using these measurements show that probably all the iron is accounted for between what remains in the inner wall of the evaporator and that combined with oxygen to form the iron oxide of the outer wall. In other words, nothing has left the pipe and nothing has been deposited on it from the evaporator heater.

The surface of the adiabatic and condenser sections of both L-2 and L-8 had only a thin black coating. The hypothesis might be made from these observations that the evaporator oxidation resulted from radiative heating. The heating elements operated at a very high temperature to maintain the heat pipe evaporator at 800 °C. Molecular oxygen in contact with the hot heater elements may have partially dissociated into atomic oxygen. Atomic oxygen would be more reactive with the iron constituent of the pipes. The pipe surfaces outside the heater would come in contact with molecular oxygen only and, therefore, be subjected to less serious oxidation.

Figure 14(c) shows a longitudinal section of the evaporator end of pipe L-2. The necking-down of the screen and tube on the right was caused by a tubing cutter. The light colored area adjacent to the internal surface is due to light reflection during photography. There was no evidence of sodium attack on either wick or pipe surfaces
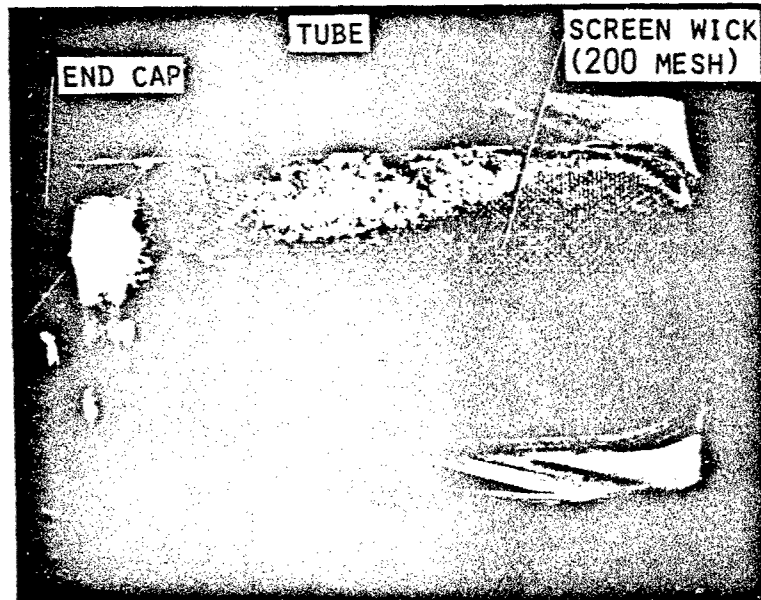
(c) LONGITUDINAL SECTION OF EVAPORATOR END OF 304L PIPE L-2.

FIGURE 14. – EXTERNAL/INTERNAL CORROSION IN STAINLESS STEEL 304 PIPE.

The next two pipes in Fig. 13 are 310S stainless steel. A thin black film covered most of pipe S-1 with some slight roughness of the external surface of the evaporator section. Pipe S-3 had no coating on the adiabatic or the condenser sections but the surface of the evaporator was spattered with small, hard particles about a millimeter in diameter. It is noteworthy that the small amount of oxidation on these pipes occurred over a period of 25,000 and 15,000 hr, respectively, at temperatures to 880 °C.

The absence of attack by the working fluid, sodium, on internal surfaces of pipe S-1 is evident in the longitudinal section of the evaporator end, Fig. 15. This was typical of 310S pipes with sodium. No failure occurred in S-1 or S-3. Both were shut down when testing was terminated in November 1981. Pipe S-2, Table 2, failed due to over-temperature of the evaporator when the heater failed to shut down and not by external oxidation or sodium corrosion.

The next two pipes in Fig. 13 are Hastalloy X pipes HX-7 and HX-9. Neither had failed when the facilities were shut down. Both pipes had a very thin, smooth, black coating over the entire length. There was very little roughness on the evaporator surface.

A longitudinal section and a cross section of the evaporator end of HX-7 is pictured in Fig. 16. The metal fiber wick in this end of the pipe did not have a cylindrical shape. Adverse temperature profile changes indicate that deformation of the wick may have begun around 7500 hr into the test. However, the deformation could have occurred during manufacture. Observation of Fig. 16 will show that typically, sodium had no effect on internal surfaces of Hastalloy X pipes.

The two Haynes 188 pipes, HA-5 and HA-6 exhibited strong resistance to oxidation. As seen in Fig. 13, both had a very thin, hard, smooth, black film over the entire
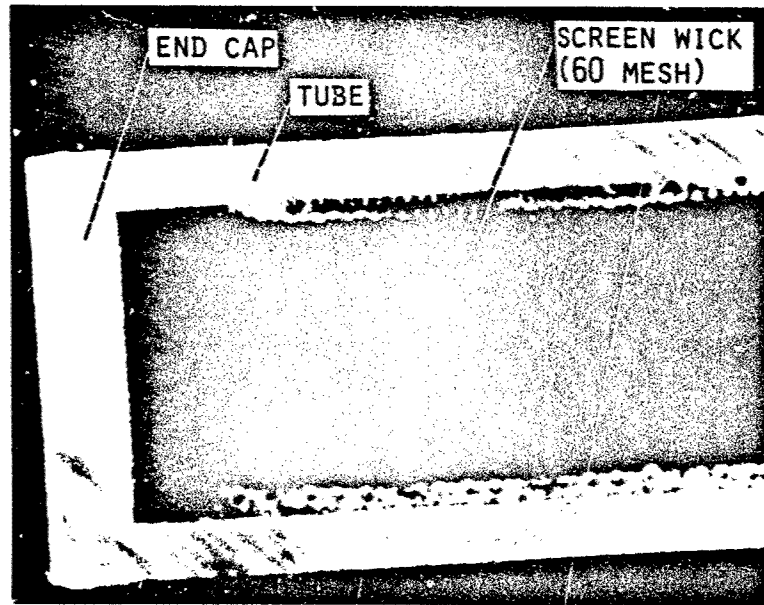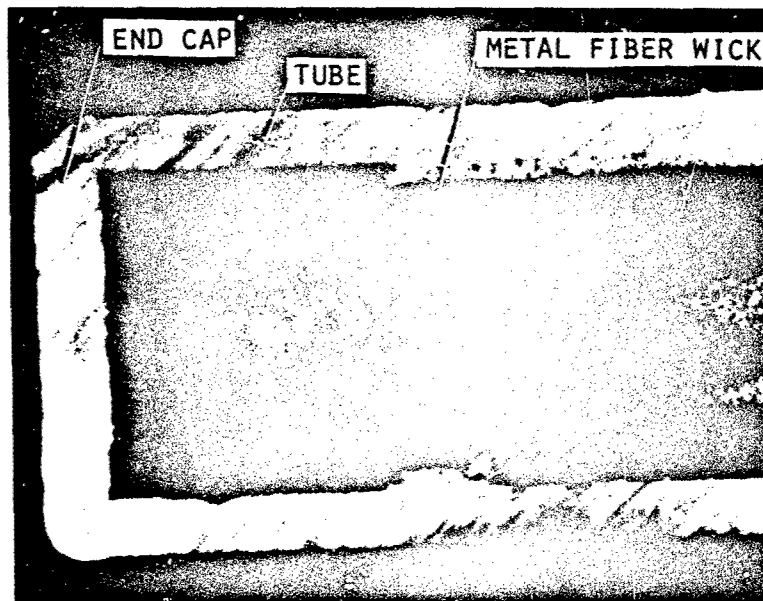
52

FIGURE 15. - LONGITUDINAL SECTION OF EVAPORATOR END OF 310S STAINLESS STEEL PIPE S-1.

(A) LONGITUDINAL SECTION.
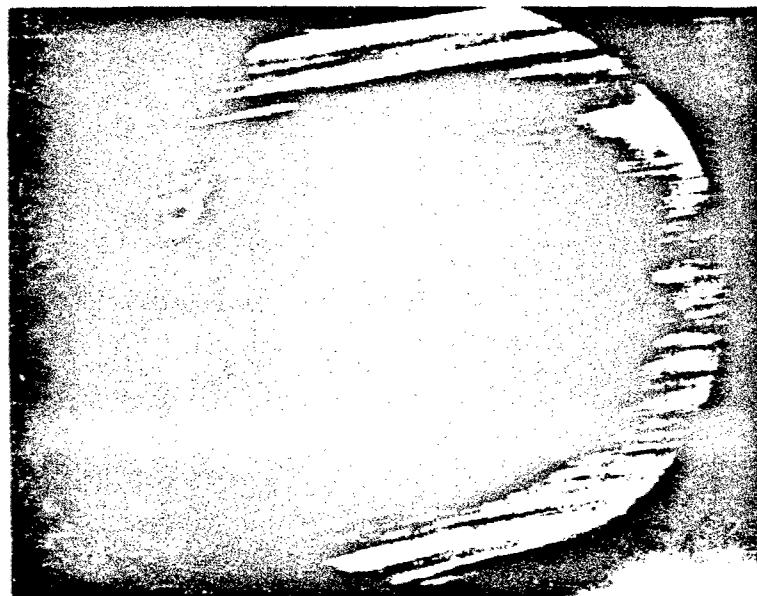
(B) CROSS SECTION.

FIGURE 16. - SECTIONS OF EVAPORATOR END OF
HASTALLOY PIPE HX-7.

external surface. There were no deposits or bumps and no erosion or roughness on the evaporator sections.

A longitudinal section of the end of the evaporator or HA-6 can be seen in Fig. 17. The photo clearly shows no evidence of sodium attack on the internal surfaces of the tube nor on the metallic fiber wick. The dark color of the bottom section of the tube is due to polishing and lighting effects.

Pipe HA-6 was the only sodium filled Haynes 188 pipe to fail. Failure was obvious from the soft white sodium oxide deposits on cool surfaces inside the test housing such as view ports and cooling water supply tubes. Cracks in the tube wall near the evaporator end were suspected of causing the leakage of working fluid, but the exact location was not definitely determined. One suspicious area is shown in Fig. 18. Cracks just above and below the dark area may extend to the inner surface of the pipe. The small diameter white tube along the top of the pipe is the alumina tube carrying the thermocouple wires to T_1. T_1 is located under the shield to the left. Unfortunately, the loss of the pieces cut from the pipe in the area of the cracks for metallurgical examination precludes further observation at this writing.

Two of the three Hastalloy B pipes operated in an air environment, HB-1 and HB-3, are shown in Fig. 13. These pipes operated for 1186 and 547 hr, respectively. The adiabatic and condenser sections of both had a thin, smooth, hard, black film on the surface. The evaporator surface area of HB-1 was roughened slightly, but the first 21.6 cm of HB-3 were deeply pitted and the diameter was reduced somewhat along the first half.

Figure 19(a) shows the end of the evaporator of HB-1 as removed from the test station. A knob of rough material covered the end except for a hole through the pipe. This material was probably sodium oxide since it was washed away with cooling water when the end pictured in

55

FIGURE 17. - LONGITUDINAL SECTION OF EVAPOR-
ATOR END OF HAYNES 188 PIPE HA-6.

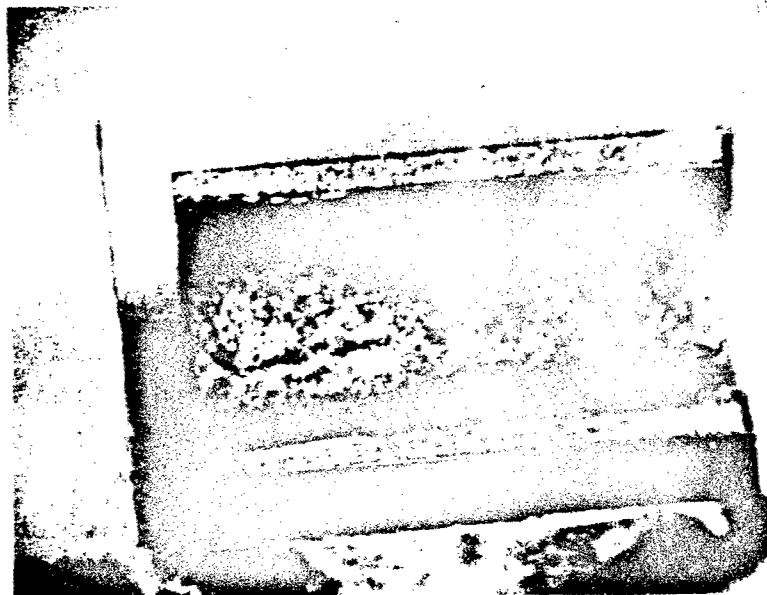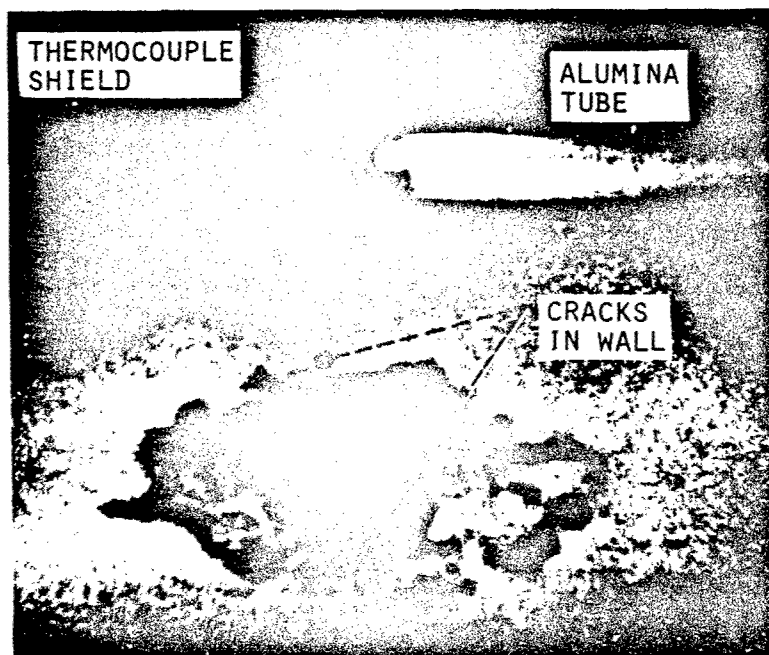FIGURE 18. - SUSPECTED FAILURE AREA IN HAYNES
188 PIPE HA-6.
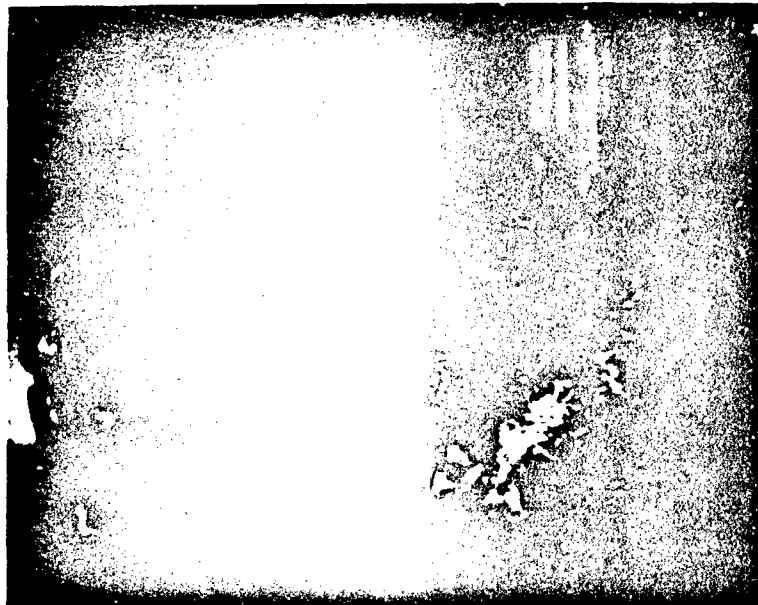
(A) External sodium oxide deposit around hole.

(B) Cut end sample with deposit removed.

Figure 19. - Failure area in Hastalloy B pipe HB-1.

Fig. 19(b) was being cut from the pipe with an abrasive wheel. With the pipe tilted evaporator end down during testing, a puddle of sodium could exist on the bottom at the end. Since there was little or no sodium attack of the internal surfaces as evident in Fig. 20, the hole probably was not initiated from the inside. Considering the nature of the hole formed and the large knob of sodium oxide covering the end, one might theorize that after an initial crack or hole caused by external oxidation, a torch was formed and burned out the observed hole. However, the orientation of the pipe in the test facility is unknown.

A cross section of the pipe and wick at the T_1 location is shown in Fig. 20(b). Again, no pronounced effect of sodium on the Hastalloy B materials can be seen.

No reason for removing pipe HB-2 from the test station was recorded. However, poor temperature profile and loss of a thermocouple may have been responsible. The data show that the pipe performance (temperature profile) deteriorated after the pipe was removed for replacement of a thermocouple at about 2900 test hr. The recorded notes do not show failure of the pipe and, as mentioned earlier, HB-2 is not available for further observation.

Pipe HB-3 failed in the same place as HB-1 except that the hole formed was not so large.

Vacuum Environment

Total test hours, maximum temperatures experienced, and causes of failure for the fourteen pipes tested in a vacuum environment are summarized in Table 4. As can be seen in Fig. 21, the evaporator ends are free of external oxidation, but some discoloration appears due to vapor transport from hotter components of the heater.

Neither of the 304L pipes, L-3 or L-9, failed in 29,000 and 23,000 hr, respectively. As mentioned earlier they were sodium. Results in air environment showed failure was due to external oxidation. The vacuum environment

58

TABLE 4

VACUUM ENVIRONMENT RESULTS

Material-pipe number	Test time, hr	Maximum temperature, °C	Cause of failure
304L			
L-3	29,187	890	No failure
L-9	23,505	910	No failure
310S			
S-7	1,155	860	Cracks at end cap weld
S-8	1,225	860	Crack through end cap
S-9	[a]28,450	900	Circumferential crack near downstream end evaporator
Hastalloy X			
HX-2	443	910	Lithium attack of wick, evaporator blockage
HX-5	754	940	Lithium attack of wick, cracks at end cap weld
HX-11	1,145	960	Lithium attack of wick, evaporator blockage
Haynes 188			
HA-1	97	[b]980	Radial cracks adjacent to seam weld
HA-2	273	840	Cracks in end cap weld and seam weld
HA-4	27,286	985	Failure not apparent
Hastalloy B			
HB-5	606	960	Severe lithium attack of wick and end cap
HB-6	552	970	Severe lithium attack of wick and end cap
HB-8	435	[b]980	Severe lithium attack of wick, end cap and wall

[a] - total hours at test temperature, time of failure not known
[b] - estimated temperature

59
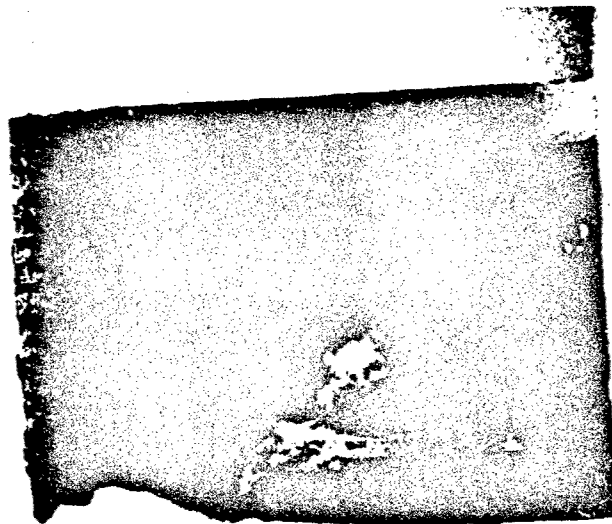
(A) CROSS SECTION OF EVAPORATOR TIP.

SEAM WELD

METAL FIBER WICK

THERMOCOUPLE T_1
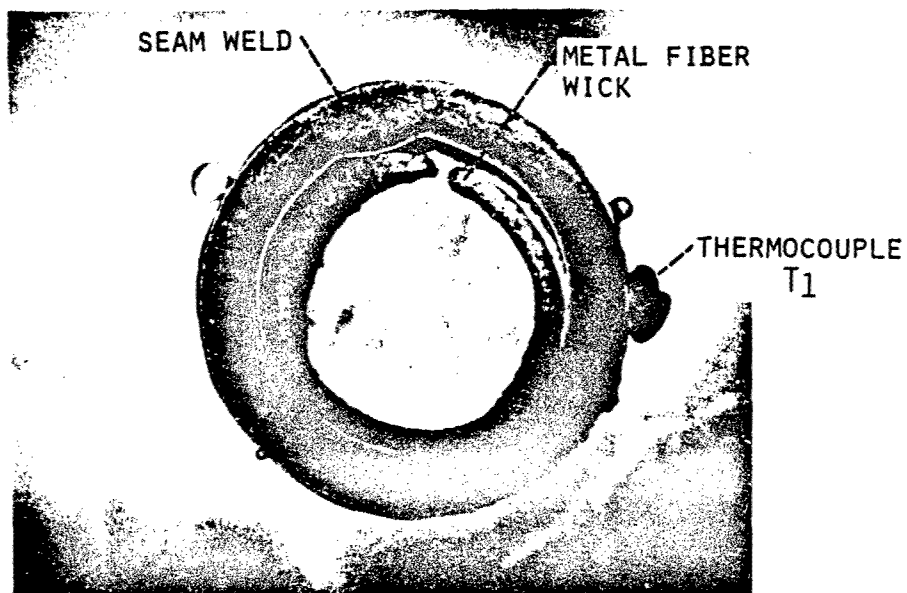
(B) CROSS SECTION AT T_1.

FIGURE 20. – SECTIONS OF HASTALLOY B PIPE HB-1.
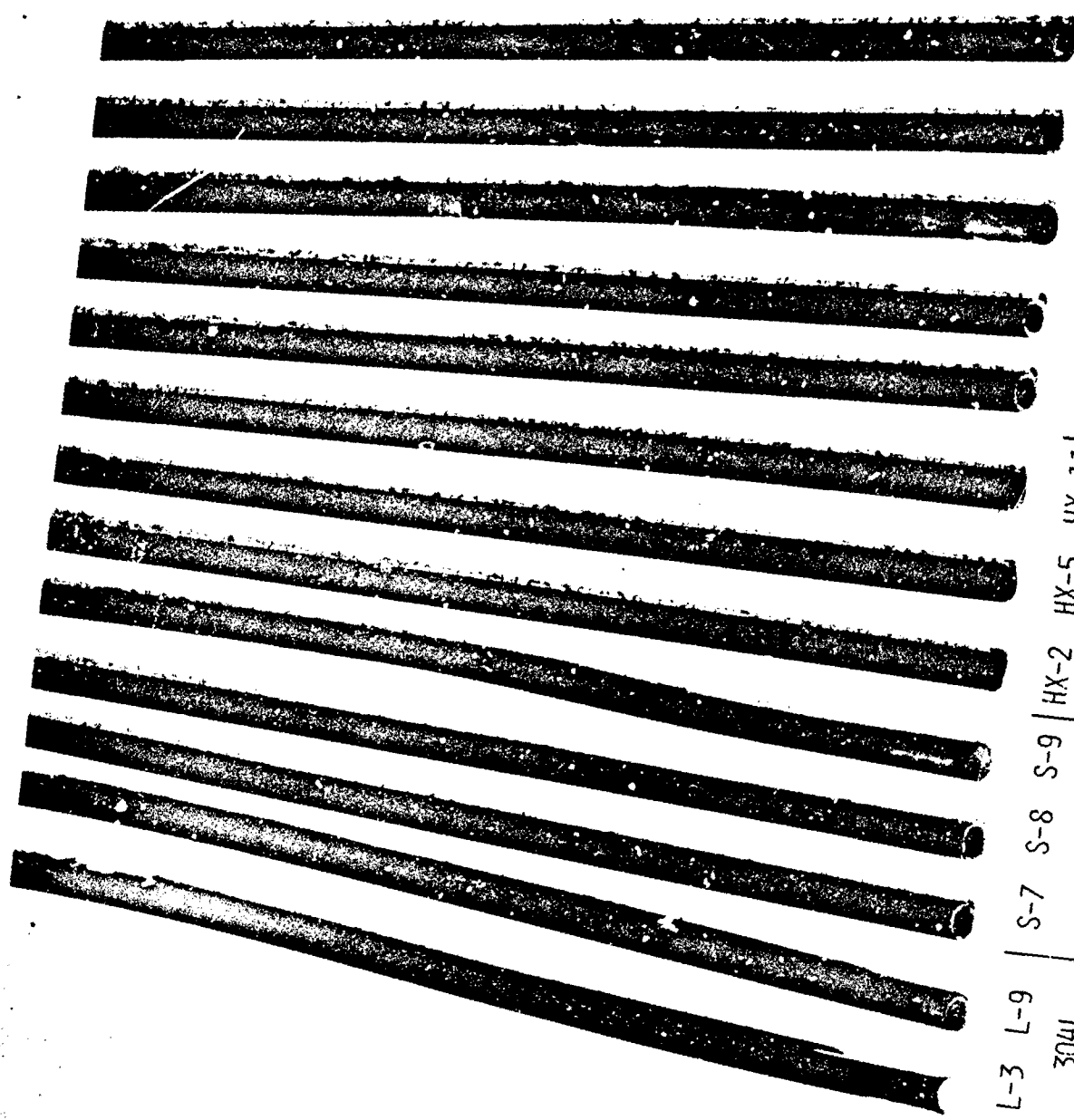
L-3 L-9 | S-7 S-8 S-9 | HX-2 HX-5 HX-11 | HA-1 HA-2 HA-3 | HB-5 HB-8
304L | 310S | HASTALLOY X | HAYNES 188 | HASTALLOY B

FIGURE 21. - EVAPORATOR ENDS OF HEAT PIPES OPERATED IN VACUUM ENVIRONMENT.

left the external surfaces clean and without any oxidation, while the compatibility with sodium, as illustrated in the air pipes (Fig. 14(c)), precluded internal failure.

All three 310S stainless steel pipes, S-7, S-8, and S-9 failed due to cracks in the evaporator wall or the evaporator end cap. A longitudinal section of S-8 can be seen in Fig. 22. The spherical shapes on the wick are merely air pockets in the plastic potting material used to mount the sample for metallurgical examination. The microscopic circumferential cracks observed adjacent to the end cap weld that caused failure are too small to be seen in the Polaroid photo. However, the extent of lithium attack is evident.

Failure of pipes S-7 and S-8 was obvious at about 1200 hr into the test by the appearance of lithium oxide on cool surfaces such as viewports. Therefore, these stations were shut down and the pipes were removed. No such deposits were observed in the case of S-9 and, since the temperature profile was so poor from the start time of failure was not apparent. S-9 remained on test until all facilities were shut down. When the pipe was removed just prior to this writing, lithium oxide was found deposited on the internal structure of the test station. A circumferential crack observed near the downstream end of the evaporator is believed to be the cause of the lithium leak.

The pipes constructed of Hastalloy X exhibited very poor compatibility with lithium. HX-2 and HX-11 failed when lithium attack penetrated far enough into the evaporator ends of the pipes to cause leakage. The extent of the lithium attack can be observed on the three photos of the evaporator end section of HX-11, Fig. 23. The three spheres in Fig. 23(a) are air bubbles in the potting plastic used to mount the section for metallographic polishing. The area of lithium penetration has a porous cellular appearance much like a sponge. The attack penetrated to about 0.15 cm (Fig. 23(b) and (c)). Apparently, failure

FIGURE 22 (B)

TRAPPED
AIR
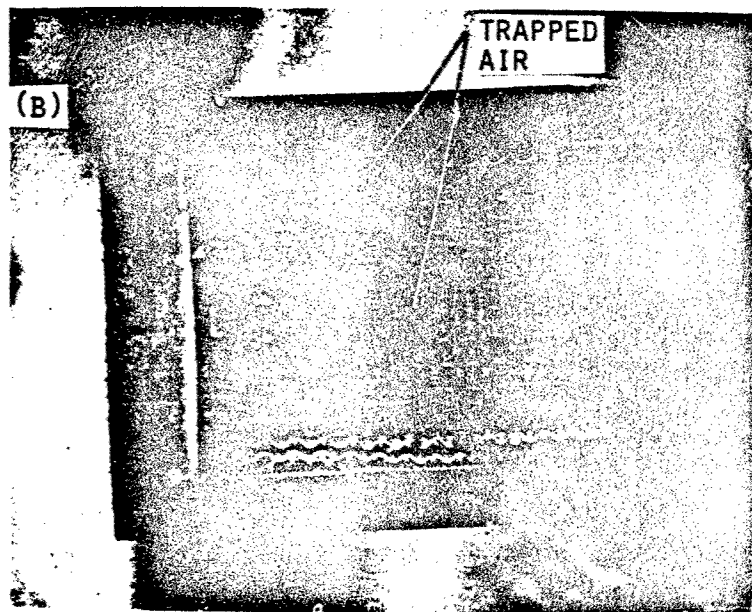
(A) LONGITUDINAL SECTION, MAGNIFICATION 6X.
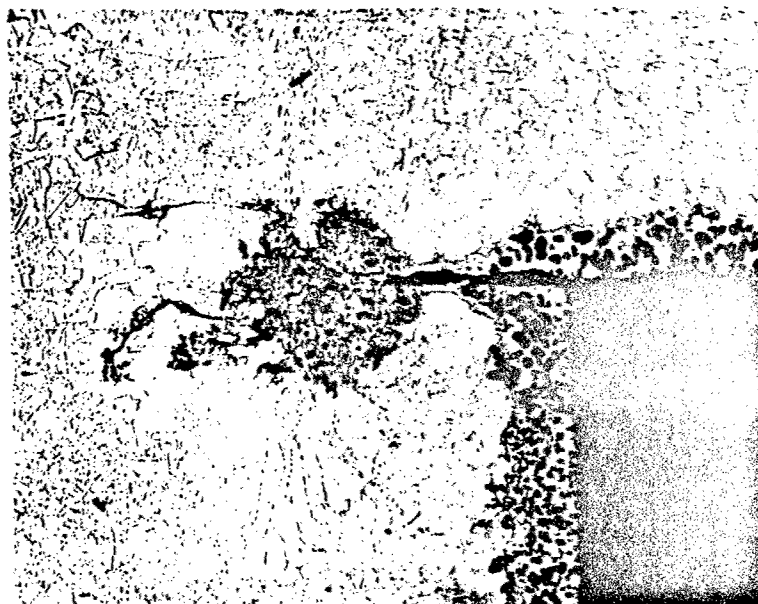
(B) EVAPORATOR END CAP JOINT, MAGNIFICATION
100X.

FIGURE 22. - LONGITUDINAL SECTION OF 310S
STAINLESS STEEL PIPE S-8.

63
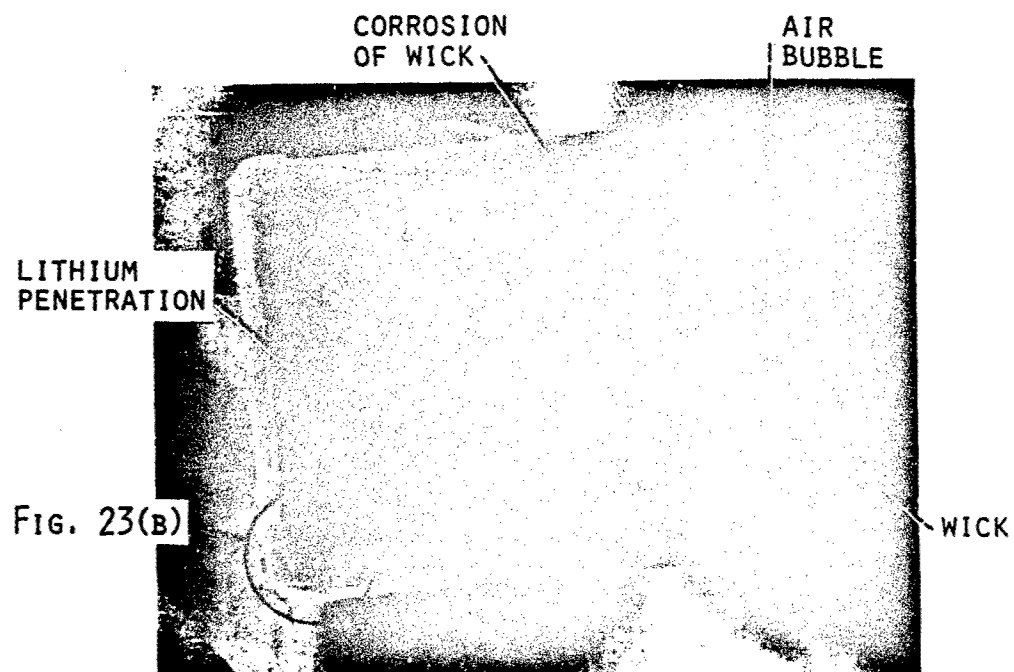
(A) LONGITUDINAL SECTION OF EVAPORATOR END.

FIGURE 23. – LITHIUM ATTACK ON INTERNAL SUR-
FACES OF EVAPORATOR END OF HASTALLOY PIPE
HX-11.
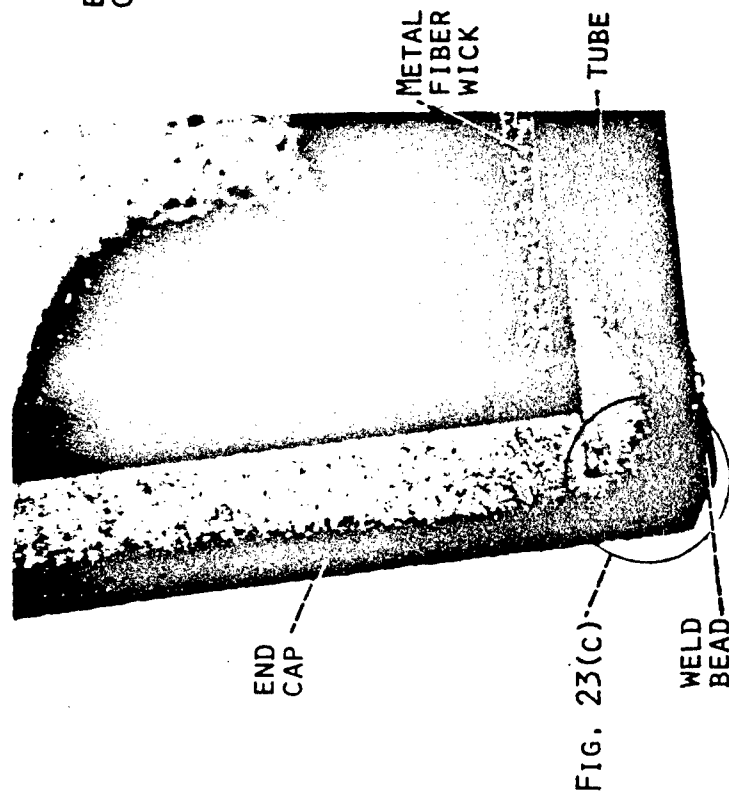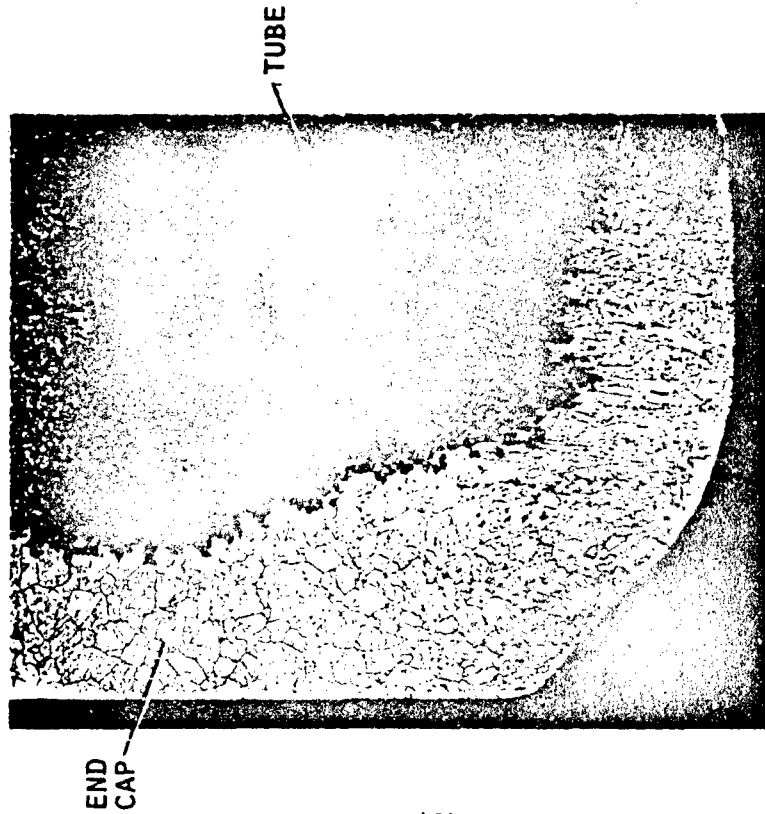
(c) Lithium penetration into end cap to tube joint area, magnification 50X.

(b) End cap to tube joint, magnification 10X.

Figure 23. - Lithium attack on internal surfaces of evaporator end of Hastalloy X pipe HX-11.

65

occurred when the pipe wall or end cap became thin enough to permit leakage of lithium. The same lithium attack was also evident in HX-5, except that leakage was due to a crack adjacent to the end cap weld as shown in Fig. 24.

Even before actual leakage occurred, a curious phenomenon was taking place in the evaporators of these Hastalloy pipes. Lithium attack of the metal fiber wick and subsequent transport of the wick material to an area about 5 to 7 cm long and centered at ∼10 cm from the evaporator tip, caused a venturi-shaped constriction. The build-up in HX-11 completely closed off the evaporator at this point. The first 10 cm were thus isolated from the rest of the pipe. A cross section through the blocked area is shown in Fig. 25(a). The extent of this constriction in the case of HX-2 is shown in Fig. 25(b). Only a small hole was left in the center of the deposit. More will be discussed concerning the nature of this type of deposit under the paragraphs relating to the Hastalloy B pipes.

Two of the Haynes 188 lithium pipes, HA-1 and HA-2, failed after very few test hours. Both failures were due to cracks in the wall adjacent to the seam weld, or adjacent to the tube-to-end cap weld. Figure 26(a) shows a typical wall crack and Fig. 26(b) is a photomicrograph of cracks penetrating into the tube wall from the external surface.

No such cracking occurred in HA-4 and no lithium oxide deposits were observed on the test station structure when the pipe was removed. Apparently, this pipe did not fail. As with the other lithium filled pipes, the temperature profile was very poor from the beginning so that no change indicating failure was apparent. Figure 27 is a view of a longitudinal section of the evaporator end of Haynes 188 pipe HA-4. It is typically free of attack by lithium. Pipe HA-4 was on test for over 27,000 hr.

FIGURE 24. - CIRCUMFERENTIAL CRACK
ALONG END CAP WELD IN HASTALLOY X
PIPE HX-5.

67
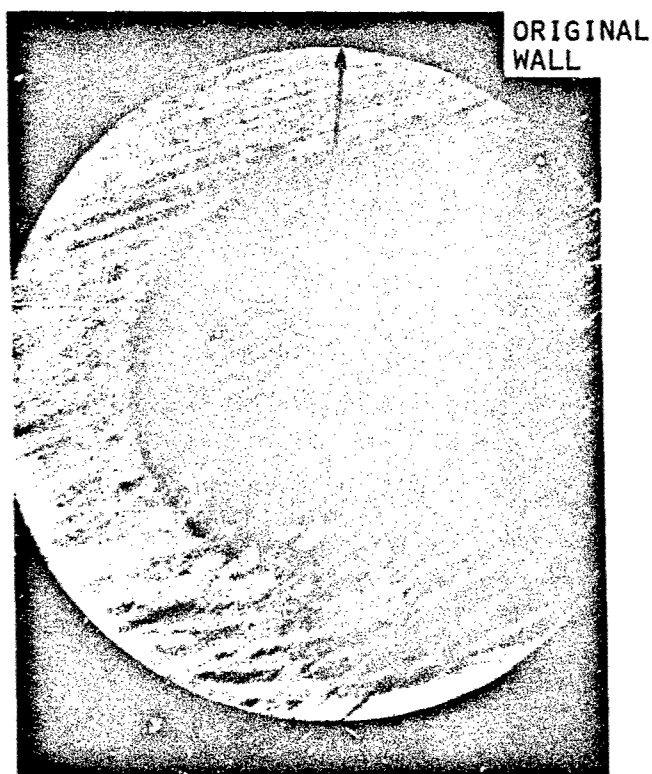
(A) CROSS SECTION THROUGH CONSTRIC-
TION IN EVAPORATOR OF HX-11.
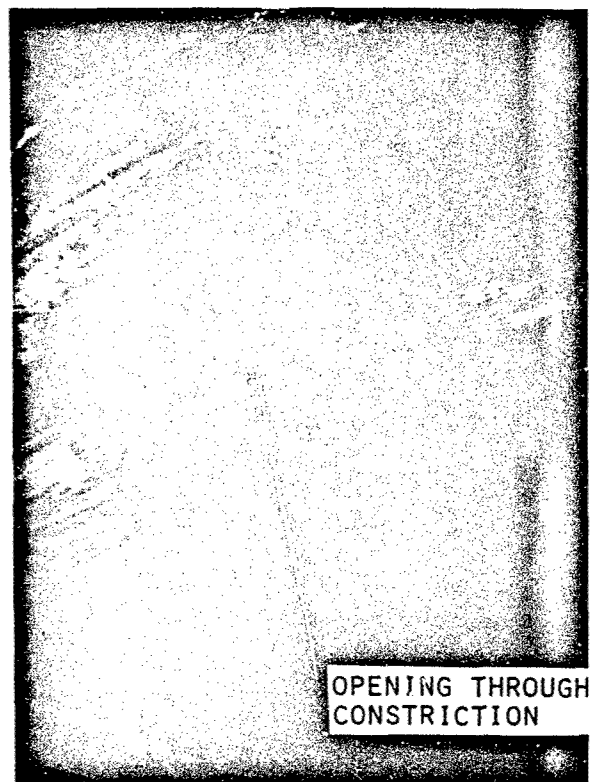
(B) CROSS SECTION THROUGH CONSTRI-
TION IN EVAPORATOR OF HX-2.

FIGURE 25. - BLOCKAGE OF INTERNAL EVAPORATOR AREA IN HASTALLOY X PIPES.

(A) Cracks in external surface, magnification 100X.

(B) Section at cracks, magnification 100X.

Figure 26. - Wall cracks in evaporator end of Haynes 188 pipe HA-1.
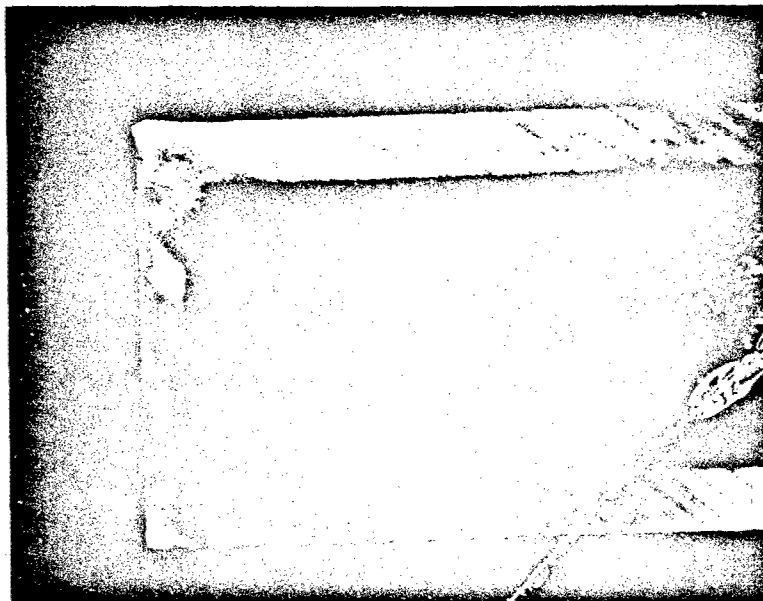
FIGURE 27. - LONGITUDINAL SECTION
OF EVAPORATOR END OF HAYNES 188
PIPE HA-4.

70

As with the Hastalloy X group, the Hastalloy B heat pipes were extremely sensitive to lithium corrosion. The extent of the corrosion is apparent in Figs. 28 through 30. Again, the spherical shapes are air bubbles in the potting plastic and have no bearing on the results. In some of the Polaroid photos, the penetrated area appears darker than the surroundings. This effect is due only to the angle of lighting when the photo was taken.

A leak developed through the center of the end cap of pipe HB-5, as seen in Fig. 28(a), because lithium had penetrated to within about one half millimeter of the outside surface. The depth of the lithium corrosion into the end cap and tube wall can be seen in Fig. 28(b). Failure of pipe HB-6 occurred in exactly the same way. Figure 29(a) shows how lithium has removed some of the material from the end cap of HB-6 and left a considerable depth of voids. The lithium oxide visible on the outside surface of the end cap is over the area of leakage. The manner in which lithium attack progresses into the grain boundaries can be viewed in Fig. 29(b). This photo clearly shows the joint between end cap and tube, and the weld.

In most cases, the pronounced lithium attack has been on the end cap and immediate area. As Fig. 30 shows, there was also severe corrosion of the tube wall, at least in the first 3 cm or so of the evaporator. The deterioration of the metal fiber wick is also obvious in the figure.

In addition to the lithium attack on the end caps and adjacent tube walls, severe attack of the metal fiber wicks of the Hastalloy B pipes and the Hastalloy X pipes occurred. Transport of the metallic particles from areas in the evaporator, adiabatic section, and the upstream end of the condenser section resulted in a large solid deposit typically 5 cm in length, beginning about 10 cm from the evaporator end. Longitudinal sections of HB-6 can be seen in Fig. 31. Missing in the picture are a 2.5 cm long section of evaporator end, a 1.9 cm section cut from the
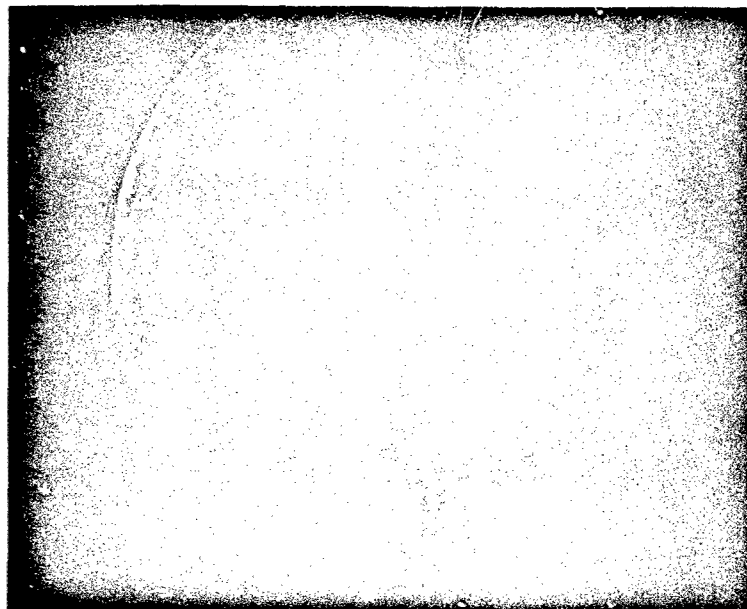
(A) External surface of end cap.
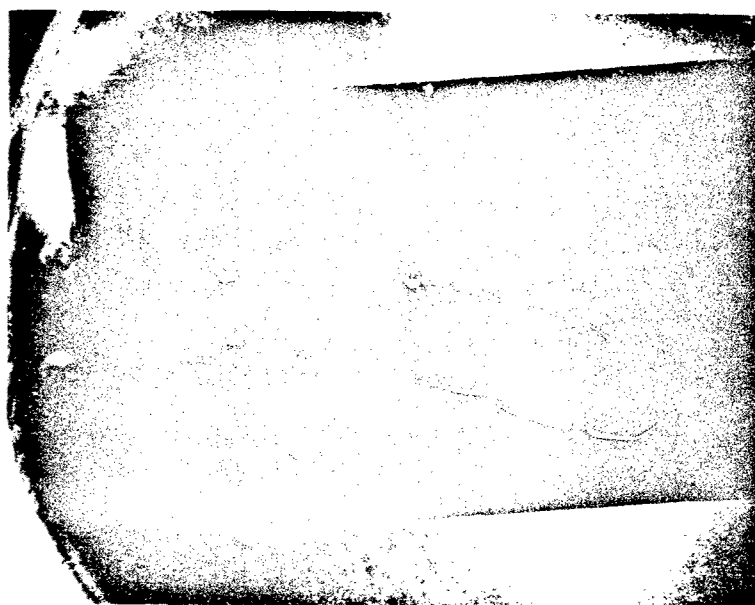
(B) Longitudinal section.

Figure 28. - Lithium attack in evaporator end
of Hastalloy B pipe HB-5.
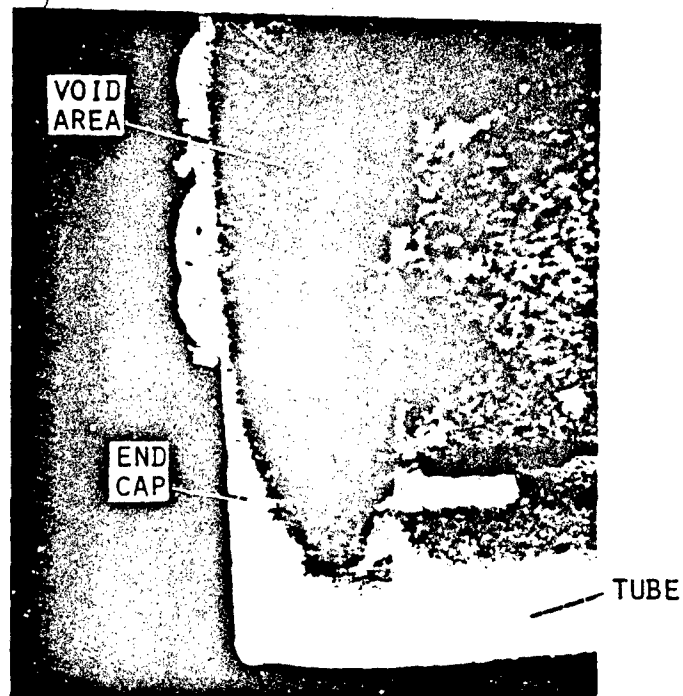
(A) VOIDS IN END CAP CAUSED BY LITH-
IUM ATTACK.
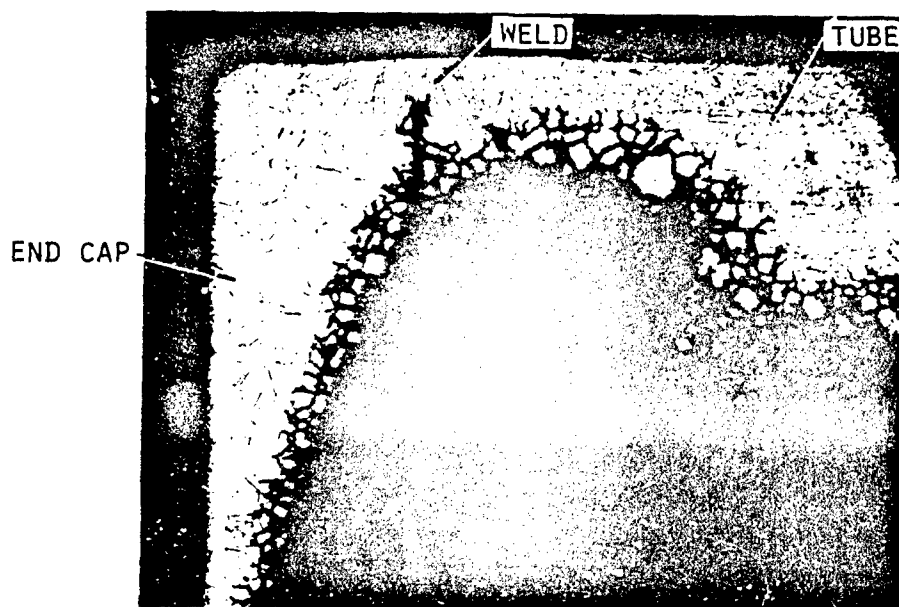
(B) PHOTOMICROGRAPH OF END CAP TO TUBE JOINT,
MAGNIFICATION 30X.

FIGURE 29. - LITHIUM ATTACK ON EVAPORATOR END
OF HASTALLOY B PIPE HB-6.
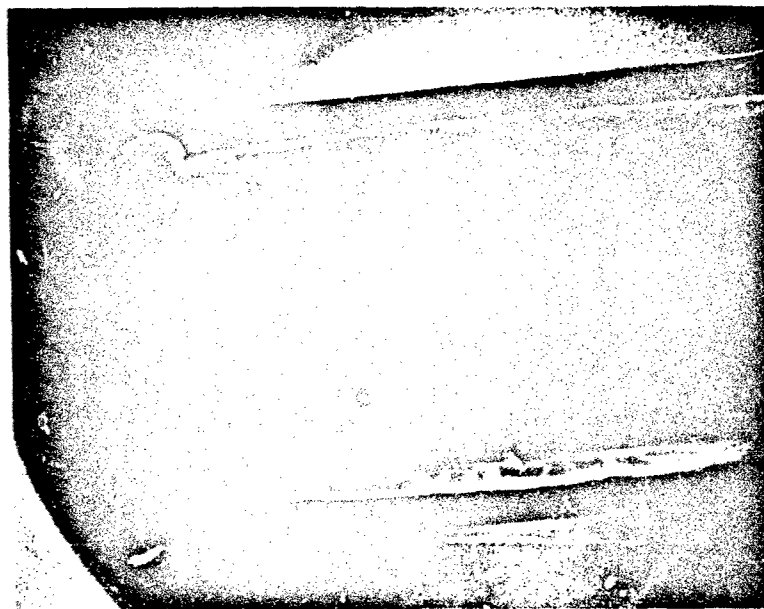
FIGURE 30. - LONGITUDINAL SECTION OF EVAPORA-
TOR END OF HASTALLOY B PIPE HB-8.

EVAPORATOR SECTION

ADIABATIC SECTION
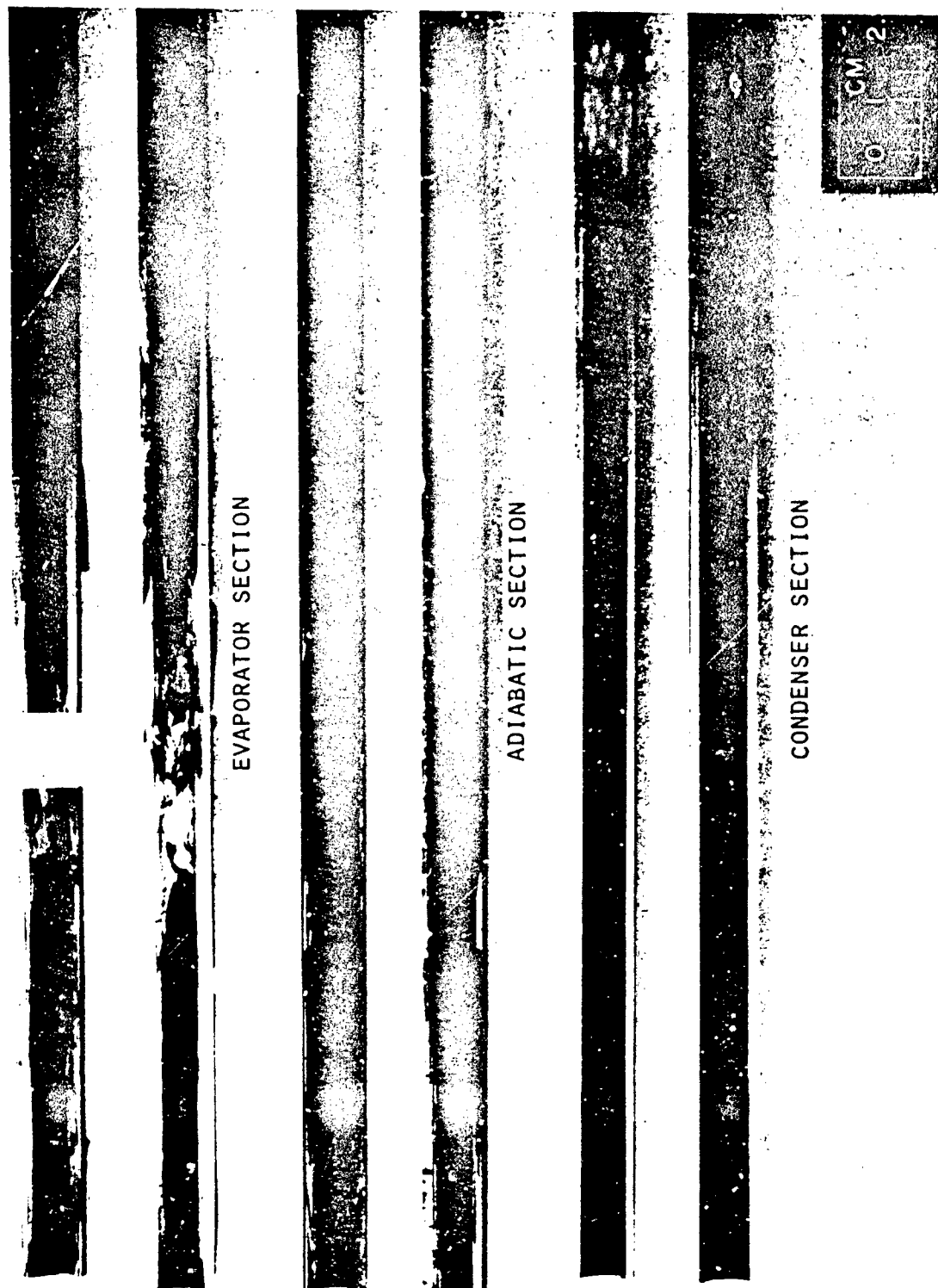
CONDENSER SECTION

FIGURE 31. - LONGITUDINAL SECTIONS OF HASTALLOY B PIPE HB-6 SHOWING EXTENT OF LITH-IUM CORROSION ALONG ENTIRE LENGTH OF PIPE.

75

deposit area, and a 13 cm long section of the condenser
end. The wick in the evaporator end is fused to the tube
wall over its entire length. Most of the wick in the
adiabatic section, particularly in the downstream end, is
gone as it is in the first half of the condenser section.
In some of the Hastalloy B and Hastalloy X pipes, the
transported material agglomerating in the evaporator actu-
ally closed off the area and prevented the flow of fluid
and vapor. Figure 32(a) shows a cross section cut from
the closed area of HB-6. Figure 32(b) shows a cross sec-
tion through the evaporator about 5 cm from the end cap,
and another through the condenser about 3 cm from the end
of the pipe. X-ray diffraction analysis indicates the
deposit to be nickel. Hastalloy X and Hastalloy B are
typically 40 to 70 percent nickel.

The depth of attack in the tube wall and in the
metallic fiber wick seems to be much less severe in HB-5
than it was in HB-6 and HB-8. The only explanation is that
the data indicate HB-6 and HB-8 were at T_1 temperature
greater than 900 °C for 300 and 400 hr compared to 160 hr
for HB-5. However, the depth of attack into the end caps
looks about the same in HB-5 as in HB-6.

RELATIVE CREEP

Excessive creep due to internal pressure over long
time periods in space applications and axial deformation in
1-g applications might be detrimental to the power system
involved. Therefore, at the start of the program, one of
the parameters to be studied was the relative creep rate
of the materials. Measurements were taken of two pipes of
each material; one to be tested in a vacuum environment
and the other to be tested in an air environment. Length
dimensions were taken between scribe marks at the location
of T_{spare} and T_2 and between T_2 and T_3. Also,
three diametrical measurements at 60° increments at T_1,
T_2, and T_3 were recorded. These measurements were to

76
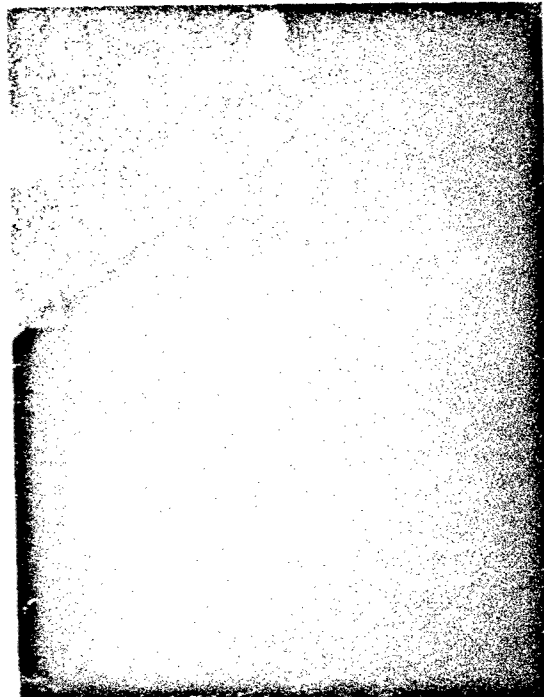
(A) SECTION THROUGH BLOCKED AREA OF
    EVAPORATOR.
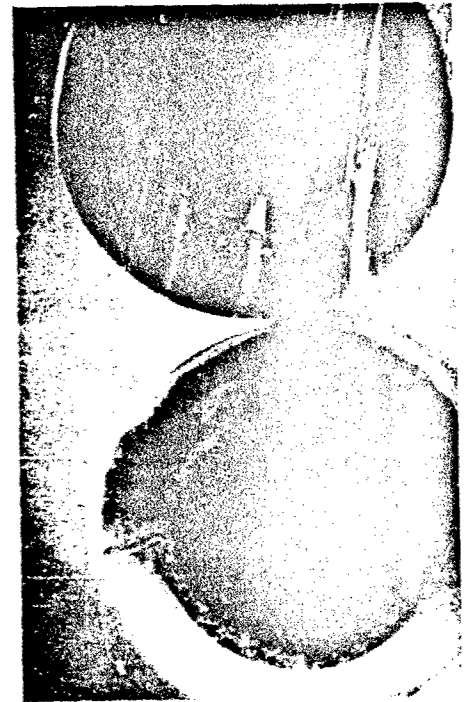
(B) CROSS-SECTIONS OF EVAPOR
    AND CONDENSER.

FIGURE 32. - CONSTRICTION OF EVAPORATOR BY DEPOSITS TRANSPORTED FROM OT
    AREAS OF HASTALLOY B PIPE HB-6.

be compared to those taken at the same places after testing.

Due to early failures of many of the pipes and particularly because of de-emphasis of the program, post-test measurements were not made. However, some qualitative comparisons of axial deformation at the temperatures experienced may be formed from the data of Table 5.

The pipes are listed in ascending test hours for each material. The hours listed at 800 °C include, of course, the hours at 900 °C. All of the pipes were supported essentially on knife edges at 30.5 cm in from each end. The ends of the pipes sagged downward, generally causing a uniform curve or "bowing". Deformation is the dimension between the centerline at each end and the centerline at the point of maximum "bowing".

The test data were examined to determine if the temperatures above 800 °C were experienced generally in the early hours of testing, but no correlation could be made. However, in four of the five material groups, the rate of deformation seems to indicate that most of the sagging occurred in the early part of the tests since the rate decreases with increased hours of testing.

TABLE 5

PIPE DEFORMATION

Pipe number	Hours at 800 °C	Hours at 900 °C	Deformation, cm	Rate $\frac{cm \times 10^2}{100\ hr}$
304L				
L-2	260	0	0.80	30.7
L-8	300	0	0.25	8.3
L-9	21,670	6,810	2.30	1.6
L-3	28,800	0	1.90	0.7
310S				
S-7	900	0	0.15	1.7
S-8	1,150	0	0.15	1.3
S-3	16,800	0	0.80	0.5
S-1	19,700	0	0.90	0.5
S-9	28,250	820	1.85	0.7
Hast. X				
HX-2	230	40	0.10	4.3
HX-5	380	20	0.20	5.3
HX-11	1,140	380	0.20	1.8
HX-9	1,500	1,500	0.15	1.0
HX-7	1,870	21,870	0.0	0.0
Haynes				
HA-1	70	50	0.15	21.4
HA-2	170	0	0.15	8.8
HA-5	400	400	0.0	0.0
HA-6	1,280	1,280	0.0	0.0
HA-4	29,900	26,900	0.35	0.1
Hast. B				
HB-5	290	160	0.10	3.4
HB-3	320	0	0.0	0.0
HB-8	430	400	0.30	7.0
HB-1	570	570	0.15	2.6

SECTION V
ANALYSIS OF PERFORMANCE

Since this program was basically a materials evaluation program, a relatively small amount of attention was paid to pipe performance. However, the poor temperature profiles in the lithium pipes and the varying capabilities of the sodium pipes required that some consideration be given here to what performance... should reasonably be expected of the pipes. The relatively sparse instrumentation impedes efforts at extensive data analysis, but there is enough to shed light on performance observations.

Frequently it is useful in analyzing heat pipe behavior to examine the heat pipe performance limits which have been derived. Within the operating ranges of the heat pipes in this program, three limits have been defined (Ref. 6). These are the viscous limit, the sonic limit, and the wicking limit. Appendix A discusses these limits. For this report the concept of a viscous limit did not prove useful for reasons dealt with briefly in Appendix A.

A simple model of a heat pipe operating at low vapor density and low heat transport was constructed (Appendix B). Using the model, the theoretical performance of sodium and lithium pipes representative of those in this program was determined. The theoretical sonic limit was computed for such pipes and placed on the performance charts. The wicking limit determined from experimental observation was also located on the charts.

SODIUM

Figure 33 shows the predicted performance of sodium filled pipes with internal dimensions similar to those in the present program. In preparing the figures, no adiabatic section was assumed so that all computations would be on the same basis. The air pipes in this program had shielded adiabatic sections while in vacuum they radiated

from the nominal adiabatic section as well as from the condenser.

In Fig. 33(a) an emissivity of 0.25 was assumed, representing bright stainless steel in a vacuum. While Fig. 33(b) pertains to an emissivity of 1.0, representing either a specially coated or badly oxidized pipe, operation in vacuum was assumed. No heat loss by convection was accounted for in the computations.

Lines of heat pipe length ratio ℓ/ℓ_e (total length of heat pipe divided by evaporator length) versus transported heat are shown for various evaporator stagnation temperatures. The ratio ℓ/ℓ_e essentially shows the length of pipe required to dissipate heat Q. If, at a given Q, ℓ/ℓ_e, and temperature, an actual pipe is longer than ℓ/ℓ_e, then a portion of the pipe will be cold and a sharp drop in temperature will occur at about ℓ/ℓ_e. If, on the other hand, an actual pipe is shorter, the pipe will have to seek a higher temperature consistent with the specified Q and ℓ/ℓ_e.

Lines of approximate Mach number M at the evaporator exit are indicated. Because of the assumption of incompressible flow, the lines of constant temperature are terminated at M = 0.3. The sonic limit line, M = 1.0, was computed by Busse's equation (Ref. 7), and located on the figures by a rough extrapolation of the lines of ℓ/ℓ_e versus Q established at lower Mach numbers.

Also shown in Figs. 33(a) and (b) are hatched regions representing approximate wicking limit for 100 mesh screen as computed from experimental data taken in the program. The width of the zone suggests uncertainty in the computation, but is in no way proportional to the uncertainty. Appendix A discusses the computations leading to the location of this region. An analytic determination of the wicking limit using published values of wick permeability and wicking capability gives a heat transport as low as 75 W at ℓ/ℓ_e of 3, the physical dimension of the
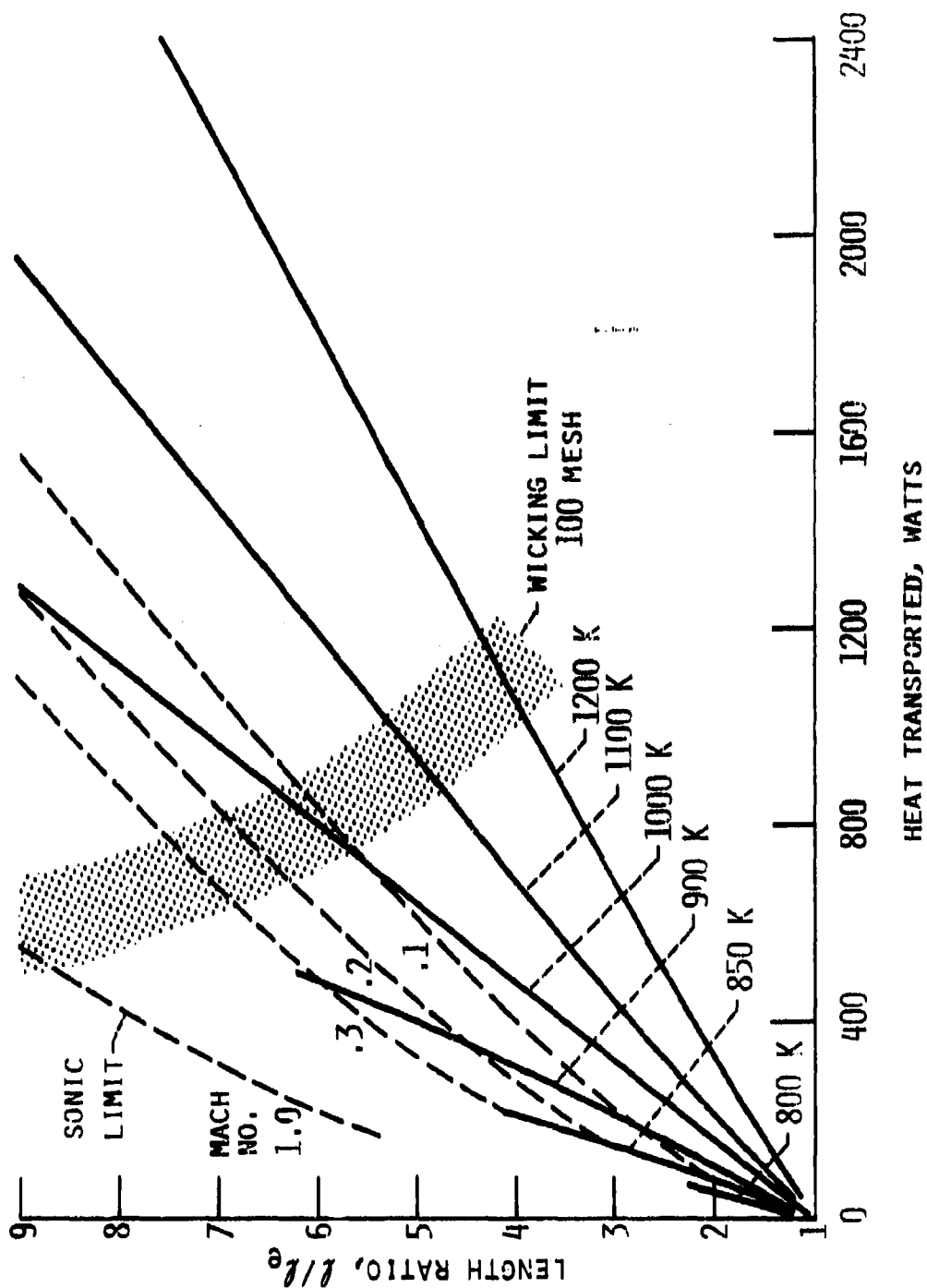
FIGURE 33. LENGTH OF SODIUM-FILLED PIPE REQUIRED TO DISSIPATE TRANSPORTED HEAT AT SEVERAL TEMPERATURES.

(A) CONDENSER EMISSIVITY, 0.25.

83
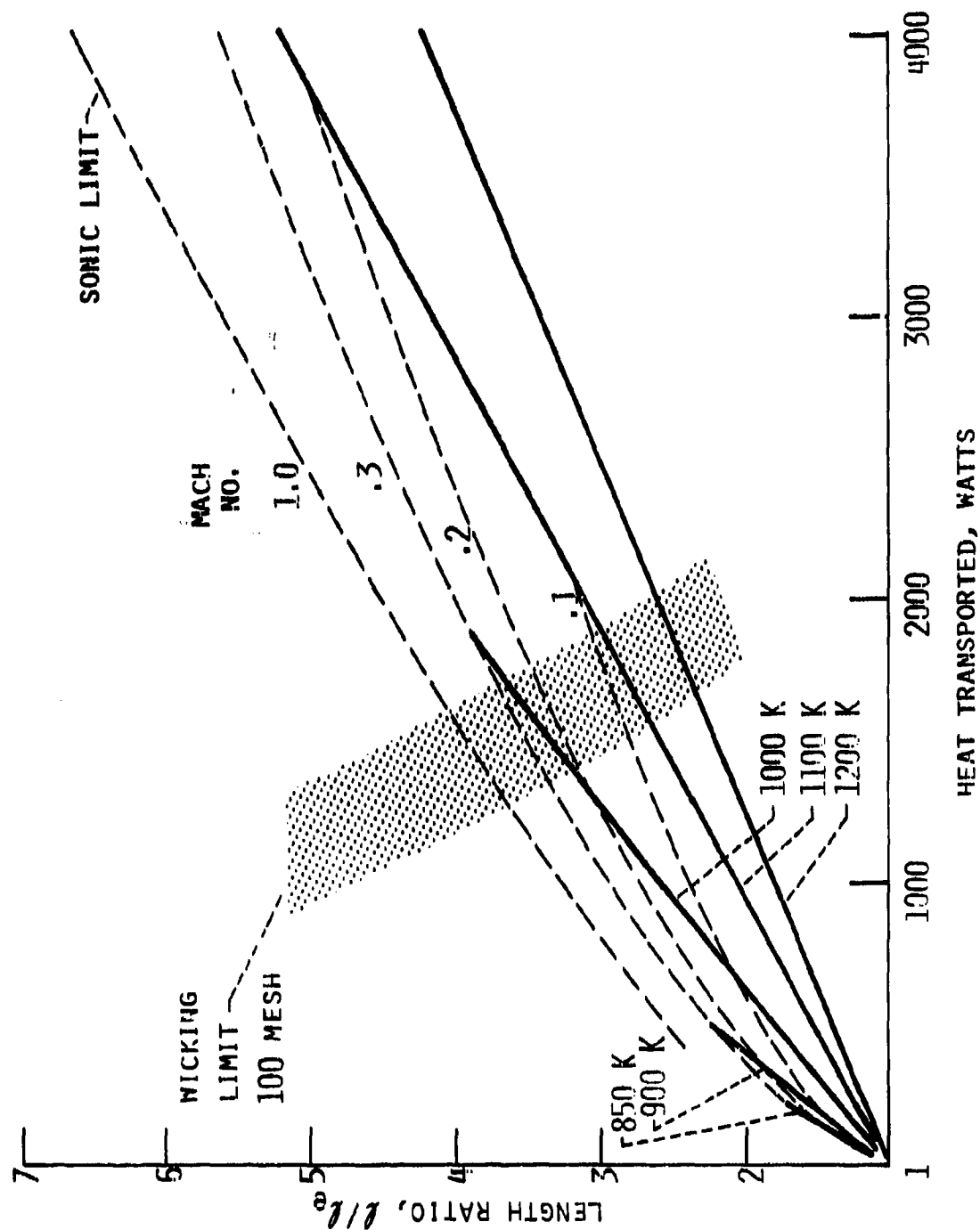
FIGURE 33. - LENGTH OF SODIUM-FILLED PIPE REQUIRED TO DISSIPATE TRANSPORTED HEAT AT SEVERAL TEMPERATURES.

(B) CONDENSER EMISSIVITY, 1.0.

heat pipes (Appendix A). Apparently a rolled screen wick such as employed in this project has a flow resistance much lower than that computed from published laboratory measurements (Refs. 6 and 8). Probably the screen layers do not remain in tight contact. The wick structure then takes on the character of an artery with much diminished flow resistance.

The attainable operating region for sodium pipes resembling those in the superalloy program is below the sonic limit line and to the left of the wicking limit zone. The figures show that even for sodium pipes having the extreme length-to-diameter proportions of the superalloy pipes, there is a substantial region of satisfactory operation. This is in agreement with observation.

Comparison of Figs. 33(a) and (b) emphasizes the obvious fact that high emissivity results in more heat transfer, and consequently a shorter heat pipe with less fluid resistance. If physical constraints require a long adiabatic section not considered in the figures, fluid resistance will increase, lowering the heat transport.

LITHIUM

Figure 34 shows the predicted performance of lithium filled heat pipes with internal dimensions resembling those in the present program. Again, no adiabatic section was assumed in the figure. For comparison purposes, the vapor channel diameter was assumed to be the same as for Fig. 33. Figure 34(a) pertains to an emissivity of 0.25, while Fig. 34(b) is for an emissivity of 1.0.

The wicking limit in Fig. 34(a) represents a computation for metal felt wicks. The wicking limit falls to the right of the grid in Fig. 34(b). While no known wicking limit was encountered in the tests with the lithium pipes, evidence of incipient dryout was observed in sodium pipes with metal felt wicks. As described in Appendix A, this information was used to deduce a metal felt flow
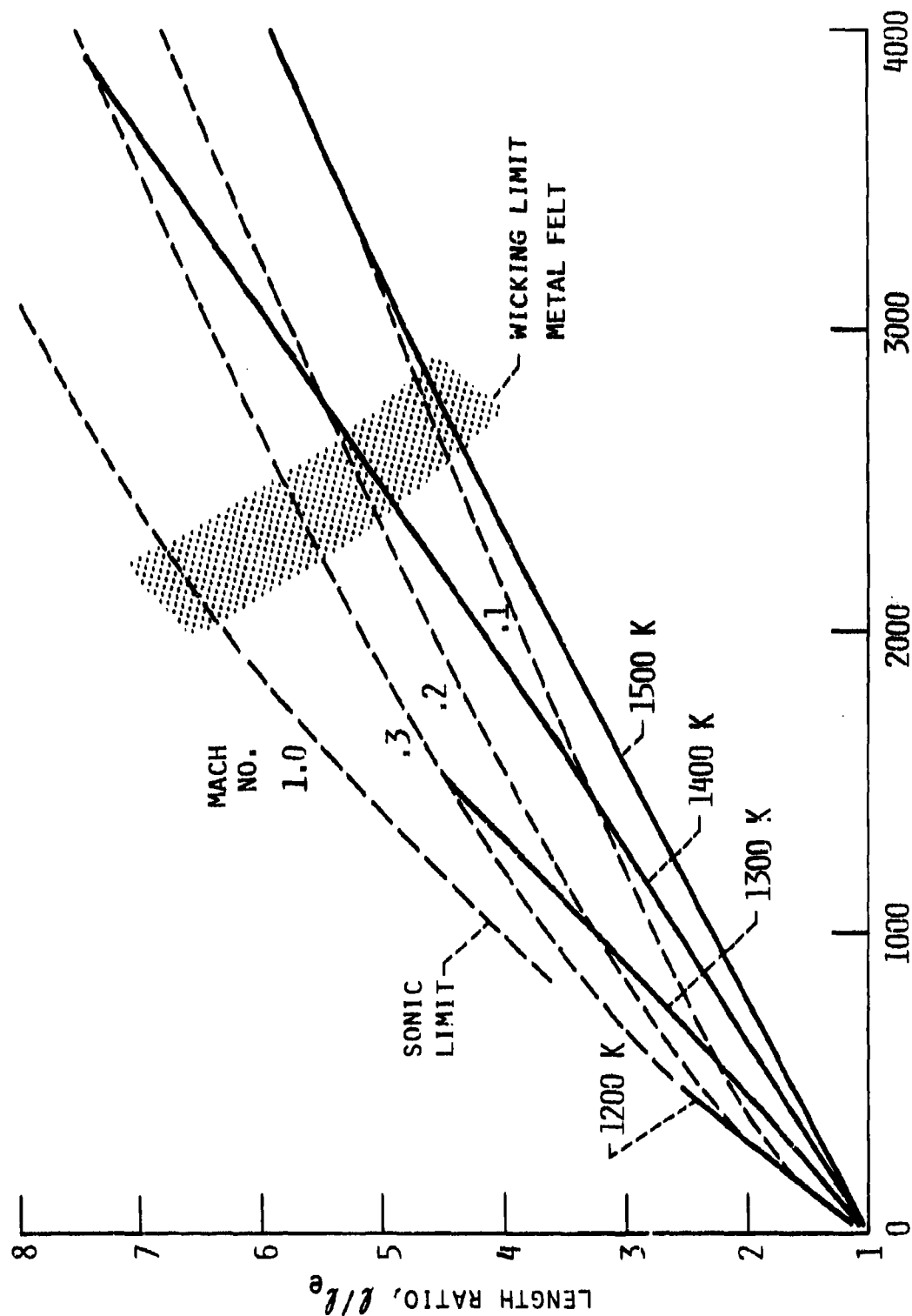
85

FIGURE 34. LENGTH OF LITHIUM-FILLED PIPE REQUIRED TO DISSIPATE TRANSPORTED HEAT AT SEVERAL TEMPERATURES.

FIGURE 34. LENGTH OF LITHIUM-FILLED PIPE REQUIRED TO DISSIPATE TRANSPORTED HEAT AT SEVERAL TEMPERATURES.

(B) CONDENSER EMISSIVITY, 1.0.

87
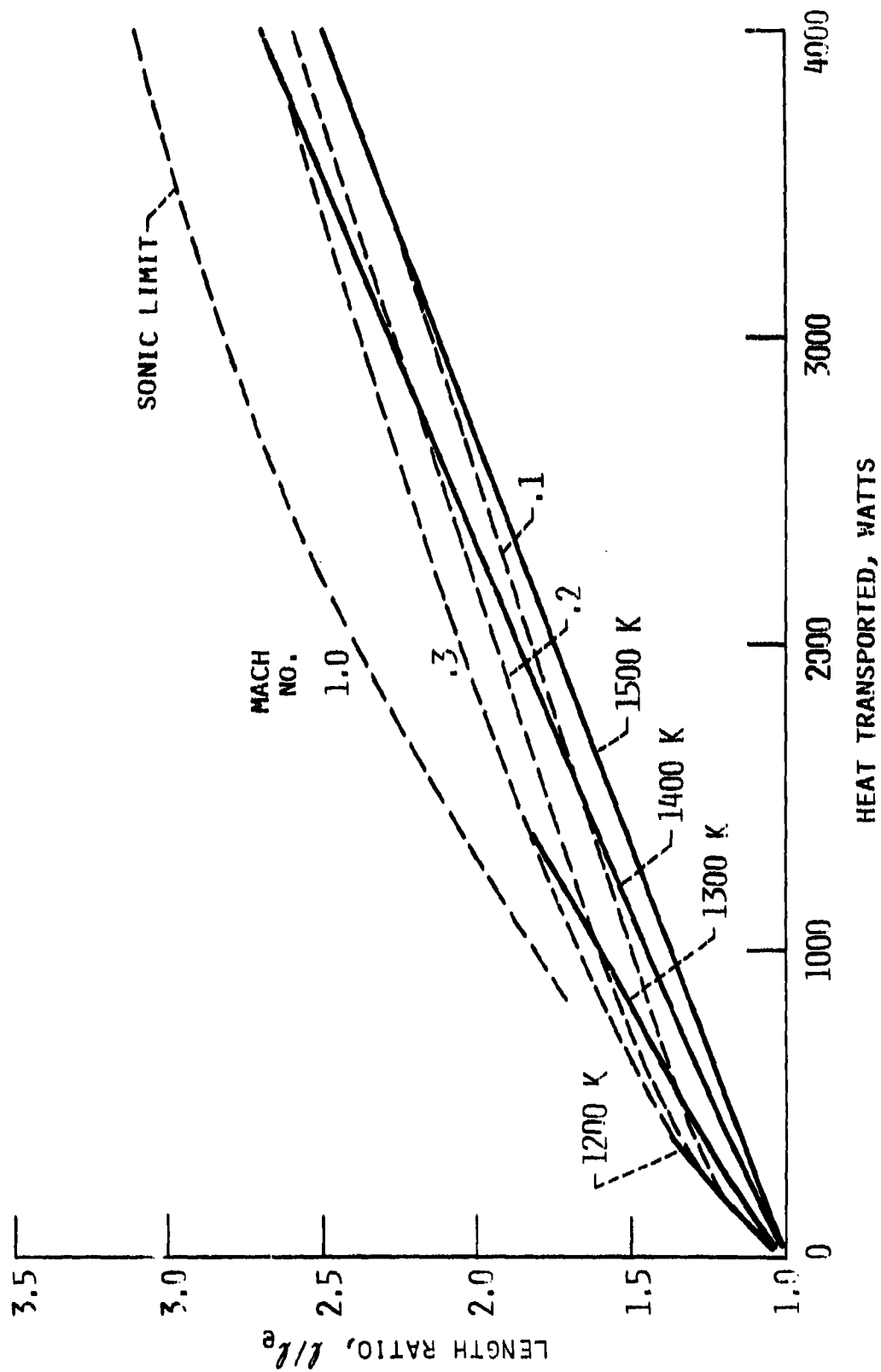
resistance. From this resistance the wicking limit was computed for lithium metal felt heat pipes. This wicking limit was in excess of any condition attained in the lithium superalloy tests.

From Figs. 34(a) and (b), the conclusion is easily reached that the lithium pipes were simply operating at too low a power input. The sonic limit was probably approached, or encountered, in all of the functioning lithium pipes. At 1200 K the sonic limit for the lithium pipes would have been reached at about 800 W. On the other hand, the superalloy materials limitations and heater restrictions prohibited the higher temperatures which would have avoided the sonic limit.

SECTION VI
CONCLUDING REMARKS

This study at the outset was focused on materials compatibility in liquid metal-superalloy heat pipes. Sodium was found to be satisfactory over long periods with all of the alloys tested. Lithium was found to be compatible only with Haynes 188, and to a limited extent with 310S stainless steel. However, both were prone to cracking.

There was no obvious external problem in any of the pipes exposed to vacuum environment, although the possibility of preferential evaporation of constituents is not precluded. In air, 304L and Hastalloy B pipes were oxidized on the evaporator surfaces, while other alloys were satisfactory.

The sodium pipes performed satisfactorily under the conditions imposed by the materials and by the test facility. The performance of the lithium pipes was poor, and was a consequence of both materials and facility limitations. A conclusion reached is that the superalloys tested in this program are unsuited to lithium heat pipes.

Because of the emphasis on materials compatibility, relatively little attention was devoted to the design of the pipes. However the differences in performance observed among member pipes of a single group suggest that large manufacturing variances were encountered in the internal structure. In large scale applications of high performance heat pipes more demanding design and quality control procedures might be desirable.

SECTION VII
RECOMMENDATIONS

Some specific recommendations applicable to future work with heat pipes and test facilities of the same type employed in this program follow.

FACILITIES

The test facilities generally proved quite satisfactory for this program, built as they were upon experience with installations for lower temperature pipes. The heaters as finally developed were adequate for the duty imposed. The air heaters were operating near their limit. The vacuum heaters, or modifications thereof, could probably be operated at higher temperatures and powers. The circulating cooling system gave no problems. On the other hand, ports and viewing holes to give better sightings of the hot pipes would have been appreciated. The pipes also could have been supported at both ends as well as at the ends of the adiabatic section. The bowing of some of the pipes, a factor in a gravity environment, could have been lessened.

INSTRUMENTATION AND DATA TAKING

Interpretation of performance data would have been greatly improved by more thermocouples, particularly in heat rejection sections. In an essentially isothermal zone such as the evaporator, two couples might suffice (one as a spare) with eight or ten more in the rest of the pipe. To monitor the temperatures, a recording system, or a visual display such as the video bargraph (Metrascope) described in Ref. 9 would be desirable. Additional attention should be given to thermocouple attachment since problems with breakage and lifting were encountered.

91

OPERATION

Whether preheating of the pipes to distribute the working fluid along the pipe was necessary is uncertain. As a precaution against a failed start up, preheating should be considered.

More power increments during start up may be desirable to better define the dynamics of the process.

APPENDIX A
REVIEW OF HEAT PIPE LIMITS
AND COMPUTATIONS

Busse (Ref. 7) has considered heat pipe limits at some
length. The material which follows is abstracted from that
source where possible.

REVIEW OF LIMITS

At the lowest operating temperature for a given pipe-
fluid combination, the viscous limit is supposedly encoun-
tered. This represents a situation in which relatively
low vapor velocities are attained. Viscous forces in the
vapor stream deplete the pressure available for driving
the column of vapor before the condenser end of the pipe
is reached. Alternatively, one may say that the heat
rejected removes all the vapor before the end of the con-
denser is reached, as explained below.

As evaporator temperature is increased in the situ-
ation above, vapor pressure and vapor velocity rise and at
some point choke, or sonic velocity, at the end of the
evaporator is reached. This is the sonic limit. Further
increase in temperature causes supersonic velocities in
the condenser, with continued choke in the evaporator end.
In the meantime, the transported heat and the vapor mass
flux continue to rise with sonic velocity maintained at
the end of the evaporator. A shock wave in the condenser
moves upstream as the temperature increases and eventually
vanishes, establishing subsonic flow throughout the pipe.
On the other hand, a change only at the condenser cannot
affect the evaporator conditions.

With continuing increase in evaporator temperature,
heat input, and, therefore, liquid velocity, the wicking
limit is encountered. An effort to pass this limit causes
dryout of the evaporator. The pressure drop in the heat

93

pipe, mostly in the wicking, exceeds the capillary surface tension forces available for pumping.

A recapitulation may be made as follows. For a given heat pipe, the viscous limit determines the active length of the pipe at the particular operating conditions. Where the sonic limit applies, the evaporator and condenser are uncoupled, and changes in condenser conditions do not affect transported heat. When the wicking limit is encountered, an effort to increase heat transport further may cause complete failure of the pipe to function. In this sense the wicking limit is altogether different from the others.

Busse (Ref. 7) has presented equations for heat transport at the viscous and sonic limits. For a heat pipe of specified cross section area the heat input Q_e to the evaporator at the sonic limit is

$$Q_e = 0.474 h_{vl} A_v (\rho_o P_o)^{1/2} \qquad (1)$$

and at the viscous limit is

$$Q_e = \frac{A_v D_v^2 h_{vl} \rho_o P_o}{64 \eta \ell_{eff}} \qquad (2)$$

where

A_v area of vapor space

D_v diameter of vapor space

h_{vl} heat of vaporization

ℓ_{eff} effective length

P_o vapor pressure at evaporator upstream end

η vapor viscosity

ρ_o vapor density at evaporator upstream end

For uniform heat addition or rejection the effective length is

$$\ell_{eff} = \ell_a + (\ell_e + \ell_{ca})/2$$

where

ℓ_a length of adiabatic section

ℓ_{ca} active length of condenser

94

ℓ_e length of evaporator

The so-called viscous limit Eq. (2) specifies how much heat can be forced through the heat pipe by the available pressure drop. At the same time, however, the condenser is rejecting heat Q:

$$Q = \pi h D_o \ell_{ca}(T_c - T_e) \tag{3}$$

where

D_o outer diameter of condenser

h   heat transfer coefficient from condenser outer wall

T_c temperature of condenser

T_e ambient temperature

For a given set of steady state conditions, it is necessary that $Q = Q_e$. If $Q < Q_e$ then Q must increase by a change in ℓ_{ca} (Eq. 3) while the resulting increase in ℓ_{eff} reduces Q_e (Eq. 2) until both Q's are equal. If the physical end of the condenser is thereby reached, the pipe moves away from the viscous limit. If $Q > Q_e$, the active length of the condenser by the same token must decrease, increasing Q_e. Because of this necessary coupling of Q_e and Q the concept of a viscous limit appears of limited utility in studying a specific heat pipe. A direct computation of conditions in a heat pipe operating in the viscous range is necessary.

The wicking limit is determined by comparing the maximum capillary pressure difference available at the evaporator upstream end,

$$\Delta p_{cap} = 2\sigma_1 / r_{eff} \tag{4}$$

to the pressure drop experienced by the working fluid departing as vapor and returning as liquid at that point (Ref. 6)

$$\Delta p = \frac{Q}{h_{v1}} \left| \frac{\mu_1 \ell_{eff}}{\rho_1 K A_w} + \frac{8 \mu_v \ell_{eff}}{\pi \rho_v r_v^2} \right| + \rho_1 g(D_w \cos\theta + \ell \sin\theta) \tag{5}$$

95

where

A_w cross sectional area of liquid channel and wick

D_w inside diameter of heat pipe wall

g gravitational constant

K wick permeability

ℓ length of heat pipe

r_{eff} effective radius of a capillary pore

r_v radius of vapor space

ρ_1 liquid density

ρ_v vapor density

μ_1 liquid viscosity

μ_v vapor viscosity

θ angle of heat pipe with horizontal, positive when condenser is below evaporator

σ_1 surface tension of liquid

If Eqs. (4) and (5) are combined, the vapor pressure drop is ignored, and the pipe is in a zero "g" environment, the maximum heat transport can be put in the familiar form (Ref. 6)

$$Q_{max} = 2\left(\frac{\rho_1 \sigma_1 h_{v1}}{\mu_1}\right)\left(\frac{KA_w}{\ell r_{eff}}\right) \tag{6}$$

The group $\rho_1 \sigma_1 h_{v1}/\mu_1$ is a figure of merit for the fluid.

COMPUTATION OF WICKING LIMIT FOR THE SUPERALLOY PIPES

A rough wicking limit for the sodium filled pipes with screen wick can be deduced from the following temperature data for pipe L-8 at the specified conditions.

Tilt	Heater power, W	Temperature, °C				Comments
		T_1	T_2	T_3	T_4	
-5°	1305	860	810	880	740	hot to end
+5°	1305	860	820	880	740	last 5 cm dark

96

The increase in elevation caused a sharp temperature drop at the end of the condenser as evidenced by darkening. This phenomenon was previously observed near dryout (Ref. 9). On the assumption that dryout was commencing at $0°$ tilt. Eq. (5) was solved for parameter KA_w. Dimensions and properties used were (Refs. 6, 10)

h_{vl}	3.74×10^6 J/kg
r_{eff}	1.3×10^{-4} m
r_v	0.00363 m
μ_l	1.7×10^{-4} N/m^2
ρ_l	748 kg/m^3
σ_l	1.15×10^{-1} N/m^2

The value of r_{eff} is estimated from a value for 100 mesh nickel screen in Ref. 6.

The heat actually transported was estimated to be about 1100 W on the basis of computed radiation and convection losses. Thus about 200 W was lost from the heater.

From the data the term $KA_w/\ell r_{eff}$ was computed. Equation 6 for the case of no adiabatic section and a level pipe was then evaluated for the temperatures in Figs. 33(a) and (b). The zone of wicking limit was then located on the figures.

A wicking limit for the lithium filled metal felt pipes was determined by more indirect means. No dryout was suspected in the lithium pipes. However, the following observations for Pipe HX-7 containing sodium were used to determine the resistance of a metal fiber wick.

Tilt	Heater power, W	Temperature, °C			
		T_1	T_2	T_3	T_4
0°	800	680	600	600	600
5°	800	720	605	605	620
10°	800	860	600	600	600

A marked increase in evaporator temperature T_1 occurred as elevation was increased. This phenomenon is

97

also a precursor or indicator of dryout (Ref. 9). The assumption was made that the pore size r_{eff} was that of 200 mesh screen, about 6×10^{-5} m. The limiting tilt before dryout was taken as 5°. The term $KA_w / \ell r_{eff}$ was computed for the wick. Equation 6 was then evaluated for lithium as the working fluid at the temperatures shown in Figs. 34(a) and (b). The zone of wicking limit appears in Fig. 34(a), but falls off of Fig. 34(b).

The results obtained would not be greatly changed by assuming r_{eff} differing from 6×10^{-5} m. In fact, doubling it to 12×10^{-5} m causes a change in Q_{max} (Eq. 6) of 23 percent.

The experimentally determined wicking limit for the screen wire pipes can be compared to a theoretical value computed from tabulated and measured wick properties. By inserting a diameter gauge snugly into the pipe the maximum internal diameter of the 200 mesh wick in one of the sodium pipes was determined. This, together with the pipe internal diameter, gives a wick cross sectional area of 1.47×10^{-5} sq m. Using a reasonable value for permeability K of 5.5×10^{-11} m^2 (Refs. 8 and 10) gives a wicking limited heat transport of 75 W at 1000 K. Obviously the assumption of tight contact in the wick layers is dispelled by this result.

ANALYSIS

A simple heat and mass transport analysis was constructed in the process of preparing Figs. 33 and 34. The many simplifying assumptions are justified by the rather sparse amount of experimental data available, and the need for only qualitative comparisons.

Only one case was considered, that of operation in vacuum with an unshielded adiabatic section. The major assumptions were

(1) Alkali metal dimers (Li_2, Na_2) were considered, and local chemical equilibrium was required.

(2) Uniform temperature across any section was assumed. The vapor and liquid were everywhere in phase equilibrium.

(3) Axisymmetric two dimensional flow was considered in the evaporator.

(4) One dimensional flow analysis could be employed in the condenser. The implied flow profile mismatch and pressure discontinuity at the evaporator-condenser interface, and possible backflow in the condenser (Ref. 11) were not considered.

EVAPORATOR

In the evaporator, the theory of Yuan and Finkelstein (Ref. 12) was employed. This theory was derived for uniform injection, or suction, through a porous wall with incompressible, laminar flow and constant fluid properties. The theory incorporates both the effects of viscosity and momentum change on the pressure drop. Reference 12 assumes a Poiseuille profile at the beginning of injection, or suction. By setting the maximum velocity of the Poiseuille profile to zero, the evaporator end condition is introduced. The equation for pressure drop from evaporator to

any station z can be written, assuming uniform axial heat input, as

$$p(0) - p(z) = \frac{-4C\mu_v}{\rho_v A_v h_{v1}} \left(\frac{Q_e}{\ell_e}\right)\left(\frac{z}{R_v}\right)^2 \qquad (7)$$

where

h_{fv} heat of vaporization of working fluid

R_v radius of vapor space

z distance from evaporator end

μ_v viscosity of vapor

ρ_v density of vapor

Yuan and Finkelstein evaluated coefficient C for the limiting conditions of low and high radial Reynolds number Re_r.

For $Re_r \ll 1$

$$-C = 1 - (3\ Re_r/4) - (11\ Re_r^2/2.70) \qquad (8)$$

and for $Re_r \gg 1$

$$-C = 0.61685 - (1.3253/Re_r) \qquad (9)$$

For the present analysis, Eq. (8) was used for Re_r < 0.05 and Eq. (9) for Re_r > 50 and a suitable fairing function was devised for 0.05 < Re_r < 50. An analysis by Busse (Ref. 11) gives very similar results to Eqs. (7) to (9).

In the application of Eqs. (7) to (9), the effects of compressibility were partially accounted for by evaluating properties μ_v, ρ_v and Re_r at the local pressure, p(z).

CONDENSER

To facilitate computation of the flow in the condenser, a simple one dimensional flow analysis was constructed. The analysis differs from the customary one dimensional flow analysis of Shapiro (Ref. 13) since the control volume is drawn to include the heat pipe wall and fluid. By this means the conduction of heat along the heat pipe wall is easily accounted for. This sketch illustrates the model:

100
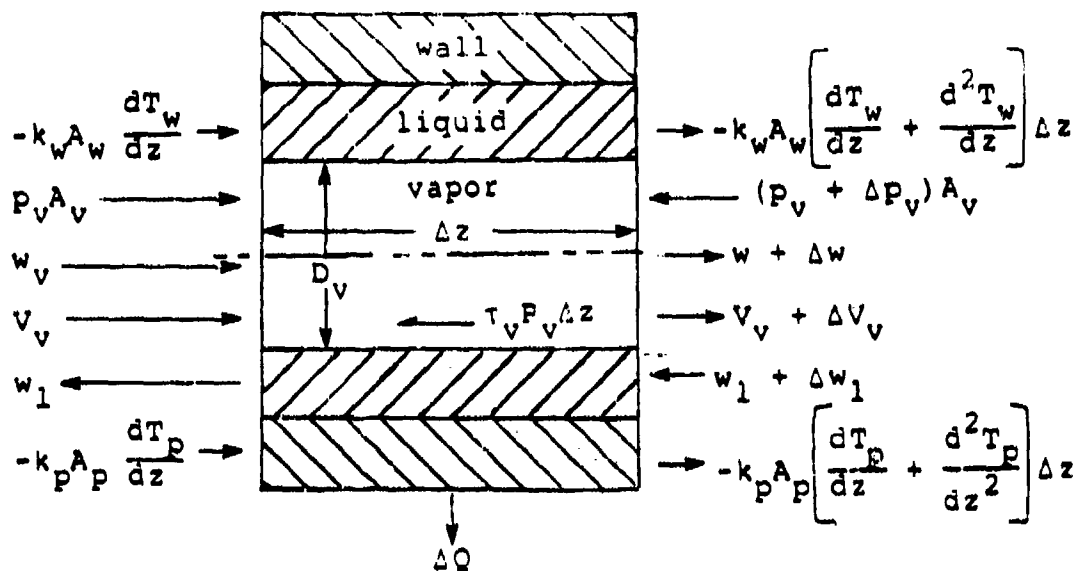
Here

A_p cross sectional area of pipe wall

A_v cross sectional area of vapor space

A_w cross sectional area of liquid channel including wick

D_v diameter of vapor space

k_p conductivity of pipe wall

k_w conductivity of liquid and wick

P_v wetted perimeter of vapor space

p_v pressure of vapor

Q heat rejected from outer wall

T_p pipe wall temperature

T_v vapor temperature

T_w liquid temperature

V_v mean vapor velocity

w mass flux of liquid

w_v mass flux of vapor

101

z distance along pipe axis

τ_v vapor shear stress

Momentum Equation

A momentum balance across the section gives

$(w + \Delta w)(V_v + \Delta V_v) - wV_v$

$$= p_v A_v - (p_v + \Delta p_v) A_v - \tau_v P_v \Delta z \qquad (10)$$

At steady state in the absence of freezing out, $w = w_v$ so the subscript has been dropped from w and V. Also needed are the continuity equation

$$w = \rho_v A_v V \qquad (11)$$

the perfect gas law

$$p = \frac{\rho R T_v}{\bar{m}_v} \qquad (12)$$

and the expressions for shear stress

$$\tau_v = f \rho_v V_v^2 / 2 \qquad (13)$$

Mach number

$$M = V/c \qquad (14)$$

and sound velocity for frozen composition

$$c = \sqrt{\gamma R T_v / \bar{m}_v} \qquad (15)$$

Here

f   friction factor

$\bar{m}_v$ mean molecular weight of vapor

R   gas constant

γ ratio of specific heats

The assumption of local chemical equilibrium in the gas is not consistent with the definition of c in Eq. 15. Combine Eqs. (10) to (15) to obtain

$$\left[1 - \gamma M^2\right] \frac{d \log_e p_v}{dz} = 2\gamma M^2 \frac{d \log_e W}{dz} - \frac{d \log_e T_v}{dz} - \frac{2f \gamma M^2}{D_v} \qquad (16)$$

102

Because of local phase equilibrium the Clausius-Clapeyron equation may be employed:

$$\frac{d \log_e p_v}{dz} = \left(\frac{h_{vl}}{RT_v}\right) \frac{d \log_e T_v}{dz} \tag{17}$$

where h_{vl} is the heat of vaporization. Combine Eqs. (16) and (17) to obtain

$$\frac{d \log_e w}{dz} = \frac{f}{D_v} - \left\{\left(\frac{h_{vl}}{RT_v}\right) \frac{(1 - \gamma M^2)}{2\gamma M^2} + \frac{1}{2}\right\} \frac{d \log_e T_v}{dz} \tag{18}$$

Energy Equation

The energy into the cross section of pipe is approximately

$$E_{in} = w\left(h_v + \frac{v^2}{2}\right) - k_p A_p \frac{d\bar{T}_p}{dz} - k_w A_w \frac{d\bar{T}_w}{dz}$$

$$+ (w + \Delta w)(h_1 + \Delta h_1) \tag{19}$$

and the energy out is

$$E_{out} = (w + \Delta w)\left(h_v + \Delta h_v + \frac{v^2}{2} + \frac{\Delta v^2}{2}\right) - k_p A_p \left(\frac{d\bar{T}_p}{dz} + \frac{d^2\bar{T}_p}{dz^2}\Delta z\right)$$

$$+ wh_1 + \Delta Q - k_w A_w \left(\frac{d\bar{T}_w}{dz} + \frac{d^2\bar{T}_w}{dz^2}\Delta z\right) \tag{20}$$

Here

h_1 enthalpy of liquid

h_v enthalpy of vapor

$\bar{T}_w, \bar{T}_p$ effective mean temperatures of the liquid and the wall

Using a frequently made assumption in heat pipe work (Ref. 8) that $\bar{T}_w$, $\bar{T}_p$ and T_v are not far different

$$\frac{dT}{dz} = \frac{d\bar{T}_w}{dz} \approx \frac{d\bar{T}_p}{dz} \approx \frac{dT_v}{dz} \tag{21}$$

103

and

$$\frac{d^2 T}{dz^2} = \frac{d^2 \bar{T}_w}{dz^2} \approx \frac{d^2 \bar{T}_p}{dz^2} \approx \frac{d^2 T_v}{dz^2} \qquad (22)$$

and defining.

$$C_c = k_w A_w + k_p A_p \qquad (23)$$

Equating E_{out} and E_{in} and using Eqs. (18), (21), (22), and (23) gives finally

$$\frac{d^2 T}{dz^2} = \left[\frac{w}{C_c} \frac{H_T h_{vl}^{(t)}}{T} + (c_v - c_1) \right] \frac{dT}{dz} + \frac{1}{C_c} \left(\frac{dQ}{dz} + w h_{vl}^{(t)} H_f \right) \qquad (24)$$

where

$\quad c_1 \quad$ specific heat of liquid

$\quad c_v \quad$ constant pressure specific heat of vapor.

Also

$$H_f = \frac{-f}{D_v} \qquad (25)$$

$$H_T = -\left[\left(\frac{h_{vl}}{RT} \right) \frac{1 - \gamma M^2}{2\gamma M^2} + \frac{1}{2} \right] \qquad (26)$$

$$h_{vl}^{(t)} = h_v - h_1 + \frac{v^2}{2} \qquad (27)$$

In the case where conduction along the wall is deemed negligible, $d^2 T/dz^2$ is set to zero in Eq. (24). Equation (24) then defines the derivative dT/dz.

The heat loss per unit length from the outer wall by combined radiation and convection (where applicable) is

$$\frac{dQ}{dz} = P_p (h_c + h_r)(T_p - T_s) \qquad (28)$$

where

$\quad h_c \quad$ coefficient of convective heat transfer

$\quad h_r \quad$ coefficient of radiant heat transfer

$\quad P_p \quad$ outer perimeter of pipe

104

T_p outer wall temperature

T_s sink or environment temperature

Assume that the net heat into the section sketched above is negligible. In the absence of a temperature gradient this is completely true. Then the heat rejected per unit length from the vapor to the outer wall, per unit length, is the same as that rejected to the environment:

$$\frac{dQ}{dz} = P_p h_{cond} (T - T_p) \tag{29}$$

The conduction heat transfer coefficient between the vapor space and the outer wall of the pipe in the assumed absence of a film resistance is (Ref. 14)

$$h_{cond} = \left[\frac{D_p \log_e\left(\frac{D_p}{D_1}\right)}{2k_p} + \frac{D_p \log_e\left(\frac{D_1}{D_v}\right)}{2k_w} \right]^{-1} \tag{30}$$

and the radiation heat transfer coefficient is

$$h_r = \sigma F_e T_p^3 \left[1 + \frac{T_s}{T_r} + \left(\frac{T_s}{T_r}\right)^2 + \left(\frac{T_s}{T_r}\right)^3 \right] \tag{31}$$

where

D   inner diameter of pipe wall

D_p outer diameter of pipe wall

F_e unit radiation conductance, equal to emissivity in this case

σ Stefan-Boltzmann constant

The convective heat transfer coefficient in a region with unrestricted air circulation can be written as (Ref. 14)

$$h_c = 1.32 \left(\frac{T_p - T_s}{D_p}\right)^{1/4} \tag{32}$$

in units of watts/meters^2 K. Equations 28 to 32 are solved simultaneously to find dQ/dz and T_p.

Properties

Reference 6 gives the following expressions for effective conductivity in wicks saturated with fluid

$$k_w = \frac{\beta - \varepsilon}{\beta + \varepsilon} k_1 \qquad (33)$$

where

$$\beta = \frac{(1 + k_s/k_1)}{(1 - k_s/k_1)} \qquad (34)$$

and

k_s thermal conductivity of solid

k_1 thermal conductivity of liquid

ε volume fraction of solid

The thermal conductivity of Haynes 188 (Ref. 15) was used as typical of the class of alloys studied here.

The conductivities of the liquid metals were from Ref. 10. Thermodynamic properties of lithium and sodium vapor and liquid were from the JANAF tables, (Ref. 16).

If the restriction of negligible wall conduction is lifted, the temperature gradient along the wall can be considered, and the profile in a pipe with an inactive length can be considered.

REFERENCES

1. E. Lantz, R. Breitwieser, and G.F. Niederauer, Development Concept for a Small, Split-Core Heat-Pipe-Cooled Nuclear Reactor, NASA TM X-2996, April 1974.

2. L.K. Tower and W.B. Kaufman, High Temperature Heat Pipe Research at NASA Lewis Research Center, Paper no. 78-438, A Collection of Papers, Third Intl. Heat Pipe Conf., Palo Alto, CA, May 1978, pp. 303-311.

3. J.F. Morris, unpublished communication, 1979.

4. D.T. Bourgette, "Evaporation of Ratioisotope Capsule Materials in Vacuum," Nuclear Metallurgy, Met. Soc. AIME, Vol. 14 pp. 248-270.

5. W.J. Waters, (private communication), NASA-Lewis Research Technology Utilization Office, 1984.

6. P.D. Dunn and D.A. Reay, Heat Pipes, 3d Ed., Pergamon Press Ltd., Oxford, 1982.

7. C.A. Busse, "Theory of the Ultimate Heat Transfer Limit of Cylindrical Heat Pipes", Int. J. Heat and Mass Transfer, Vol. 16, 1973, pp. 169-186.

8. B.D. Marcus, Theory and Design of Variable Conductance Heat Pipes, TRW Systems Group, Redondo Beach, CA, NASA CR-2018, 1972.

9. L.K. Tower and W.B. Kaufman, Procedures for Testing and Evaluating Spacecraft Type Heat Pipes, Interim Report AFWAL - TR - 84-2029, April 1984.

10. E.A. Skrabek, Heat Pipe Design Handbook Part I, Dynatherm Corporation, Cockeysville, MD, NASA CR - 134264, 1965.

11. C.A. Busse, Pressure Drop in the Vapor Phase of Long Heatpipes, Thermionic Conversion Specialist Conference, Palo Alto, CA, Oct. 1967.

12. S.W. Yuan and A.B. Finkelstein, "Laminar Pipe Flow with Injection and Suction Through a Porous Wall", Trans. ASME, May 1956, pp. 719-724.

13. A.H. Shapiro, _The Dynamics and Thermodynamics of Compressible Fluid Flow_, Vol. I, The Ronald Press Company, New York, 1953.

14. F. Kreith, _Principles of Heat Transfer, 3d Ed._, Intext Educational Publishers, New York, 1973.

15. Harold J. Hucek, Coordinating Editor, _Aerospace Structural Metals Handbook with Supplements_, Mechanical Properties Data Center, Battelle's Columbus Laboratories, Columbus, OH 1982 Publication.

16. Dow Chemical Company, Compilers and Calculators, JANAF Thermochemical Data, Thermal Laboratory, Midland, MI.